A laboratory investigation of the effect of flow rate and bedding characteristics on the interaction of a vertical water jet with an idealised soil medium

Dissertation presented in partial fulfilment for the degree, Master of Science in Engineering

Prepared by:

Kuveshan Govender

Student No: GVNKUV007

Supervised by:

Professor J.E. van Zyl

Date: August 2016

Department: Civil Engineering

Faculty: Engineering and the Built Environment

Institution: University of Cape Town

Declaration of Authorship

I know the meaning of plagiarism and declare that all the work in this document, save for that which is properly acknowledged, is my own. This dissertation has been submitted to the Turnitin module (or equivalent similarity and originality checking software) and I confirm that my supervisor has seen my report and any concerns revealed by such have been resolved with my supervisor.

Student No: GVNKUV007

Surname: Govender

Date: August 2016

Signature: Signed by candidate

Summary

Water conveyed through pipes systems installed beneath the ground surface has become standard practice in which treated fresh water is transported to communities. This kind of water delivery is successful in many regards but also results in considerable amounts of water wastage in the form of undetectable leakage. This is a serious concern since fresh water reserves throughout the world are being depleted faster than it is replenished; yet, there exists a large gap in understanding how leaks outside water distribution pipes behave.

Recent studies that have investigated external leakage behaviour have discovered that when water under pressure passes through a leak opening (orifice); a water jet is formed, which interacts with the surrounding soil (bedding material) in a manner that causes the granular medium to fluidise. This fluidisation process was seen to exhibit complex behaviour, which restricted shallow leaks under relatively high pipe pressures from growing and reaching the bed surface. As a result, leaks are able to remain bound beneath the ground surface with reduced chances of being detected and repaired.

The goal of this study was to conduct experiments aimed of performing a sensitivity analysis on how leakage conditions in the bed are affected when soil-leak characteristics including jet flow rate, bed height and the size of the granular particles in the bed are varied. In this study a vertical water jet in an idealised granular bed (glass beads) was used. The leakage conditions that were examined for each soil-leak factor comprised of measuring the height of the fluidised region and distributions of pore pressure, fluid velocity and energy within the bed.

The sensitivity analysis was based on data collected from experiments, which were conducted using an apparatus that was able to simulate an unbound pipe leak. The apparatus comprised of a glass tank, which housed the bedding material. An orifice installed at the bottom of the tank assisted in creating the water jet required for the pipe leak and, a Pitot tube positioning system above the tank allowed for positioning of straight and L-type Pitot tubes in the granular bed, which were used to measure the leakage conditions within the bed.

Results from the experiments revealed that the soil-leak factors, which were investigated had significantly affected leakage conditions, each to varying degrees. Larger jet flow rates led to an exponential increase in fluidisation height and higher maximum pore pressures, velocities and energies were measured in the bed. It was found that by varying the bed height, fluidisation height increased linearly with decreasing bed height and only the pore pressure distribution was considerably affected, where larger maximum pore pressures were measured in beds that were shallower. The effects of varying particle size included lower fluidisation heights and maximum pore pressures in beds that contained larger particles. Interestingly, the velocity and energy distribution remained substantially unaffected.

Acknowledgements

I would like to express sincere appreciation to, Professor J.E. van Zyl, for providing me with constructive supervision, unwavering support and patience throughout the course of this study.

I wish to thank the laboratory staff at the Civil Engineering department, led by Mr Noor Hassen, for their daily assistance during the experimental phase of this study.

In am grateful to the National Research Foundation for awarding me funding, which gave me financial stability.

Lastly, none of this would have been possible without the generous support and encouragement from my wife, Mrs Vishakthi Singh Govender. Thank you for so unselfishly allowing me this opportunity.

Table of Contents

List of Figures

List of Tables

Notation

English alphabet

A	Cross sectional area of soil bed
A_o	Area of orifice
A_s	Area of flow in the soil
C	Leakage coefficient
C_d	Discharge coefficient
D	Pipe diameter
D_p	Average particle diameter
d_p	Particle diameter
d_{10}	Diameter of the 10 % of the soil from the grading curve
e	Voids ratio
e_{max}	Maximum void ratio
e_{min}	Minimum void ratio
F_d	Drag force
g	Acceleration due to gravity
h_p	Pressure head
h_s	Head loss due to flow through the soil
h_{sp}	Surplus pore pressure head
h_v	Velocity head
$h_{v(h)}$	Horizontal velocity component of the velocity head
$h_{v(v)}$	Vertical velocity component of the velocity head
ΔH	Change in pressure head
I_p	Intermediate particle diameter
k	Coefficient of permeability
L	Length or height of the soil medium
L_P	Longest particle diameter
$N1$	Leakage exponent
ΔP	Change in pressure
p	Pressure
Q	Flow rate / discharge
R_e	Reynolds number
r_s	Sphere radius
S_p	Shortest particle diameter
U	Velocity averaged over the flow cross-section (superficial velocity)
$U_{mf(v)}$	Minimum fluidisation velocity

$U_{mf(T)}$	Turbulent minimum superficial fluidisation velocity
V	Velocity of the sphere relative to the fluid

Greek symbols

α	Constant dependent on the fluid properties
β	Constant dependent on the properties of the granular media
μ	Dynamic viscosity of the fluid
ρ	Dry density
ρ_f	Fluid density
ρ_s	Particle density
ϕ	Porosity ratio
φ	Particle shape factor
φ_o	Krumbein's Operational Sphericity
φ_p	Sneed and Folk Sphericity

1. Introduction

1.1 Problem statement

The uncertainty of freshwater supply for the future is a problem experienced globally. Arnell (2004) pointed out that an assessment of the world's freshwater reserves, conducted by the United Nations in 1997, revealed that "approximately a third of the world's population was living in countries deemed to be suffering from water stress" and that "two-thirds of the world's population would be living in water-stressed countries by 2025".

In South Africa the Department of Water and Sanitation (2000) estimated that based on current usage trends, "South Africa's water demand will exceed the availability of economically usable freshwater resources by 2025" and unless corrective measures are implemented further strain will be placed on the limited available freshwater reserve through increasing trends in industrialisation and urbanisation. Therefore, the preservation of water resources by reducing water wastage is a pertinent issue that concerns the wellbeing of humanity.

Water loss in water distribution systems in the form of physical leakage is of great significance since leakage results in considerable amounts of water wastage as well as large amounts of Non-Revenue water. Kingdom et al. (2006) estimated that 8 billion cubic meters of treated water could possibly be recovered should physical water losses from water distribution systems be reduced by half in all developing countries such as South Africa.

The simplest form of locating a buried leak is when it becomes visible above ground level, but not all leaks reach the soil surface, which makes them very difficult and costly to locate. Laboratory experiments (Alsaydalani, 2010 and van Zyl et al., 2013) have shown that relatively shallow leaks with high pressure heads do not penetrate the soil surface even when a pipe has a leak directed perpendicularly towards the soil surface. It was established that the formation of a fluidised region immediately outside the leak opening was responsible for dissipating significant amounts of energy, which prevented the leak from propagating to the soil surface (van Zyl et al., 2013).

Little is known of how the interaction between the soil medium and water jet is affected when soil-leak characteristic such as the jet flow rate and bedding properties (e.g. soil grain size and bed height) are varied. Understanding these relationships could give insight into the conditions that promote a buried leak to propagate to the soil surface, which could assist in methods of early leak detection, thus reducing the number of undetected leaks. This will effectively result in a reduction of water loss.

1.2 Goal and objectives

The main goal of this study was to conduct experiments aimed at understanding the effects of varying the jet flow rate, bed height and particle size during soil-leak interaction of an unbound vertical water jet beneath an idealised granular bed. This involved conducting laboratory experiments using a newly constructed soil-leak apparatus and methodology developed by Bailey (2015), which enables one to find distributions of pore pressure, velocity and energy within a granular bed. The list below describes the objectives that were set in order to achieve the main goal.

i. Prepare a review and develop an understanding of the relevant literature regarding soil-leak interaction.

ii. Test the existing experimental set-up and modify where necessary.

iii. Conduct controlled experiments to obtain distributions of pore pressure, fluid velocity and energy for various jet flow rates that enables assessing its influence during soil-leak interaction of a vertical upright water jet in an idealised granular bed.

iv. Conduct controlled experiments to obtain distributions of pore pressure, fluid velocity and energy for various bed heights that enables assessing its influence during soil-leak interaction of a vertical upright water jet in an idealised granular bed.

v. Conduct controlled experiments to obtain distributions of pore pressure, fluid velocity and energy for various particle size distributions that enables assessing its influence during soil-leak interaction of a vertical upright water jet in an idealised granular bed.

vi. Perform a sensitivity analyse of the data recorded during the experimental phase and discuss findings.

vii. Discuss potential implications for leak detection based on the outcome of the experiments.

viii. Draw conclusions and finally make recommendations for future investigations.

1.3 Layout of dissertation

This dissertation was organised into the following five chapters:

- Chapter 1 gives the problem statement as well as the objectives set to achieve the main goal of the investigation.
- Chapter 2 contains a literature review of material relevant to the subject of this study.
- Chapter 3 gives a detailed description of how the experimental apparatus functioned, modifications made to the setup, characteristics of the soil materials used and techniques that were employed during the experimentation phase of this study. Results from validation

experiments that were carried out to ensure accurate readings were obtained are also given in this section.

- Chapter 4 presents the results obtained from the main experiments. In addition, a detailed discussion of the trends and relationships established from analysis of the results forms part of this chapter.
- Chapter 5 contains the conclusion of the investigation. A summary of the findings is presented and recommendations for improving the experimental setup and future investigations are given.

Supporting data is given in the form of appendices at the back of this report. The appendices contain the following information:

- Appendix A gives the raw data obtained from the geotechnical tests that were conducted on the soil materials used in the experiments.
- Appendix B contains the raw data that was attained during the various validation experiments.
- Appendix C gives the raw data that was obtained in a standard experiment as well as in the sensitivity tests that investigated the effects of the jet flow rate, bed height and particle size distribution in the bed.
- Appendix D presents the raw data attained in an additional investigation, where the leakage conditions at the centre and side orifice was investigated.

2. Literature review

This chapter provides a review of literature centred on understanding various mechanisms that were observed during the soil-leak interaction. It begins by considering the various definitions of the fluidisation phenomenon, before explaining the relevant fundamental theories of orifice hydraulics and fluid flow through a porous medium.

Thereafter, focus shifts to pertinent observations and findings from studies where the combined flow mechanism (from an orifice into granular material) was investigated. Moreover, in this section notable experimental setups and techniques used to investigate the fluidisation phenomenon are also described.

2.1 Definition of fluidisation

The term “fluidisation” has been used within the disciplines of chemical engineering, soil mechanics and earthquake engineering. As a result, there are a number of definitions and terms that can be used to describe the fluidisation phenomenon.

In the field of chemical engineering, Kunii and Levenspiel (1991) defined fluidisation “as the operation by which solid particles are transformed into a fluid-like state through suspension in gas or liquid.” This process commonly occurs in biological reactors where a fluid (gas or liquid) is injected at the bottom of a confined bed of granular material. Once the bed becomes fluidised, the suspended material within the fluid is easily collected and transported through a network of pipes. Other functions of the fluidisation process in the chemical engineering field include reacting gases with solid catalysts.

In the context of soil mechanics, Powrie (2004) explained that soils, which experienced a strong upward flow such as regions in front of retaining walls may fluidise or “boil” when the uplift force due to seepage becomes greater than the weight of the soil. Moreover, Powrie (2004) categorised the fluidisation condition according to the size of the area being fluidised; he referred to the condition as “quicksand” if it covered a large area and “piping” if it was localised. However, in soil mechanics the term “piping” is often used to describe the process of backward erosion, which is usually identifiable by a continuous passage in the soil, brought about when erosive forces generated by seeping water encourages soil particles to become dislodged and transported away from the soil matrix. Interchanging the word “piping” with “fluidisation” could create a level of misconception since, as stated by Ma (2011), the term “piping” is commonly used in relation to the effects of fluidisation.

Foda et al. (1997) defined fluidisation as a condition that arises when contact stresses between particles in a granular medium reduce to zero with the net effect of the granular material losing its shear strength and starts to behave like a fluid. They interchangeably used the term “liquefaction” with fluidisation, stating that when fluidisation occurs in soil it is referred to as liquefaction. Interestingly, the term liquefaction is often used in earthquake engineering to describe the process when large volumes of saturated soils behave like a liquid when acted upon by large stresses such as those created during an earthquake (Ma, 2011).

Therefore, the terms "fluidisation", "piping", "quicksand" and "liquefaction" have been used to describe a common process where a region of saturated soil (or granular material) that was once a ridged and stationary body is transformed to behave in a fluid-like manner. During the transformation process the saturated soil medium loses its net shear stresses due to an applied force (such as those created by a strong seepage flow or an earthquake), which effectively results in the soil particles becoming mobile. If the force is applied from below the permeable soil body and exceeds the weight of the soil, the particles become suspended within the pore fluid.

In this study the description provided by Alsaydalani (2010) is adopted since it best defines the process that occurs during a pipe leak. He used the term "internal fluidisation" to name the soil-leak interaction and defined it as a phenomenon where the pore water pressure and hydraulic gradient within the granular bed immediately outside the leak opening increases due to a strong flow, resulting in the granular bed behaving like a fluid and advancing to form a localised circular flow pattern. The term "internal" denotes that the fluidised mechanism is restricted to a confined space and does not reach the bed surface.

2.2 Orifice hydraulics

An orifice can be defined as an opening, usually circular or of regular shape through which fluid flows in the form of a jet. When considering water supply pipes, an orifice is an opening that develops in the wall of the pipe, usually during failure of the pipe material. Orifices are often characterised by having a relatively larger opening (area) compared to the thickness of the surrounding wall (Finnemore & Franzini, 2002).

Under free discharge condition, flow through an orifice often occurs at velocities high enough that produce a turbulence flow regime (Alsaydalani, 2010). The velocity of water flowing through an orifice can be quantified using the Torricelli equation shown in equation (1). The Torricelli equation was derived using the conservation energy equation, which describes the conversion of potential pressure energy to kinetic energy.

$$u = \sqrt{2gh_P} \tag{1}$$

Where:
u is the fluid velocity (m/s)
g is acceleration due to gravity (m^2/s)
h_P is the pressure head (m)

Discharge through an orifice can be determined using equation (2). This expression is commonly referred to as the orifice equation.

$$Q = C_d A_o \sqrt{2gh_p} \quad (2)$$

Where: Q is the fluid flow rate (discharge) (m^3/s)
C_d is the discharge coefficient
A_o is the orifice area (m^2)

The discharge coefficient (C_d) is the product of the velocity coefficient (C_v) and the contraction coefficient (C_c). It is added to the equation to take into account energy losses that occur at the orifice due to friction (C_v) as well as the reduction of the jet area downstream of the orifice (C_c), known as the vena contracta. Experiments have shown that C_c is the ratio of the reduced jet area over the orifice area and can range from 0.61 to 0.66 whilst C_v can range from 0.97 to 0.99 (Chadwick, Morfett & Borthwick, 2004).

Elements such as thickness, roughness and shape of an orifice have been found to influence C_d. Figure 2.1 shows some typical orifice openings and its effect on C_v and C_c. In figure 2.1a an example of an orifice with a sharp edge is shown and in figure 2.1b a square shoulder. These orifice openings are considered to be standard. The orifice shown in figure 2.1c and 2.1d are not standard since flow through them is affected by the wall thickness, roughness of the surface and the radius of curvature in the case of figure 2.1b. One might notice that, increasing the wall thickness of the orifice to a point where the vena contracta does not occur resulted in C_c becoming 1 and therefore negligible, however, in this case C_v cannot be ignored (Finnemore & Franzini, 2002).

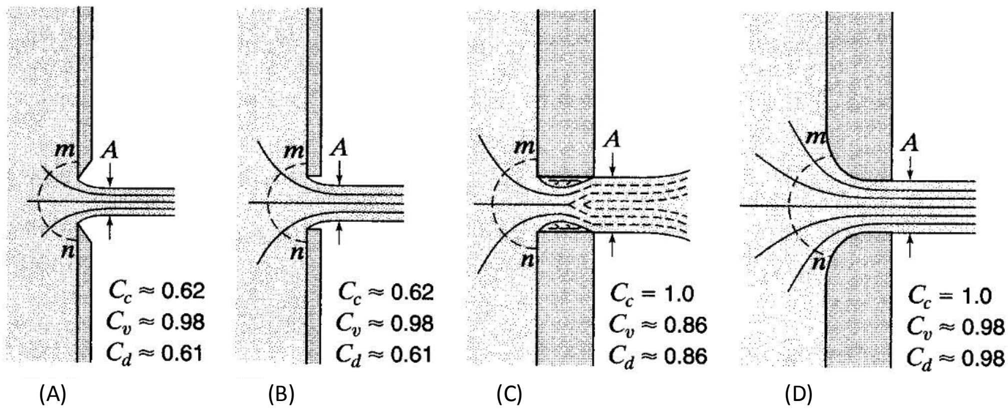

Figure 2.1: Orifice types

(Finnemore & Franzini, 2002)

Practitioners have expressed equation (2) in more general terms to quantify leakage in water networks, as seen in equation (3). This empirical form of the orifice equation is commonly referred to as the N1 equation.

$$Q = ch^{N1} \quad (3)$$

Where: C is the leakage coefficient
N1 is the leakage exponent.

In this expression, N1 has an exponential relationship to discharge and thus has more influence than the leakage coefficient. In effect this allows for total leakage in the water distribution networks to be evaluated according to the N1 term. Theoretically, N1 should have a fixed value of 0.5 but field studies have shown that N1 can range from 0.5 to 2.8. The interaction of the soil surrounding the leak has been suggested by Clayton and van Zyl (2007) to be one of the causes for the variation of N1. Van Zyl et al. (2013) explained that the soil surrounding a leak can affect the leakage rate either by increasing the pressure outside of the leaks or by simply blocking the leak openings.

2.3 Flow through saturated granular material

Flow through granular material can be laminar or turbulent. It is important to make this distinction since in each case, flow features such as energy loss and velocity profiles within the soil can be significantly different. Therefore, theories pertaining to each flow regime have been suggested and are reviewed below.

2.3.1 Laminar flow

In 1856, Darcy showed empirically that the flow rate of water through a fully saturated bed of soil is linearly related to the ratio of the head loss over the length (or height) of the soil medium (the hydraulic gradient defined by the symbol (i)) and is proportionally dependant to the permeability and cross sectional area of the soil bed. This is shown in equation (4) (Greenkorn, 1981):

$$\mathrm{Q} = \mathrm{Ak}\left(\frac{\Delta \mathrm{H}}{\mathrm{L}}\right) \tag{4}$$

Where: k is the coefficient of permeability (m/s)
A is the cross sectional area of soil bed (m^2)
ΔH is the change in pressure head (m)
L is the length or height of the soil medium (m)

The permeability (k) of a soil (also known is as hydraulic conductivity) is primarily reliant on the average size of the pores in the soil, which is effectively related to the distribution of particle sizes. Allen Hazen as cited in many textbooks (for example Craig (2004)) showed that the permeability of sand can be approximated using equation (5). From this equation it is evident that the presence of a small quantity of fines in coarse grained soil will result in k being significantly reduced compared to the same soil without the fines.

$$\mathrm{k} = 10^{-2}\mathrm{d}_{10}^{2} \tag{5}$$

Where: d_{10} is the diameter (m) of 10 % of the soil from the grading curve.

Darcy's law is only valid for liner laminar flow (Greenkorn, 1981). Laminar flow is characterised by the fluid having low velocity where the streamlines are not necessarily parallel but remains in discrete layers (Finnemore & Franzini, 2002). Flow regimes (such as laminar or turbulent) are usually classified using the dimensionless Reynolds number (Re). Re is determined by taking the ratio of the fluids inertial force over the viscous force. The Re for a pipe flowing fully as shown in equation (6).

$$\mathrm{Re} = \frac{\mathrm{UD}\rho_f}{\mu} \quad (6)$$

Where: Re is the dimensionless Reynolds number
U is the velocity averaged over the flow cross-section (superficial velocity (m/s))
D is the diameter of the pipe (m)
ρ_f is the fluid density (kg/m^3)
μ is the dynamic viscosity of the fluid (kg/(m.s))

The Re for flow through a porous medium contained in a pipe can be determined as illustrated in equation (7) (Greenkorn, 1981). In this equation the superficial velocity is also used, however, the average particle diameter is used instead of the pipe diameter.

$$\mathrm{Re} = \frac{2}{3(1-\phi)} \frac{\mathrm{UD_p}\rho_f}{\mu} \quad (7)$$

Where: D_p is the average particle diameter (m)
ϕ is the porosity ratio

When a fluid experiences laminar flow the inertial force of the fluid is relatively low, this allows viscous forces to dominate, resulting in a low Re. According to Greenkorn (1981) laminar flow through a porous medium occurs at an Re of less than 1. Harr (1962) found that when Re ranged from 1 to 10 the flow was in a transitional phase between laminar and turbulent.

2.3.2 Turbulent flow

During laminar flow, Darcy's law suggested that when a fluid passes through a granular bed a linear relation existed between the pressure drop and the flow rate. However, when the flow becomes turbulent it was found that the pressure drop was higher than what was predicted by the Darcy equation (4). To account for the difference Forchheimer (1901) introduced a second non-linear term to form the empirical Forchheimer equation (Hlushkou & Tallarek, 2006):

$$\frac{\Delta \mathrm{H}}{\mathrm{L}} = \alpha \mathrm{U} + \beta \mathrm{U}^2 \quad (8)$$

Where: α is a constant dependent on the fluid properties
β is a constant dependent on the properties of the granular media

By employing different methods of investigation Ward (1946) and Ahmed and Sunada (1969) found the constants α and β to have the expressions shown in equation (9) and (10) respectively. Ward (1964) used the method of dimensional analysis while Ahmed and Sunada (1969) used the Navier-Stokes equations to develop the theoretical relationships for the constants. Venkataraman and Rao (1998) validated these equations by comparing results from previous studies spanning four decades. During the validation process, experimental data was collected for a wide range of granular material, which had varying particle diameters, porosity and permeability.

$$\alpha = \frac{1}{k} \tag{9}$$

$$\beta = \frac{6.72(1-\phi)}{g\varphi D_p \phi^{3/2}} \tag{10}$$

Where: φ is the particle shape factor

In 1952, Ergun studied the non-linear relationship established between pressure drop and fluid velocity by conducting experiments that allowed gas to flow through a fixed bed containing a crushed porous medium. In his study he took into account the effects of the fluid properties, porosity, orientation, size and shape of the particles in the granular medium and found that the energy loss through the porous bed per unit length can be expressed as follows (Alsaydalani & Clayton, 2014):

$$\frac{\Delta H}{L} = A\frac{(1-\phi)^2}{\phi^3}\frac{\mu U}{d_p^2 \varphi} + B\frac{(1-\phi)}{\phi^3}\frac{\rho_f U^2}{d_p \varphi} \tag{11}$$

Where: d_p particle diameter (m)

Equation (11) has two terms where the first takes into account energy loss resulting from laminar flow and the second term accounts for energy losses due to high fluid velocity (inertial losses). After analysis of a large amount of experimental data, Ergun (1952) found that the values of 150 and 1.75 for A and B respectively give the best representation. According to Hlushkou and Tallarek (2006), a large number of empirical equations have been reported that describe fluid flow through granular material and its dependence on medium properties; however, the Ergun (1652) equation has become the most popular and widely accepted.

Hlushkou and Tallarek (2006) illustrated using figure 2.2 the three regimes of liquid flow through a fixed porous bed; namely, linear laminar, non-linear laminar and turbulent flow. During linear laminar flow, viscous forces in the fluid dominates and pressure drop is linearly proportional to the fluid velocity (or flow rate). Darcy's law is only valid during this flow regime. During nonlinear- laminar flow both viscous and inertial forces affect the fluid dynamics and pressure drop is no longer linearly proportional to the fluid velocity but flow is still laminar. Finally, during a turbulent flow regime inertial forces dominates and pressure drop is proportional to the square fluid velocity.

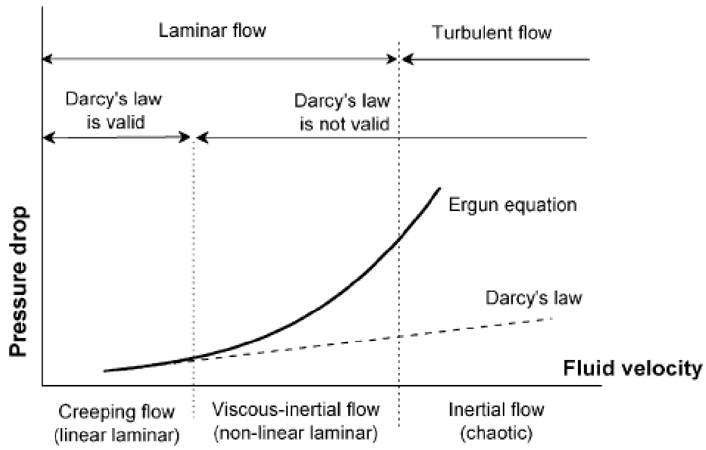

Figure 2.2: Characterisation of different flow regimes in fixed beds.
(Hlushkou & Tallarek, 2006)

The competancy of the Ergun equation against experimental data for a wide range of velocities (creeping to turbulent flow) in a fixed particulate bed is illustrated in Figure 2.3. Additionaly, figure 2.3 provides values of Re_{inter} (determined using the particle diameter and interstital velocity [U/ϕ]) that can be used to find ranges for the three flow regimes in packed beds with varying porosities (Hlushkou & Tallarek, 2006):

- $Re_{inter} \leq 1$ (Linear laminar, creeping or Darcian flow)
- 1 < Reinter < 500 (nonlinear-laminar or viscous-inertial regime)
- $Re_{inter} \geq 500$ (Inertial or turbulent regime)

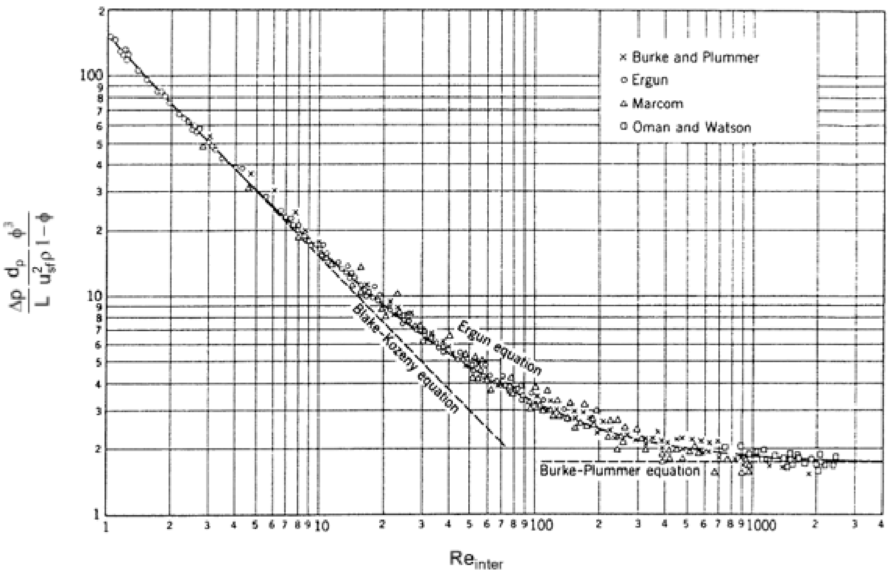

Figure 2.3: Normalised plot of the Ergun equation for flow through packed beds
(Bird, Stewart & Lightfoot, 2002)

Deviation from Darcy's law during non-linear laminar flow could be attributed to local energy losses (also referred to as "shock", "minor" or "fitting" losses) that can occur through expansion, contraction and changes in flow direction within the porous bed (Niven, 2002). Referring to non-Darcian flow and turbulent flow interchangeably would be incorrect (Hlushkou & Tallarek, 2006).

2.4 Flow from an orifice into granular material (combined flow)

It has been observed that flow issuing from an orifice into a granular bed resulted in the formation of a fluidised area. Thus, to study this flow mechanism various experimental setups have been developed. This section first gives a description of notable experimentation designs and techniques with the aim of providing a perspective on how the fluidisation process was simulated in a laboratory setting, and to illustrate the advancement of investigation in this field. Thereafter, relevant observations and findings regarding characteristics of the fluidised area are presented.

2.4.1 Experimental designs and techniques used to study combined flow

2.4.1.1. Zoueshtiagh and Merlen (2007)

Zoueshtiagh and Merlen (2007) developed the experimental setup in figure 2.4 to study the mechanism of an upright vertical water jet under a bed of granular material. The setup consisted of a 24 cm diameter cylindrical tank made of transparent Plexiglass, which was used to house granular material. A circular disk at the bottom of the tank formed the base. The setup allowed for the tank volume to vary. This was achieved by sliding the disk up or down parallel to the vertical axis, which effectively increased or decreased the height of the tank. A hole at the centre of the disk allowed for attachment of hollow sub cylinders (orifice) of varying internal diameters. A 210 μm grid was placed above the injection hole to prevent particles of the granular bed from falling through the orifice into the inflow system.

The technique adopted by Zoueshtiagh and Merlen (2007) when preparing each experiment was to first fill the tank with the granular material to a predetermined bed height (e.g. height S in figure 2.4). Water was then injected through the orifice (sub cylinders) until the tank was full. The top of the tank was left open for excess water to overtop. This outflow system ensured that the water level in the tank remained constant and did not fluctuate during experimentation. Once the tank was filled, the inflow of water was stopped and the tank was left to slowly defluidise (drain). The objective of this step was to achieve constant packing of the granular particles within the bed. This approach was based on a study by Ojha et al. (2000), where it was found that slow defluidisation leads to a constant packing fraction of the granular particles within the bed irrespective of grain size.

During experimentation, the flow rate of water flowing into the tank was measured using a flow meter positioned upstream of the orifice. A charged-coupled device (CCD) video camera was initially placed above the setup to capture the motion of the granular bed. However, this gave a limited view. Thus, to capture both top and lateral views of the bed the camera was replaced by a mirror set at a 45° and the camera moved horizontally in line with the optical path of the mirror. The arrangement of these components in this manner allowed the setup to investigate the influence of flow rate, orifice size and bed height on the fluidisation process as well as make observations. The following conclusions were reached in the study:

- The fluidised region was observed to occur in three stages as the flow rate was increased. First the bed remained motionless, following this the bed surface was deformed but only above the injection point and the last stage was complete local fluidisation of the bed height, which took the form of a vertical chimney.
- The onset of fluidisation and the size of the fluidised region appeared to be unaffected by the size of the water jet i.e. orifice size.
- The height of the bed was found to influence the flow rate required for the onset of fluidisation. A linear relation was observed where deeper beds required greater flow rates for fluidisation to occur.

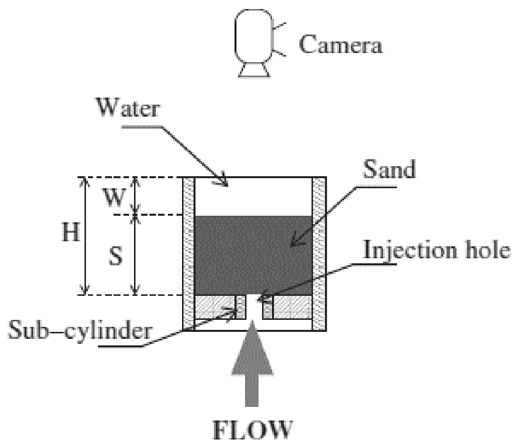

Figure 2.4: Schematic drawing of Zoueshtiagh and Merlen's experimental setup

(Zoueshtiagh & Merlen, 2007)

2.4.1.2. Van Zyl et al (2013)

With the main aim of investigating pressure distribution within the fluidised area, van Zyl et al. (2013) developed the setup shown in figure 2.5. This setup consisted of a supply line and a rectangular tank made of Perspex. At the base, a nozzle protruded 98 mm into the tank and 2 mm away from the front wall. This formed the entry point for the water jet. The nozzle was designed in a way that one of three circular orifices sizes (2, 4 and 8 mm) could be selected and used independently to produce the jet. Additionally, the nozzle could be turned to a closed setting to prevent granular particles from entering the supply pipe when the water supply was stopped. An alternate method of closing the system was to plug the orifice with a rubber stopper, which was attached to a metal wire. Pressure readings within the fluidisation zone were obtained by inserting pressure tappings through 1 mm holes that were drilled through the front wall of the tank. The pressure tappings were made of blunted hypodermic needles that had a 0.9 mm internal diameter. They were positioned centrally to the orifice and at specific heights above the orifice. The needles were long enough to reach inside the tank and provide sufficient space for attachment of sight tubes outside the tank. Each pressure tapping was connected to a sight tube that was used to read pressures at the specific points. van Zyl et al. (2013) referred to the increase in the measured pressure readings as "excess pore pressure", which effectively was a measure of pore pressure above hydrostatic conditions.

In preparation for experimentation, the empty tank was first filled with water and then the granular material was "rained" into the tank to a bed height of 400 mm. "Raining" the material caused the granular material to separate into individual particles and release the air that was trapped between the particles. Trapped air bubbles in the bed blocks voids and reduces permeability, which ultimately affects pressure readings and the fluidisation process (van Zyl et al., 2013 and Ma, 2011). Water in the tank was allowed to overflow through pipes placed 100 mm above the bed surface. This insured that the bed remained fully saturated during testing. The flow rate of the inflowing water was measured using an electromagnetic flow meter. During fluidisation its geometry was traced using a scale attached to the front wall of the tank (van Zyl et al., 2013). The findings from this study were:

- The distribution of pore pressure against depth, and height of the fluidised zone were influenced by the jet flow rate but were unaffected by the orifice size.
- The geometry of the locally fluidised region was observed to contain three zones namely, inner fluidised, mobile and static bed zones.
- Results illustrated that fluidisation did not reach the bed surface in shallow leaks with relatively high pressure heads in the pipes.
- The inner fluidised and mobile bed zones followed by the orifice were identified to be responsible for dissipating majority of the leak energy, which prevented the leak from reaching the surface. Energy loss due to the orifice was shown to be dependent on C_d.

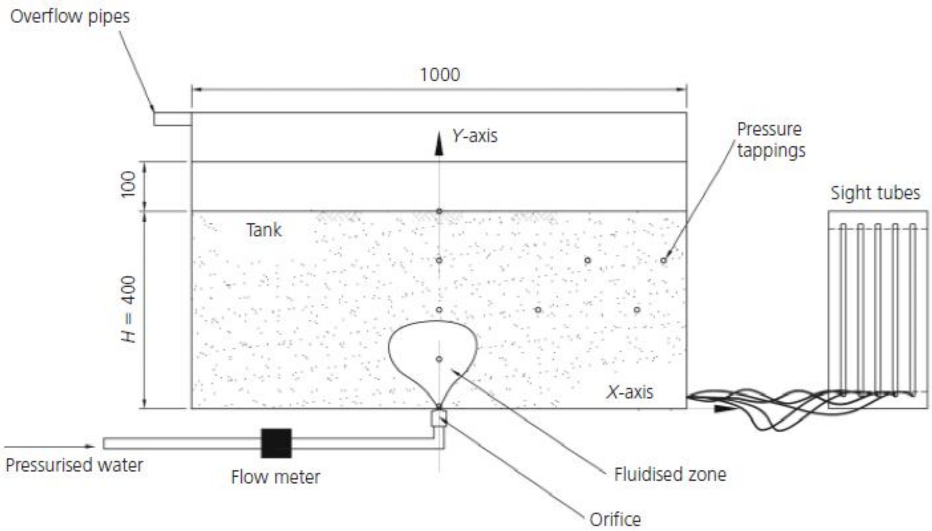

Figure 2.5: Schematic drawing of van Zyl et al. experimental setup

(van Zyl et al., 2013)

2.4.1.3. Alsaydalani (2010)

Alsaydalani (2010) developed an apparatus (figure 2.6) similar to that of van Zyl et al. (2013) to investigate the effects of orifice size and soil grain characteristics on the onset of fluidisation. However, a significant difference in his apparatus design was the shape of the orifice and flow dynamics of the upright jet that was projected into the tank. A rectangular orifice that resembled a longitudinal pipe crack and spanned the width of the tank was positioned on the tank base. This configuration allowed a two dimensional flow (upwards and along the length of the tank) of water into the tank. The third flow dimension (along the width of the tank) was prevented due the restriction of the tank walls.

The orifice was squire edged and had a wall thickness of 10 mm. It was constructed by leaving a gap between two aluminium plates that rested on an empty machined box. The length of the gap remained constant while the width was made adjustable to a tolerance of a fraction of a millimetre. This was achieved by turning a screw that pulled or pushed one plate while the other remained stationery on the box. This experimental setup was also designed to measure pore pressure differences before and during the fluidisation process (i.e. excess pore pressure) by placing pressure tapping perpendicular to the centreline of the vertical water jet for varying flow rates.

The findings from the study were:

- The excess pore water pressure profiles were unaffected by the size of the orifice. Thus, it was concluded that the size of the orifice did not influence the process or properties of the fluidisation mechanism.
- The size of the granular particles in the bed was found to have an influence on the onset of fluidisation. Lower flow rates were required for fluidisation to occur in beds made up of smaller diameter particles.
- The form (sphericity) of the granular particles was observed to influence excess pore water pressures in the bed, which ultimately affected the onset of fluidisation. It was discovered that the build-up of excess pore water pressure increased with decreasing form. The build-up of pore pressure lead to a greater potential for fluidisation to begin.
- Results from experiments that investigated the influence of bed height on the onset of fluidisation suggested that higher flow rates are required to fluidise beds with greater depths.

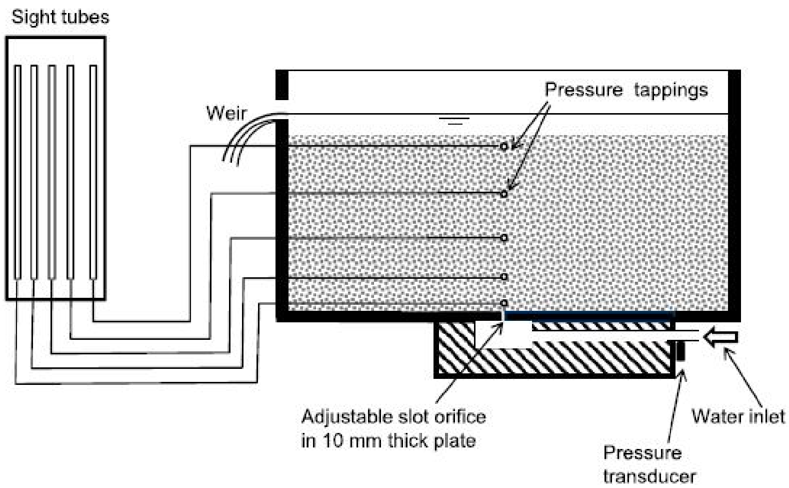

Figure 2.6: Schematic drawing of Alsaydalani's experimental setup.
(Alsaydalani & Clayton, 2014)

2.4.1.4. Philippe and Badiane (2013)

In a separate study, Philippe and Badiane (2013) used the experimental setup shown in figure 2.7 to investigate characteristics of the fluidisation phenomenon. Their setup also consisted of a rectangular tank manufactured out of Plexiglass, however three circular "injection ports" were installed at the base of the tank at equal distances apart. Each port could be controlled separately allowing for usage of a single port or simultaneous use of any two or all three ports. The latter was used to investigate the interaction of two upright fluidised regions that were in close proximity to each other. However, that investigation is not within the scope of this study. The diameter of each port was adjustable from 14 mm to 6 mm by adding a perforated cylindrical piece. As seen in figure 2.7, the top of the tank was extended to accommodate for an overflow system, which ensured that the fluid was kept at a constant level during experimentation. A perforated grid was screwed onto the tank base just above the injection ports to presumably prevent granular material from falling into the supply line.

The material preparation routine for experimentation was to pour the sample material into the tank to a predetermined height (H_o) and thereafter slowly fill the tank with fluid via the ports located at the bottom. A glass stick was then inserted into the saturated granular bed and moved around in a systematic manner to release any trapped air as well as to create a reproducible state of compaction. After each round of testing the soil sample was homogenised with the glass stick in order to recover its initial setting condition.

Philippe and Badiane (2013) used a combination of interesting optical techniques and materials to observe and analyse the fluidisation process within the granular bed. The first technique was to select a fluid and granular material that had the same refractive index. The purpose of this grouping was to allow the immersed granular particles to become translucent. This was achieved by selecting a granular material made of glass beads (also known as ballotini) and submerging it into a fluid made of a mineral oil mixture. The next optical technique employed was used to visualise the internal structure of the grains during fluidisation. This involved inserting small amounts of fluorescent dye into the fluid and then illuminating the point of interest within the granular bed using a laser light, see figure 2.7. Directing the laser light at a particular point caused the fluorescent dye (diluted in the fluid) to emit its own light and by utilising an optical filter it was possible to obtain only the light emitted by the fluorescent dye. The final result were images in which the fluid appeared clear and the glass beads as black dots. The images and observations of the fluidisation process obtained using these optical techniques are presented in the section that follows (see figure 2.10). Results from experiments conducted using this setup yielded the following results:

- Development of the fluidisation mechanism was observed to the point of it breaking the bed surface. Three stages were identified as the flow rate was increased. They were termed the, static, cavity and chimney regimes. Details of each of these stages are given in the next section.
- The onset of fluidisation of the entire bed height (chimney regime) as a function of flow rate and bed height was found to influence by the size of the granular particles that formed the bed.
- The onset of fluidisation in the chimney regime as a function of flow rate and bed height was found not to be dependent on the size of the injection area (orifice).

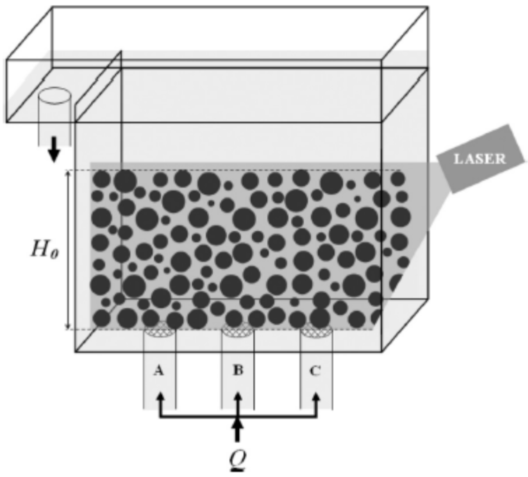

Figure 2.7: Schematic drawing of Philippe and Badiane's experimental setup

(Philippe & Badiane, 2013)

2.4.2 Development and geometry of the fluidised area

This section reports observations made on the development of fluidisation within a granular bed. All observations presented are of a vertical water jet positioned in a bed of granular material.

Zoueshtiagh and Merlen (2007) (setup described in section 2.4.1.1) observed three distinct regimes from outside the bed when flow rate was gradually increased. A description of each regime is given below.

- ***Regime (i): Motionless bed***

  At a low flow rates the external appearance of the bed remained unchanged and motionless. The bed "seemed to act like a rigid porous medium"(Zoueshtiagh & Merlen, 2007).

- ***Regime (ii): Deformation of the bed surface***

  The second regime was characterised by an increase in flow rate to the point where local deformation was observed at the bed surface, directly above the injection. The deformation on the bed surface was reported to be influenced by material type, since deformation was more pronounced in some granular beds compared to others. This regime was said to be a transitory stage between the bed behaving like a porous medium and the final regime.

- ***Regime (iii): Local fluidisation of the bed***

  The third and final regime was distinguished by the formation of a fluidised area that occurred above the injection hole. This occurred when the flow rate was increased to values higher than those in region (ii). It was reported that, at first an "explosion" occurred at the bed surface, which resulted in the development of a "bowl-shaped crater" and thereafter the fluidised area formed. The fluidised area was described as having a cylindrical shape similar to that of a "vertical chimney". Another notable observation in this regime was that granular particles within the fluidised area were in constant motion, creating a dome shape above the bed surface while a fluctuating movement of the granular particles was witnessed within the crater. Particles outside the crater remained stationary. Figure 2.8 shows typical images of the formation of the fluidised area.

It was noted that increasing the flow rate further, increased the size (height and diameter) of the dome as well as intensified the movement of the particles that created the dome. Motion analysis of these particles suggested that the granular particles were projected upwards and when the vertical velocity reached zero the particles began to fall outward. The motion and concentration of the particles forming the dome remained constant over several hours, which suggested that a recirculating motion of the granular material occurred within the fluidised area. Additionally, the number of domes that formed per experimental run varied between one and three. The double and triple domes were reported to be very unstable (lasted for only a fraction of a second) and were noticed for relatively smaller flow rates and bed heights.

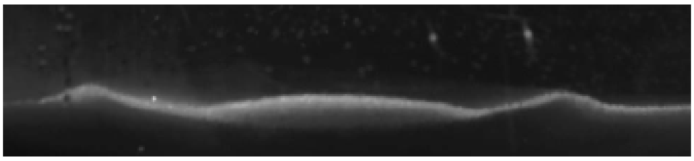

(a) Bowl-shaped crater formed after bed explosion.

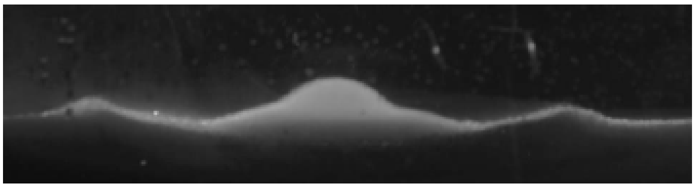

(b) A small dome composed of moving grains within the previously formed cavity.

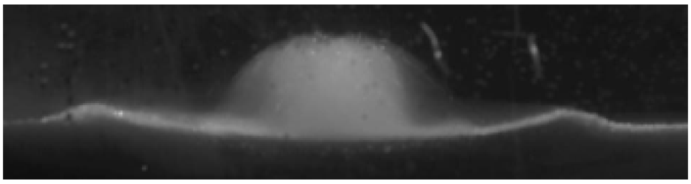

(c) A larger dome.

Figure 2.8: External observation of the formation of the fluidisation area

(Zoueshtiagh & Merlen, 2007)

The configuration types of the domes can be seen in figure 2.9. Zoueshtiagh and Merlen (2007) assumed that the formation of multiple domes was due to bubbling fluidisation. This is a stage observed in the fluidisation process when bubbles form within the granular bed and begin to rise to the surface. It occurs when the velocity of the injected fluid exceeds the minimum fluidisation velocity (see section 2.4.3). However, bubbling fluidisation is a stage mostly observed in granular beds that were fluidised by a gaseous fluid.

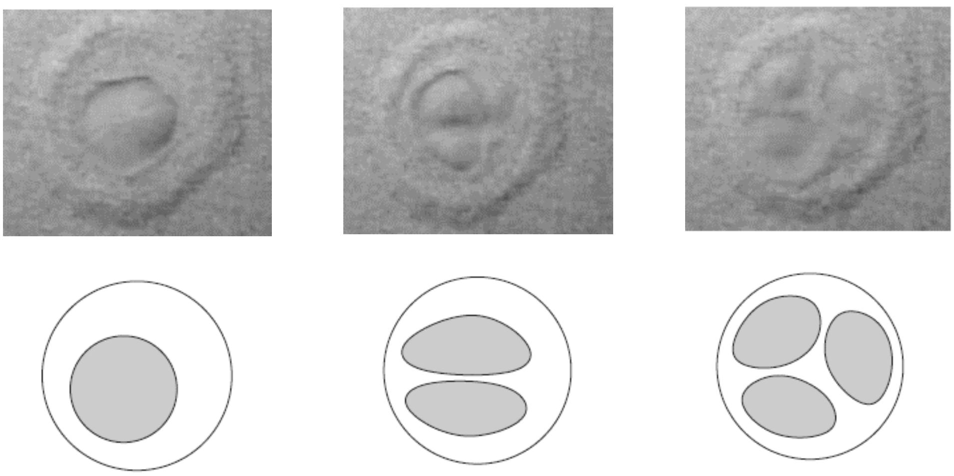

Figure 2.9: Dome configurations during the fluidisation process

(Zoueshtiagh & Merlen, 2007)

Experiments conducted by Philippe and Badiane (2013) (setup described in section 2.4.1.4) made it possible to observe the fluidisation process from within the granular bed. This was advantageous since the development of unbound fluidisation could be analysed in greater detail. As the flow rate was gradually increased, Philippe and Badiane (2013) also observed three stages that led to fluidisation of the entire bed. The three stages were:

- ***Static regime***

  In this regime the granular bed remained stationary except for a "small expansion at initial pressurisation"(Philippe & Badiane, 2013).

- ***Cavity regime***

  Development of a cavity of fluidised grains above the injection hole was the distinctive feature of this regime. The cavity was confined and did not extend to the bed surface and it was reported that, in this regime only grains within the cavity were in motion.

- ***Chimney regime***

  Increasing the flow rate beyond the cavity regime resulted in the fluidisation area being extended towards the surface of the bed, thus, giving an appearance of a chimney of fluidized grains. It was also noticed that a steady state of this system was obtained by a upward movement of grains carried by the flow in the centre of the chimney and the downward movement of an outer "avalanche that continuously refuelled the system"(Philippe & Badiane, 2013).

Images of the three regimes are given in Figure 2.10. In this figure image 2.10a, 2.10e and 2.10i shows the static, cavity and chimney regime respectively. Images to the right are manipulated pictures (using an image processing program) that show areas where particles are in motion for each of the three stages. For example, pictures 2.10b and 12.0c are manipulated images of 2.10a. The last column of images on the right of figure 2.10 gives the height of the respective fluidised regimes.

Philippe and Badiane (2013) used the images to differentiate between the cavity and chimney regime by simply observing the height of the fluidised zone and the depth of the stationary bed above the cavity as seen in figure 2.10g. Another difference between the two regimes as pointed out by Philippe and Badiane (2013) was the location of the movement of the particles. In the case of the cavity regime, the movement of grains only occurred inside the cavity while in the chimney regime particle outside the chimney were in motion. Evidence of the latter is shown in figure 2.8j by the large blurred area that surrounds the chimney.

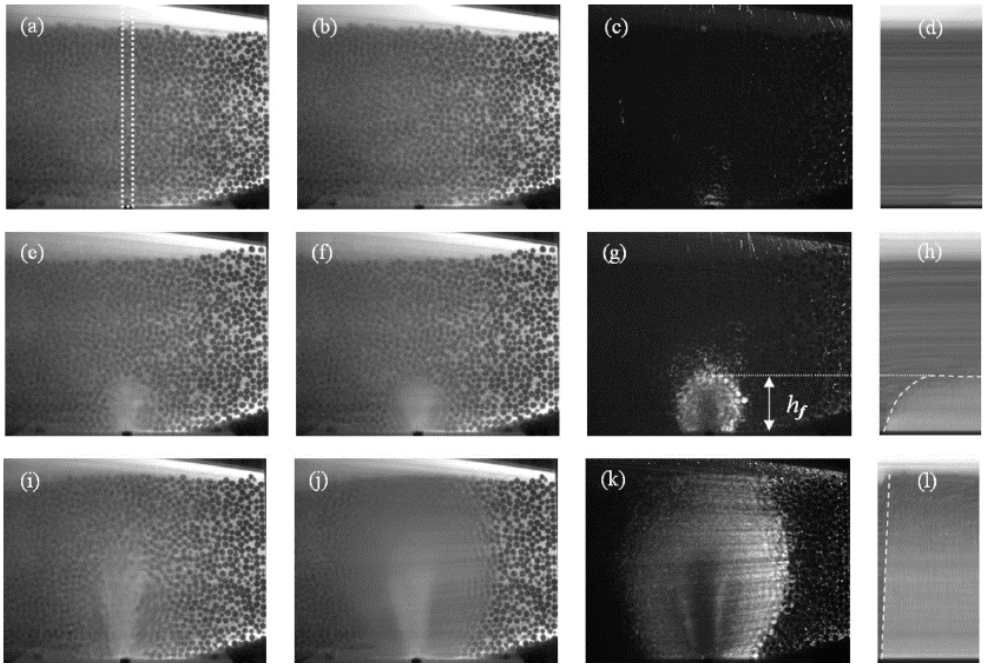

Figure 2.10: Observed formation of the fluidised area from within the granular bed
(Philippe & Badiane, 2013)

Van Zyl et al. (2013) made observations of the mechanism of fluidisation, by cutting a 6 mm diameter tube along the longitudinal axis and placing it against a transparent tank wall. Increasing flow rates of 130, 220 and 320 l/h were passed through the pipe, which was positioned below a fully saturated bed of glass beads. Fluidisation occurred within seconds and stabilised as the waters jets were introduced into the bed. Three distinct zones were noticed within the fluidised area. They were termed the fluidised, mobile bed and static bed zones. The shape, size and motion of the particles inside the zones were recorded using transparent tracing papers. Figure 2.11 shows an example of a traced drawing. The arrows in the figure show the observed direction of flow of the fluid and particles. As reported by van Zyl et al. (2013), a description of the fluidised, mobile bed and static zones is given below.

- ***Fluidised zone***

  The fluidised zone occurred at the centre. It stretched vertically up from the orifice to the roof of the cavity, where it terminated in a vortex movement. The width of the zone remained roughly constant. It was observed that this zone was made up of high velocity, upward flowing fluid that contained particles of the granular bed. The size and shape of the zone was stable, however the terminating vortex at the head moved side to side in an erratic fashion. The flow patterns at the head were also unstable, this sometimes resulted in the formation of a double vortex, where one vortex moved in a clockwise direction and the other in an anti-clockwise direction (see figure 2.11b).

  Furthermore, the fluidised zone increased with increasing flow rate until it broke the bed surface, resulting in piping. This finding was consistent with the observations made in the third regime by Zoueshtiagh and Merlen (2007) and perhaps the temporary double and triple dome configuration they witnessed just before the fluidised area broke the bed surface was a result of the vortices and not bubbling fluidisation.

- ***Mobile bed zone***

The fluidised zone was surrounded by a mobile bed zone. The latter was described as being a layer of packed granular material (no visible gaps) that "moved steadily from above the fluidised zone towards the orifice" (van Zyl et al., 2013). Particles within the zone were picked up at the mouth of the orifice by the fluid in the fluidised zone and deposited outwards at the terminating head(s). The area of the mobile bed zone was larger than that of fluidised zone. The observed motion of the mobile bed here agreed with the observations made in the chimney region by Philippe and Badiane (2013). Thus, it confirmed Zoueshtiagh and Merlen's (2007) speculation that a recirculating motion of the granular material occurred within the fluidised area.

- ***Static bed zone***

This zone occurred outside the mobile bed zone, which was the remaining portion of the granular bed. The granular particle in this zone "remained stationary and unaffected by the water jet" (van Zyl et al., 2013).

It was pointed out that the growth of the fluidised area seemed to be sensitive to the initial packing conditions of the granular material since significant differences were noticed in the sizes and shape of the fluidised and mobile bed zone. Additionally, van Zyl et al. (2013) acknowledged that the Perspex tank wall may have influenced the fluidisation mechanism but assumed that it did not significantly change the soil-leak interaction.

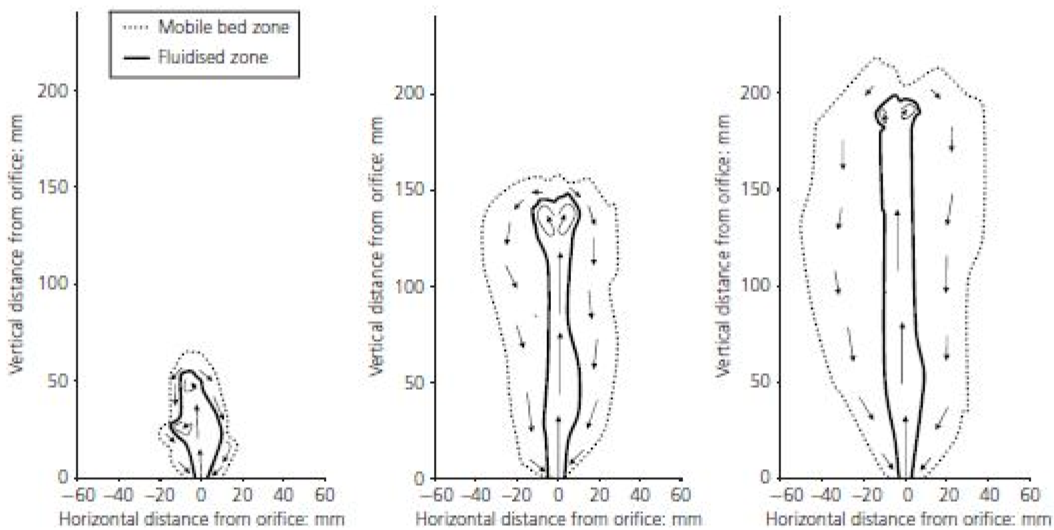

(a) Fluidisation at 130 l/h (b) Fluidisation at 220 l/h (c) Fluidisation at 320 l/h

Figure 2.11: Tracing of the geometry of a fluidised cavity

(van Zyl et al., 2013)

2.4.3 Minimum fluidising velocity

Initiation of fluidisation in a porous media as defined by Leva (1959) occurs when the granular particles are subjected to an upward fluid flow that creates a drag force sufficient to support the weight of the particles. Beyond this point the particles that once formed a fixed porous bed becomes suspended. The measure of the jet velocity at this instance is known as the minimum fluidising velocity. At the point of minimum fluidisation the upward acting pressure (pressure drop per length) balances the buoyant weight of the material, which can be expressed as follows (Niven & Khalili, 1998):

$$\frac{\Delta P}{L} = (1 - \phi)(\rho_s - \rho_f)g \qquad (12)$$

Where: ρ_s is the particle density (kg/m^3)

By equating equation (12) with the Ergun equation (11) and ignoring kinetic energy losses, Leva (1959) determined the minimum fluidisation velocity shown in equation (13). However, this derivation has limitations since it is only valid for particle fluidisation with a Re < 20 and for sands with a particle size < 0.6 mm (Niven & Khalili, 1998).

$$U_{mf(v)} = \frac{d_p^2 g(\rho_s - \rho_f)}{150\mu} - \frac{\varphi_s^2 \phi^3}{1 - \phi} \qquad (13)$$

In sands where particles are greater than 0.6 mm the kinetic energy losses cannot be neglected (Niven & Khalili, 1998). Wen and Yu (1966) considered this and by directly equating (11) and (12) they obtained a quadratic equation with only one positive solution, shown below. This formula was called the turbulent minimum superficial fluidisation velocity ($U_{mf(T)}$).

$$U_{mf(T)} = \frac{1}{\rho_f D_p}\left\{-33.7\mu + \sqrt{[33.7\mu]^2 + 0.0408\rho_f d_p^3(\rho_s - \rho_f)g}\right\} \qquad (14)$$

It must be noted that the equations derived above where based on a one dimensional fluidisation configuration i.e. an evenly distributed source, flowing in an upward direction beneath a bed of solid particles confined by lateral boundaries. Weisman et al. (1988) found through an experimental study that the minimum superficial fluidisation velocity of a horizontal jet in an unbound domain compared favourably with the velocities calculated using equation (14). For an initial bed depth of 25.4 cm and 42 cm, it was found that $U_{mf(T)}$ was 0.039 cm/s and 0.048 cm/s respectively. Using equation (14) the $U_{mf(T)}$ was 0.044 cm/s.

In addition Niven and Khalili (1998) explained that for fluidisation to occur from a buried pipe an energy input greater than that required for fluidisation might be necessary. The additional energy is required to overcome the interlocking of soil particles located downstream of the orifice and can be referred to as a fluidisation activation energy.

2.4.4 Influence of orifice size on the fluidisation process

Zoueshtiagh and Merlen (2007) and van Zyl et al. (2013) examined the influence of orifice size on fluidisation by varying the orifice size at a constant flow rate. The orifice diameters used when combining the studies were 2, 3, 4 , 8, 15 and 35mm. Van Zyl et al. (2013) observed the shape of the excess pressure profile, the maximum excess pressure and the height of the fluidised zone and concluded that the fluidisation zone remained unchanged for the different orifice sizes. Zoueshtiagh and Merlen (2007) measured the radius of the fluidised area at increasing heights using a specially constructed vernier calipers. A plot of radius against height gave insight into the shape and size of the fluidised areas for the various orifice diameters. The findings of this analysis agreed with the conclusions made by Van Zyl et al. (2013). It is important to note that in these experiments a circular orifice openings was used.

Alsaydalani (2010) used a rectangular orifice opening to investigate the effect of orifice size on fluidisation. Two types of granular materials were used; both had an average particle size of 0.9 mm. One soil type was used for a 0.234 mm and 0.336 mm width orifice opening and the other soil type was used for a 0.62 mm and 0.92 mm width orifice. Excess water pressures at the centre of the orifice were measured at fixed heights above the orifice for each experiment. Observations of the pressure profiles at a constant flow rate revealed that the excess pressure along the centre of the orifice for the various heights was not affected by the size of the orifice for both soil types.

Therefore, the results of the studies presented above showed strong evidence that orifice size did not influence fluidisation. This conclusion was found to be true for circular and rectangular shaped orifices, which can be seen as idealised circular and longitudinal pipe cracks respectively.

2.4.5 Relation between the jet flow rate and the fluidised zone

Van Zyl et al. (2013) and Alsaydalani and Clayton (2014) observed similar trends regarding the relation between the flow rate of the injected water jet and fluidisation. In general, both studies found that the size of the fluidised zone and the magnitude of the average excess water pressure within the fluidised zone increased when the flow rate was increased.

An example of the observed trends is shown in figure 2.12 where excess water pressure at heights above the orifice for increasing flow rates was plotted. One can notice that, for all flow rates, excess water pressure in the bed initially increased with height until a maximum pressure was reached. In the case of the low flow rates (220 and 350 l/h) the maximum excess water pressures were roughly 1.3 and 2.1 kPa respectively whilst the high flow rates (785 and 850 l/h) produced a maximum excess water pressure of roughly 2.3 and 2.4 kPa respectively. The height above the orifice at which the maximum excess pressure occurred inside the fluidised zone also increased as flow rate increased, thus signifying vertical growth of the fluidised zone. According to van Zyl et al. (2013) the point of maximum excess pressure occurred near the head of the fluidised zone. Finally, for all flow rates at heights above maximum excess pressure, the excess pressure in the soil began to drop in a linear fashion until it reached zero at the bed surface. According to Alsaydalani and Clayton (2014) flow through the bed In this region obeyed Darcy's law.

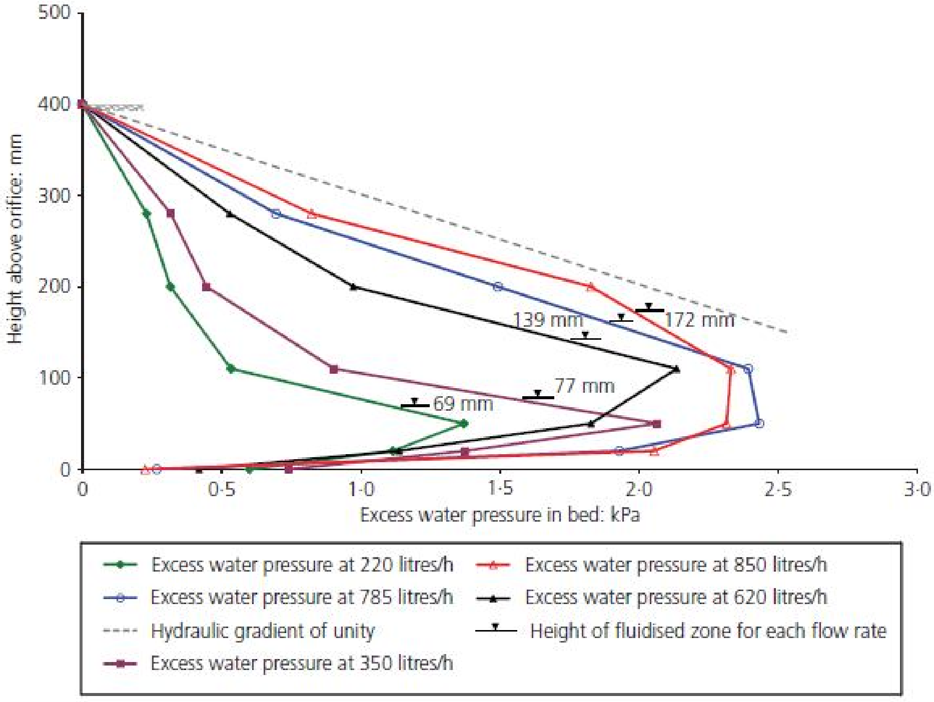

Figure 2.12: Change in pressure inside the fluidised zone with increasing flow rate

(van Zyl et al., 2013)

2.4.6 Energy losses during a pipe leak

Walski et al. (2006) investigated two elements that were responsible for energy losses during a pipe leak. The first was head loss due to flow through the orifice (h_o) and the second was head loss due to flow through the soil (h_s) medium surrounding the pipe leak. The orifice equation (2) was used to determine h_o and Darcy's law (4) was used to compute h_s. In this study a theoretical model was developed to understand conditions related to which head loss dominated. Essentially, the model, shown in equation (15) measured the ratio of orifice head loss over soil head loss and the result was a dimensionless "orifice/soil number" or OS number.

Walski et al. (2006) obtained a wide range of OS numbers by conducting experiments using two types of apparatus, which they called "tall" and "short". Both were cylindrical in shape and allowed water to be injected through an orifice located at the base. The tall apparatus was 1.85 m high with a narrow cross sectional diameter of 10.2 cm, while the short apparatus was 0.48 m high with a relatively wide cross sectional diameter of 38 cm.

$$OS = \frac{h_o}{h_s} = \frac{KA_sQ}{2gL}\left(\frac{1}{C_dA_o}\right)^2 \quad (15)$$

Where: A_s is the area of flow in the soil (m^2)

A pressure plate was placed just above the orifice in the tall apparatus to prevent the bed from expanding and fluidising. The range of OS numbers were found by varying the orifice size, flow rates and applied pressure using both experimental setups. Results showed that for an OS equal to 1, both head loss due to the orifice and the soil contribute equally and both are important. When OS is small (<0.1) the soil losses are dominant and for a large (>10) OS the orifice losses are dominant. Walski et al. (2006) concluded that in "most real world cases the OS number will be large" suggesting that losses due to orifice flow will dominate and losses due to flow through the soil will be small or negligible.

Clayton and van Zyl (2007) conveyed concerns with the above approach of simply combining the orifice equation with Darcy's law of soil seepage to explain the system. One of the main reasons for their concern was the incompatibility of the velocities between the orifice flow and seepage flow. In soil seepage, the velocity head component is very small and is safe to ignore but the orifice equation predicts relatively high velocity heads for the flow of fluid existing the orifice (Clayton & van Zyl, 2007).

Furthermore, Clayton and van Zyl (2007) stated that the soil-leak interaction downstream of the orifice is very complex and it is likely that a non-linear relationship exists between head loss and flow. The latter was explained to occur due to interaction of soil particles with the orifice, deformation of the soil geometry (in seepage theory the geometry of the bed remains unchanged) and fluidisation of the soil bed, all of which is a result of the high velocity of the water jet that leaves the orifice. Studies presented in section 2.4.2 gave observations of flow from an orifice into a granular medium that supported Clayton & van Zyl's (2007) explanation of the complexity of the soil-leak interaction downstream of the orifice. The most notable observation was the formation of a highly turbulent fluidised zone that occurred inside the soil bed without breaking the bed surface; this strongly implied a non-linear relationship between head loss and flow in that region.

In a fluidisation example with, a circular orifice of 2mm diameter, the flow rate of 850 l/h and the granular bed with a porosity of 30 %. Van Zyl et al. (2013) showed that, by simplifying the shape of the fluidised area to half a sphere only 3 % of the available energy in the above example is dissipated in the static bed. This implies that 97 % of the available energy is lost at the orifice and in the fluidised and mobile bed zones. The contribution of energy loss at the orifice depends on the value of C_v. Van Zyl et al. (2013) considered a C_v where energy loss was the highest, i.e. a C_v of 0.62. This resulted in 38 % of the available energy being lost at the orifice and a significant 59 % in the fluidised and mobile bed zones. The latter will increase proportionately should C_v approach 1 (where no energy is lost at the orifice). This example illustrated that the fluidised and mobile bed zones of the fluidised area can be viewed as an energy dissipation mechanism that prevented the leak from reaching the soil surface.

2.4.7 Effect of soil characteristics on internal fluidisation

2.4.7.1. Influence of bed height

According to Zoueshtiagh and Merlen (2007), the flow rate required to achieve local fluidisation within a bed is influenced by the bed height. Alsaydalani (2010) used the bed heights of 150, 220 and 300 mm to determine the effect of the bed height on fluidisation. The results of the experiment revealed that fluidisation occurred at a flow rate of 450, 730 and 1042 l/h for the respective bed heights in ascending order. The excess pore pressure measured within the beds at the point of fluidisation were 2.63, 4.78 and 7.38 kPa respectively. It was established that as the bed height increased, the flow rate and pressure required to initiate fluidisation also increased, thus a direct relationship existed. Alsaydalani (2010) explained that this relationship exists due to the increase in bulk weight of the bed.

Ma (2011) used a horizontal jet to determine the influence of the bed height. Results from the experiment indicated that as the height of the bed increased, higher flow rates were also required for the fluidisation zone to occur. This finding was believed to occur due to increasing in-situ pressures that acted against the flow of the injected fluid. At deeper depths the horizontal pressures that acted upon the particles in the region of the orifice increased, thus higher flow rates and pressures were required to initiate the fluidisation process.

Therefore, based on the result from the studies presented above it is clear that bed height influences the onset of fluidisation. Higher flow rates and pressures were required to fluidise beds with increasing height. However, studies that have investigated the effects of bed height regarding the behaviour of pressure and velocity distributions within the fluidised zone are scarce. Thus, further research is required to fully understand the effect that bed height has on the fluidisation zone.

2.4.7.2. Influence of particle size

Alsaydalani (2010) examined the effect of particle size on fluidisation of an upright vertical water jet. Granular material that had a particle size of 0.9 and 1.6 mm was used. Results from this experiment indicated that, at any given flow rate the bed consisting of finer grained material experienced larger excess pressures compared to the bed with larger grained particles. A significant difference in pressures were observed for the different particle sizes. For instance, at a flow rate of 812 l/h the excess pore pressure downstream of the orifice for the 0.9 mm granular material was 7 kPa while the 1.6 mm granular material produced an excess pore pressure of only 2.7 kPa. Considering the results from the experiment it was concluded that when the flow rate is increased, beds with finer grained material will experience significantly larger excess pore pressures in the fluidised zones compared to beds made of larger particles, and the build-up of pore water pressure within the bed would lead to a higher chance for fluidisation to occur. Thus, beds consisting of finer particles will fluidise at lower flow rates (i.e. more quickly) compared to the beds of larger particles.

Ma (2011) used a horizontal water jet submerged into two granular beds that contained particles sizes that ranged from 90-150 μm in one bed and 600 μm-1.18 mm in the other. Results from this experiment indicated that fluidisation occurred at a lower flow rate in the granular material with finer particles and at a higher flow rate in the granular material with coarser particles. This result was consistent with the findings of Alsaydalani (2010). Another trend Ma (2011) observed was that, with same amount of increase in flow rate the dimensional increase in the geometry of the fluidised zone in the bed that contained the finer particles was greater compared to the larger particles. Ma (2011) explained this trend using Stoke's law, a mathematical expression that describes the drag force required to move a sphere through a viscous fluid at a specific velocity. This expression is shown in equation (16).

$$F_d = 6\pi\mu r_s V \tag{16}$$

Where: F_d is the drag force (N)
r_s is the radius of the sphere (m)
V is the velocity of the sphere relative to the fluid (m/s)

Given Stoke's law, one can notice that the drag force generated on a sphere, which acts against the particles' weight is directly proportional to its diameter. Therefore, according to Ma (2011), in the bed consisting of smaller particles a lower flow rate resulted in formation of the fluidised zone, since smaller drag forces were required to suspend the particles. Additionally, increasing the flow rate further caused a larger dimensional increase in the geometry of the fluidised area.

2.4.7.3. Influence of particle shape

The term "sphericity" is used to describe the shape of a particle. It is a measure of how closely an object resembles a sphere. Wadell (1933) illustrated that the measurement of sphericity of a particle can be determined by taking the cubic root of the ratio of the volume of the particle to the volume of its circumscribing sphere. Many other approaches have been recognised that estimates the sphericity of particles. For example, Krumbein (1941) suggested that particles can be assumed to be tri-axial ellipsoidal (where the lengths of all three semi-principal axes are different) in shape and can exhibit three diameters, namely largest, intermediate and shortest. To measure the sphericity of a particle, Krumbein (1941) used the three diameters to form equation (17) that was named "Krumbein's Operational Sphericity" (φ_0).

$$\varphi_0 = \sqrt[3]{\frac{I_p \times S_p}{L_p^2}} \tag{17}$$

Where: L_p is the longest diameter (m)
I_p is the intermediate diameter (m)
S_p is the shortest diameter (m)

Sneed and Folk (1958) used the same parameters described in equation (17) to develop equation (18), which measured the sphericity of a particle in motion within a fluid. They developed this equation based on the premise that a tri-axial ellipsoidal particle in motion has a tendency to align the side with the largest surface area perpendicular to the flow direction.

$$\varphi_p = \sqrt[3]{\frac{S_p^2}{L_p \times I_p}} \tag{18}$$

In a more recent study, Abbireddy et al. (2009) showed (by also adopting the premise that, particles were tri-axial (scalene) ellipsoidal) that sphericity can be determined using equation (19). They named this expression the "Scalene Ellipsoid Equivalent Sphericity (SEES)"

$$\mathrm{SEES} = \frac{\mathrm{S_p}}{\mathrm{L_p}} = \frac{(\mathrm{w}/\mathrm{n}\rho_s)\left(6/\pi\,\mathrm{L_p I_p}\right)}{\mathrm{L_p}} \tag{19}$$

Where: W is the mass of the sample (kg)

n is the number of particles in the sample determined by counting or using appropriate software

The magnitude of S_p can be measured directly from images (i.e. the smallest diameter of an inscribed circle drawn on each elevation plane when the particle is dropped onto a level surface) or indirectly by determining L_p and I_p. Abbireddy et al. (2009) assumed that L_p and I_p was the respective measure of the diameter of a circumscribed and the largest inscribed circle, using an image of the top view of the dropped particle.

To find the influence of particle shape on fluidisation, Alsaydalani (2010) used particles that had a measured sphericity of 0.55 and 0.92. A sphericity reading of one indicates a sphere shaped particle and a reading close to zero denotes a particle shape that is not a sphere. The results from the experiment described an indirect relationship between particle shape and excess pore pressure. It was determined that for any given flow rate the excess pore pressure measured in the granular bed with particles of lower sphericity was always larger than the particles with higher sphericity. It was also observed that fluidisation of the bed containing the low spherical particles occurred at a flow rate of approximately 1050 l/h at a corresponding excess pore pressure of 7.52 kPa whereas, a relatively larger flow rate of almost 1500 l/h, corresponding to an excess pore pressure of 8.8 kPa was required to fluidise the bed consisting of particles with higher sphericity.

According to Alsaydalani (2010) the build-up of pore water pressure in bed with less spherical particles lead to fluidisation at a lower flow rate. Furthermore, Alsaydalani and Clayton (2014) explained that these results are consistent with the Ergun model (described in section 2.3.2). The model assumes that the upward drag on each particle is a function of its maximum projected area and since objects with low sphericity have a low buoyant weight they will require reduced pressures for fluidization. It is clear from these findings that particle shape had a significant effect on fluidisation, however more research is required before firm conclusions can be drawn.

2.4.7.4. Influence of particle roughness

In the field of chemical engineering, Eastwood et al. (1969) found that beds consisting of particles with increasing roughness had "considerably" higher voids ratios (defined as the ratio of the volume of voids to the total volume of solids). The voids ratio (e) is related to porosity (ϕ) as shown in equation (20). One can notice from equation (20) that as the voids ratio increase the porosity will also increase but will always remain lower.

$$\phi = \frac{e}{1+e} \tag{20}$$

Where: e is the voids ratio

Therefore, beds with increasing particle roughness will have a larger voids and porosity ratios. The Ergun equation (11) predicts that packed beds with higher porosity should have lower pressure drops; however, this was not observed in studies conducted by Crawford and Plumb (1986) and Jordi et al. (1990). They found that particle surface roughness increased the pressure drop during both viscous and inertial flow regimes. Therefore, a level of inconsistency exists in the literature regarding the effects of particle roughness on fluidising a granular bed, which emphasises the need for further investigation.

2.5 Measurement of pore pressure and fluid velocity in the fluidised region

2.5.1 Experimental setup and equipment

The apparatus described in this section was developed by Bailey (2015) and was used in the current study. The setup is shown in figures 2.13 and 2.14. It consisted of a transparent glass tank suspended above the ground by a metal stand. Two orifice openings where installed on the base of the tank to create vertical upright water jets. One orifice was located at the centre while the other was located against one of the tanks wall. The orifice against the tank wall allowed for visualisation of the fluidised regions. The orifice openings were used independently i.e. water was supplied to a single orifice opening at time while the other was shut off using a ball valve. The inlet water supply consisted of a flow meter attached to a Sensus data logger via a cable sensor. This configuration allowed for setting and visual monitoring of preselected supply flow rates.

Above the tank was a Pitot tube positioning system, which made use of steel rulers to accurately position straight and L-type Pitot tubes inside the tank. The Pitot tube are shown in figure 3.3. Using a flexible transparent pipe, the Pitot tube being used was connected to a glass sight tube from which the excess pore pressure and velocity readings within the fluidised bed were read and recorded.

The fluidised area within the bed was assumed to be symmetric about any vertical plane that passed through the centre of the orifice, which allowed for the Pitot tubes to be strategically placed at points along a single plane (for example Y-Z) to obtain the “Pressure”, “Stagnation pressure” and “Dynamic pressure”. Bailey (2015) defined “pressure” as the increase in bed pressure created by internal fluidisation. To obtain this reading the L-type Pitot tube was utilized and inserted into the bed from the surface in a manner were the tip of the Pitot tube was perpendicular to the flow at the point of interest. The “Stagnation pressure” at the same point was measured by positioning the tip of the L-type Pitot tube parallel but opposite to the direction of fluid flow and was defined as the sum of “Pressure” and “Dynamic pressure”. The “Dynamic pressure” component resembled the velocity head created due to the fluid flow and was determined by subtracting “Pressure” from the “Stagnation pressure”. The straight Pitot tube was used to obtain “Stagnation pressure” in the vertical direction for each point.

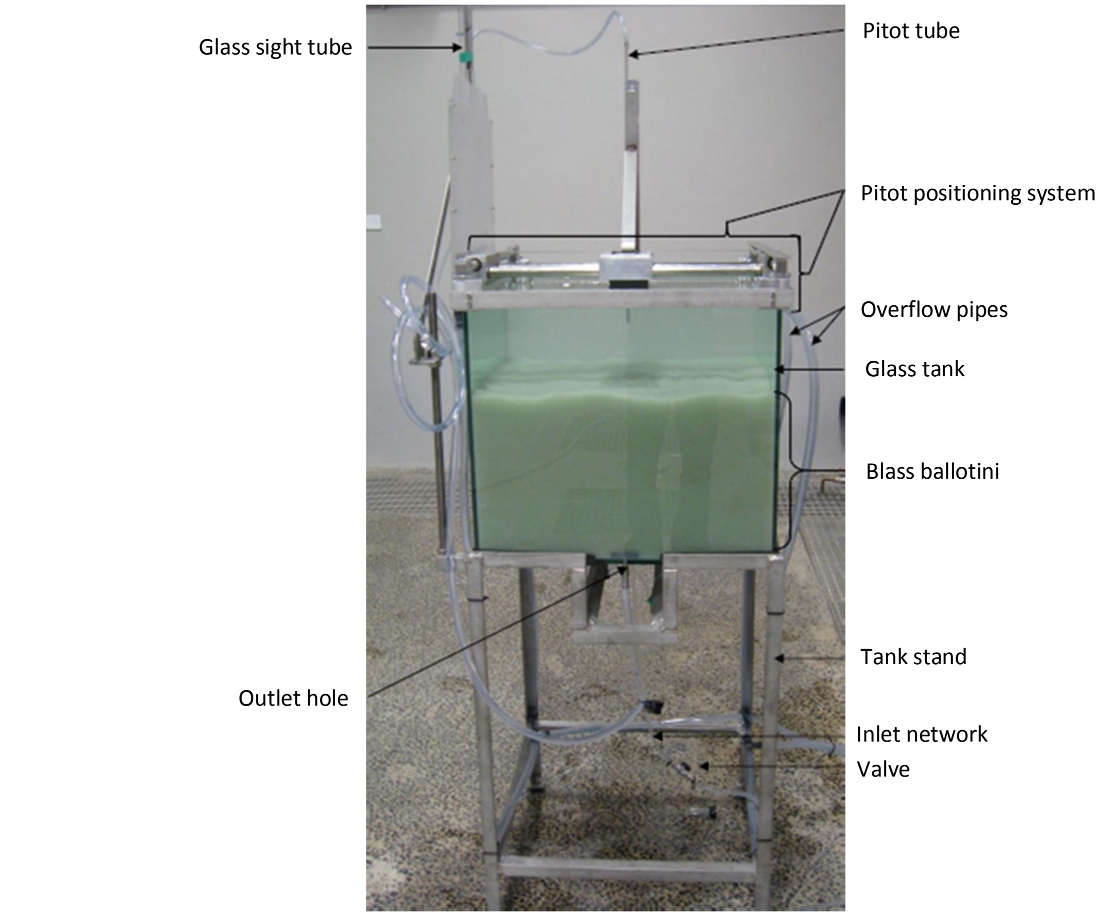

Figure 2.13: Side view of the complete experimental setup

(Bailey, 2015)

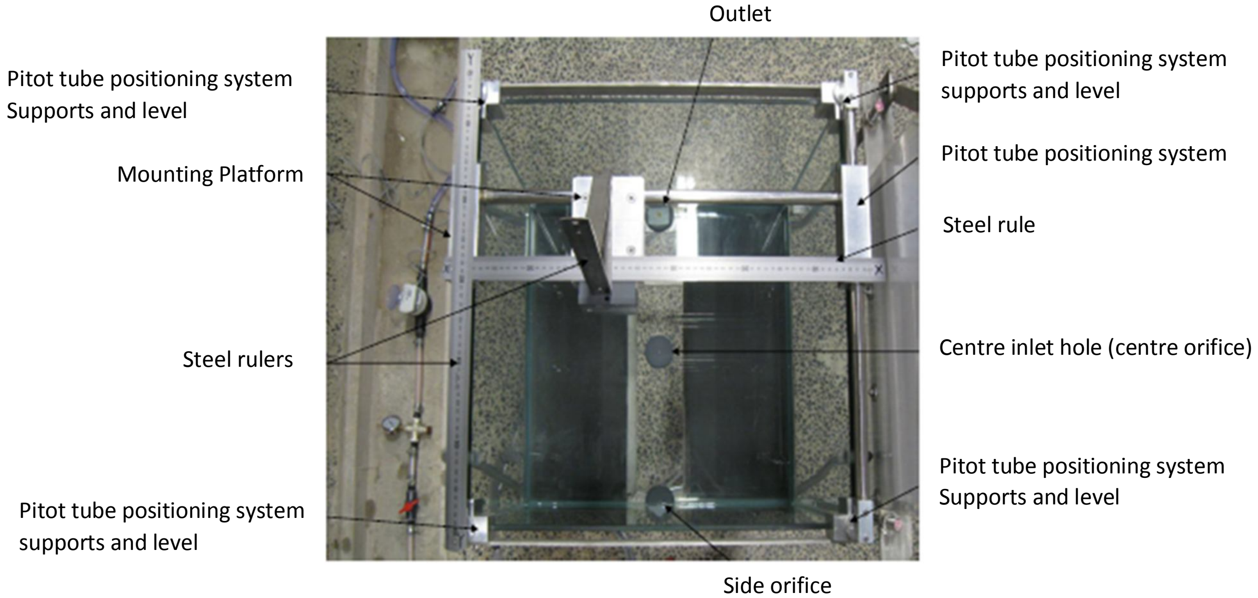

Figure 2.14: Top view of the experimental setup

(Bailey, 2015)

In an effort to test the experimental setup, Bailey (2015) simulated a 2 l/min leak below a 300 mm high bed consisting of ballotini with particle diameters ranging from 0.6 to 0.85 mm. In this test the centre orifice was used.

The various pressures described above were obtained for each point on a grid in the Y-Z plane. The points were spaced 10 mm apart reaching a maximum Z and Y value of 200 and 60 mm respectively. From the measured data the pressure, velocity in the horizontal and vertical directions and energy head at each point were determined and plotted on graphs for analysis. Some of the findings are given below.

2.5.2 Vertical velocity distribution

A graph of the vertical velocity component (i.e. flow perpendicular to the base and toward the bed surface) for horizontal slices above the orifice is shown in Figure 2.16 is. The most significant trend in this plot is the relatively large change in velocity from points directly above the orifice to Y= 60 mm for the horizontal slices Z= 0, 10 and 20 mm. In these slices the velocity in the vertical direction was highest at points above the orifice and began to rapidly decrease with increasing distance away from the orifice. By inserting the tip of the straight type Pitot tube along the centre line of the orifice, Bailey (2015) heard a scrambling noise, which he assumed to be the height of the fluidised zone. Using this technique he established that the fluidised zone reached a height of 27 mm. The vertical velocity profiles for slices beyond this height can be seen to have relatively lower velocities with very little change. Therefore, according to figure 2.16 the velocity of the fluid in the vertical direction was the highest in the vicinity of the fluidised zone with the highest recorded velocity occurring just above the orifice.

Given that the area of the orifice and the flow rate of the fluid that was injected into the tank were known, Bailey (2015) calculated the velocity of the injected fluid using the orifice equation (2) and compared it to the vertical reading obtained immediately above the orifice. These two velocities should have a relatively low difference between them if not no difference. The calculated velocity was 4.716 m/s and the measured velocity as shown in figure 2.16 was 5.253 m/s, resulting in a difference of 0.537 m/s.

Bailey (2015) suggested two likely events that may have occurred that could explain the disparity between the velocities. The first was an impinging action that may have occurred when the ballotini particles from the mobile bed zone entered into the fluidised zone. This action could have caused the jet area to constrict, which resulted in an increase in the flow velocity at the measured point. The second possibility was the influence of friction on the flow passing through the orifice. The flow through the orifice was described to behave similar to that of steady fully developed pipe flow i.e. due to the effect of friction from the inner wall of the supply pipe and the influence of the granular particles immediately downstream of the orifice, the velocity distribution of the flow exiting the orifice followed a parabolic shape with velocity being the highest at the centre of the orifice and lowest in regions close to the orifice edges. In this experiment the straight Pitot tube was positioned close to the centre of the orifice and would have registered a reading reflective of the maximum velocity. Thus, the measured velocity was higher than the calculated velocity since when computing the velocity using equation (2) the result was average velocity across the orifice opening.

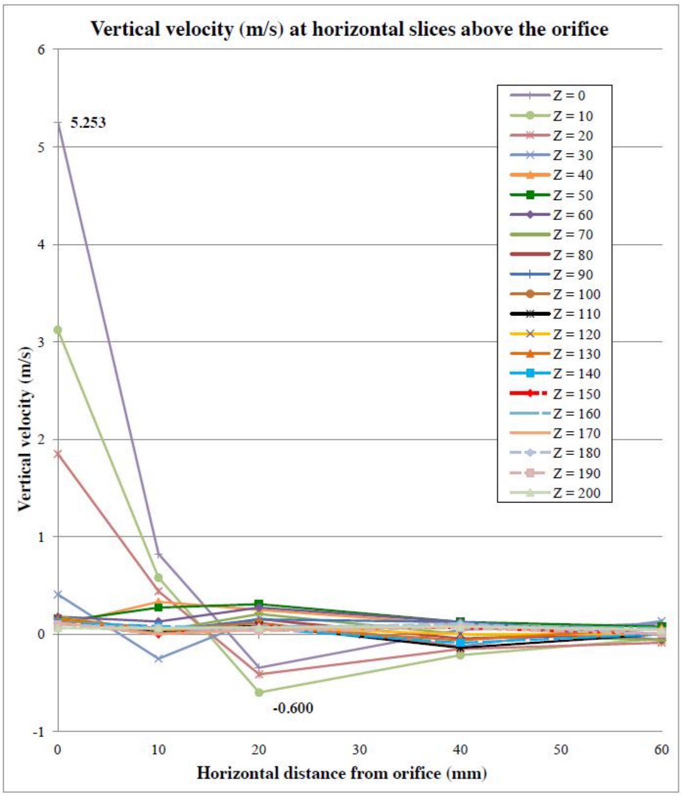

Figure 2.15: Vertical velocity component along horizontal slices

(Bailey, 2015)

2.5.3 Pressure distribution

Figure 2.17 is a plot of the pressure head along vertical slices with the exception of the slices Y= 30 and 50 mm. Measurements along those Y values were not taken during the experiment. From the graph one can notice that the maximum pressures occurred at the points (0,20), (10,20), (20,10), (40,10) and (60,20) where the co-ordinates follow the sequence (Y-slice, Z-height). However, Bailey (2015) pointed out that the maximum pressures in the fluidised bed may not have occurred at the exact heights as indicated by the graph; they may have occurred at a distance above or below but close to where the readings were taken. Nevertheless, it was noted that the pressure profiles in the graph gave a general trend where the maximum pressures close to the orifice occurred at a height Z= 20 mm and then dropped to Z= 10 mm at a small distance away from the orifice in the horizontal direction. The influence of the tank base was said to be the cause of drop in pressure. The region away from the orifice can be assumed to be in the mobile bed zone and as described in section 2.4.2, in this region the flow circulates towards the orifice from the head of fluidised zone. Thus, when the flow approached the orifice it was hindered by the base of the tank, which essentially created a localised pressure increase that resulted in the maximum pressures along those vertical slices occurring closer to the tank base as indicate in the graph (Bailey, 2015).

The bright green line in the graph illustrates a linear trend for the readings above the elevation Z= 100 mm, which implied that seepage in that region followed Darcy law (equation (4)) and flow was possibly laminar. Points below Z= 100 mm can be seen to deviate away from the green line for all vertical slices with the exception of Y= 60 mm. This outcome suggested that flow in this region was non-linear and could be turbulent (Bailey, 2015).

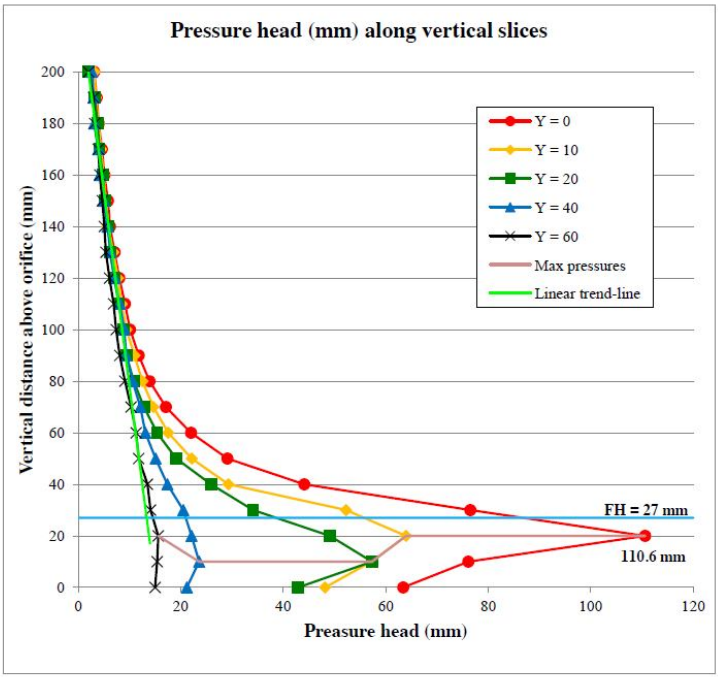

Figure 2.16: Pressure head along vertical slices

(Bailey, 2015)

2.5.4 Energy distribution

The energy measured at each point shown in figure 2.18 was effectively the energy above the constant static energy (energy before fluidisation) in the bed and was calculated by summing the pressure and velocity heads. Figure 2.18 is a plot of the energy distribution for vertical slices. The graph clearly shows that the energy in the fluidised bed was largest immediately downstream of the orifice and decreased rapidly as distance from the orifice increased in both the vertical and horizontal direction. This finding has great significance in understanding leak development since it shows that, of the available energy a relatively large amount was confined to a particular region in the fluidised zone, which possibly prevented the leak from growing toward the surface (Bailey, 2015).

Furthermore, Bailey (2015) pointed out that the drop in energy at the point (10,10) could be a measurement error or at that particular point the tip of the Pitot tube was inserted in an area where flow was drawn toward the orifice (likely in the mobile bed zone), which created a suction at the tip of the Pitot tube and therefore resulted a lower energy reading.

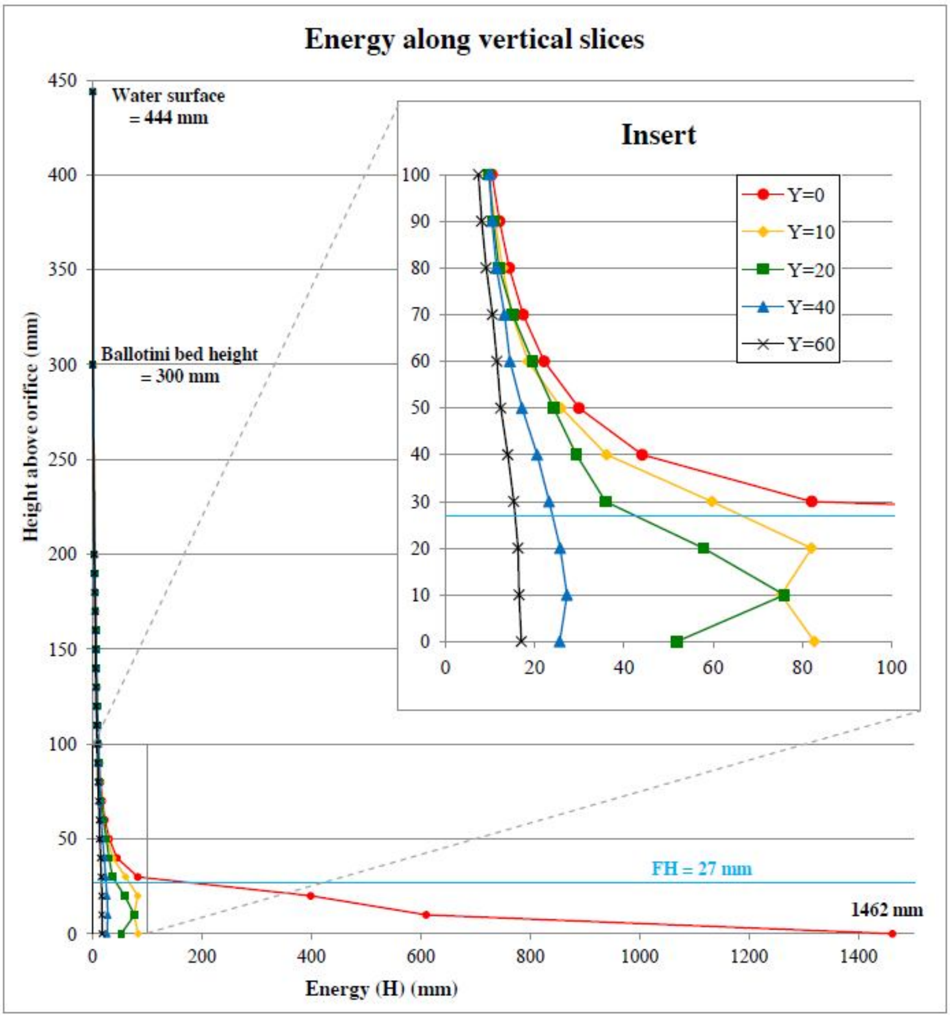

Figure 2.17: Energy along vertical slices

(Bailey, 2015)

2.6 Computational Fluid Dynamics (CFD)

"Computational Fluid Dynamics (CFD) techniques are derived from the equations governing the fluid flow in the form of partial differential equations representing the conservation of mass, momentum and energy. The partial differential equations are reduced to an approximate and equivalent set of algebraic equations, which are solved numerically to give the flow field at discrete points in the calculation domain"(Chiesa et al., 2005).

Mulitiphase flow as seen in fluidised bed manifests into mathematical complexities of non-linear equations with a result of difficult numerical solutions. With increasing computational capabilities, researchers have turned to CFD as a tool to model the complex interactions.

CFD modelling of fluidised beds has developed into a standard tool for single-phase flows while it is still in the development stage for multiphase systems. There are two different approached namely Lagrangian and Eulerian, which have been used to apply CFD modelling to Mulitiphase fluidised beds.

The Lagrangian model is fundamentally a Discrete Element Modelling (DEM) numerical methodology. It functions by consistently considering and recording the motion of each particle in the flow. This technique however seems less widely used than the Eulerian model approach. On the other hand Eulerian modelling simulates both phases making use of Eulerian-type conservation equations. In this approach the phases are seen as continuous and interpenetrating.

Interestingly, CFD models makes use of correlations which are still empirical. As a result model validation processes are required. One method of validation is to compare experimental measurements with results from the computational models. This process highlights the need for experimental data, an aspect which the current study addresses but within its limited scope.

2.7 Conclusions drawn from literature review

A literature review geared at understanding the fluidisation mechanism which occurs outside a pipe leak was conducted. Based on the material reviewed the following conclusions can be drawn.

- The terms “fluidisation”, “piping” and “liquefaction” which are used in various disciplines describe a common process where a porous medium is transformed to behave in a fluid-like manner, usually, when acted upon by a strong fluid force. Experiments conducted in various studies indicated that a granular bed can become fluidised when a fluid with a high velocity (turbulent flow regime) was allowed to pass through it. In general, the fluidisation phenomenon was found to be a scarcely researched topic, which is of most interest to the field of chemical engineering field where the focus has been mainly on granular beds that were fluidised by gas in a confined cylinder. Limited research was found that investigated the interaction of liquid-solid fluidisation of granular material.

- Although limited, various experimental setups and techniques have been developed that investigated fluidisation from a point source (orifice) in an unbound domain. This setup closely resembled the flow mechanism which occurred during a pipe leak.

- Observations of the fluidisation process strongly indicated that the formation of a fluidised area induced by a vertical water jet below a bed of granular material occurred in stages as the flow rate was gradually increased. The stages of development resulting in full fluidisation of the bed included the static, cavity and chimney regimes. Full fluidisation of the bed occurred when significantly high flow rates were applied, which caused the cavity regime to lengthen and break the bed surface, resulting in piping. Furthermore, fluidisation in the chimney and cavity regimes was shown to inhabit three distinct zones, namely the fluidised, mobile bed and static bed zones. An analysis of the movement of fluid and particles within the fluidised and mobile bed zones suggested that a recirculation pattern existed. Finally, it was shown that a vortex movement of the fluid occurred occasionally at the head of the fluidised zone.

- Mathematical models that took into account the properties and behaviour of the fluidising fluid and granular bed were developed to predict the onset of fluidisation. Equation (12) was developed to predict the pressure at the onset of the fluidisation process, while Leva (1959) and Wen and Yu (1966) developed equations (13) and (14) respectively to estimate the minimum fluidising velocity.

- Results from experiments, which investigated the influence of orifice size on fluidisation indicated that the geometry of the fluidised zone and the static pressure along its centre were not influenced by orifice size.

- Studies have discovered that the fluidised area is sensitive to the flow rate of the fluidising jet. Increasing the flow rate of the jet resulted in an increase in the size (mostly in height) of the fluidised zone and the magnitude of the average excess pressure within. An assessment of the distribution of excess pressure indicated that pressure increased as height above the orifice increased, with the maximum pressure occurring in the vicinity of the head of the fluidised zone. At heights beyond this point the excess pressure began to steady decrease in a linear fashion until it reached zero at the bed surface. Seepage in this region was pointed out to follow Darcy's law.

- Two elements were responsible for energy losses in the fluidisation mechanism initiated from a point source. The first was head loss due to flow through the orifice and the second was head loss due to flow through the soil. It was established that Darcy's law cannot be used to determine head loss in the fluidised area mainly due to the turbulent nature of the seepage flow and the changing geometry of the soil bed. Additionally, van Zyl et al. (2013) illustrated in a study that the majority of the available energy in the fluidisation mechanism described above was lost at the orifice and in the fluidised and mobile bed zones, which prevented the leak from reaching the bed surface and potentially being discovered.

- Particles size was found to have a significant effect on fluidisation induced by a horizontal and an upright vertical water jet. In both mechanisms, it was established that that beds consisting of finer grained material experienced higher excess pore pressures, which led to fluidisation at lower flow rates compared to beds with larger particles. Moreover, Ma (2011) observed that for the same incremental increase in flow rate the dimensional increase of the fluidised area was greater in the bed consisting of smaller particles.

- The sphericity of granular particles was also found to have a substantial influence on the initiation of the fluidisation phenomenon. Experiments conducted by Alsaydalani (2010) indicated that the build-up of pore water pressure increased with decreasing form, which led to the onset of fluidisation at lower flow rates.

- Investigation regarding the effects of particle roughness revealed inconsistency between theory and experimental findings. Eastwood et al. (1969) found that beds containing particles with high surface roughness had more voids. According to the Ergun equation (11) increasing the number of voids in a bed should result in low pressure drops. However, Crawford and

Plumb (1986) and Jordi et al. (1990) observed that this was not the case since large pressure drops were noticed.

- Studies centred on understanding the influence of bed height on fluidisation discovered that as bed height increased the flow rate and pressure required to initiate fluidisation also increased.

3. Method of investigation

Experiments aimed at meeting the objectives of this study were carried out in a laboratory. This chapter gives a detailed description of the existing experimental setup, modifications that were made to the setup, properties of the soil materials used and the techniques and methodologies that were employed to conduct the experiments. A description of all the experiments that were performed is also given.

3.1 Detailed description of the experimental equipment

The experimental apparatus that was used during this study was shown in figures 2.13 and 2.14 in section 2.5.1. In essence the apparatus can be broken down into of four main components, namely: the glass tank, water supply line, Pitot tubes connected to a piezometer and a Pitot tube positioning system located on top of the tank. A description of each of these components including its function is given below.

3.1.1 Glass tank

A transparent glass tank with the dimensions 566 x 566 x 488 mm was used to house the granular bed required to simulate soil-leak interaction. The tank was suspended above the ground by a metal stand. Two orifice openings where installed on the base of the tank to create vertical upright water jets. One orifice was located at the centre (referred to as the centre orifice) while the other was located against one of the tanks wall (referred to as the side orifice), see figure 3.1. They had an internal diameter of 3 and 2.8 mm respectively. The orifice openings were used independently i.e. water was supplied to a single orifice opening at time while the other was shut off using a ball valve. The tank as mentioned by Bailey (2015) was “sized to ensure that tank wall had little or possibly no disturbance on the flow of water through the granular bed”.

Pipes connected to four holes, drilled at equal distance from the top of the tank formed an overflow system to prevent water from over toping during experimentation. Finally, an outlet orifice lined with a piece of gauze was installed at the bottom of the tank for drainage purposes. The gauze prevent the granular material from entering the drainage system.

Figure 3.1: Plan view of the experimental setup showing components of the tank

3.1.2 Water supply line

A schematic drawing showing the components of the water supply line is given in figure 3.2. The apparatus was designed to receive water directly from the laboratory's water supply system, which in turn drew water from the municipal water distribution system. Pressure fluctuations that would have come from the in the water supply line were removed by throttling the flow. It was assumed that the remaining fluctuations did not affect the fluidisation zone, since it was found to be stable once established.

A ball valve (No. 1) connected to the 20 mm line served as the main control to open and shut off the supply of water to the apparatus, while another ball valve (No. 2) installed on the 6 mm pipe was used to make fine adjustments when setting the flow to the desired rate.

The flow meter installed on the line was an Aquadis+ Composite type manufactured by Itron. A Senus Cosmos Data logger was connected to the flow meter using a V2 type Itron Cyble sensor for the ease of visually setting and monitoring the flow rate, see figure 3.3.The accuracy of the flow meter was tested in the lab by measuring the volume of water contained in one minute time intervals to obtain a flow rate. This was then compared to the readings of flow registered on the data logger which was set to roughly 2 l/min. This exercise was repeated five times. The results illustrated that the water meter was over reading by approximately 1.9 % on average. According to the Itron accuracy curve (Itron, 2014) for this meter, an overestimation error of roughly 2 % is expected for the flows rates that were test. Therefore, the meter was registering flows within its manufactured capability.

Bailey (2015) found that when there was no flow through the water supply line, it often got blocked by ballotini particles, which fell through the orifice. This was the case for both the side and centre orifice. Thus, a Pressure Reducing Valve (PRV) combined with a pressure gauge was installed to prevent damage to the 6 mm pipe during high pressure build-up, which occurred when the supply line was blocked.

To unblock the water supply pipe at the beginning of an experiment, Bailey (2015) inserted a thin wire of sufficient length through the orifice from the bed surface while the flow in the supply line was turned on. The thin wire loosened the tightly packed ballotini particles that caused the blockage, which subsequently allowed the water to flow through the orifice and eventually clear the pipe. Once the bed was fluidised the pipe remained unblocked.

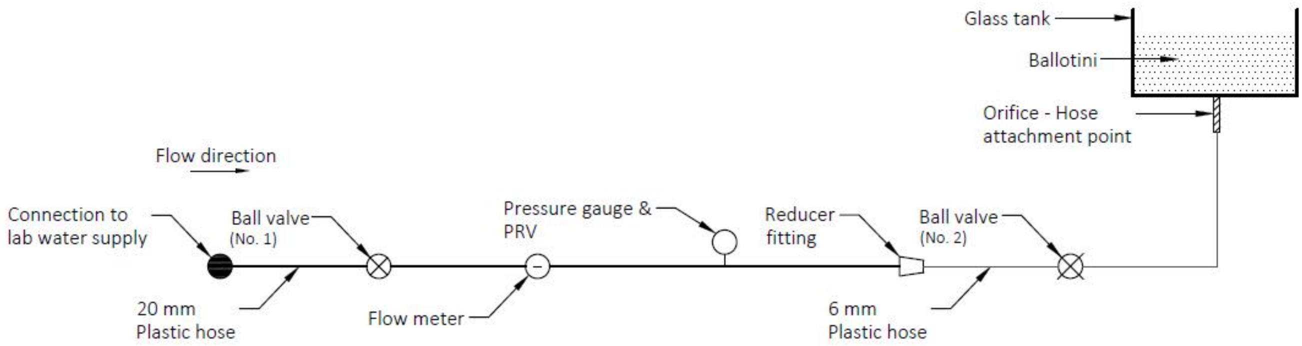

Figure 3.2: A schematic drawing of the water supply system.

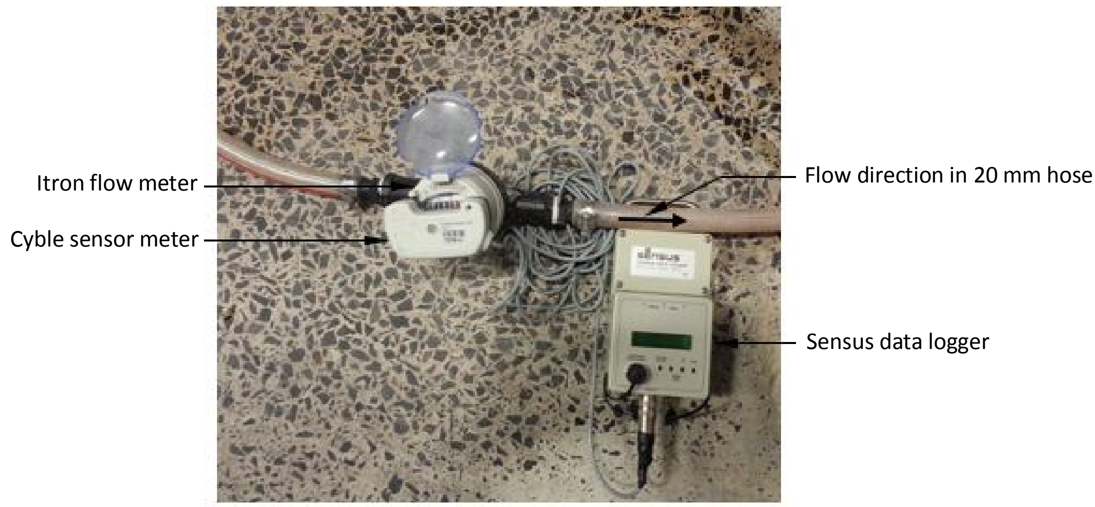

Figure 3.3: Devices used to set and monitor the flow rate during experimentation.

3.1.3 Pitot tubes

Bailey (2015) developed straight and L-type Pitot tubes to obtain measurements of velocity, pore pressure and energy head in the fluidised bed. The Pitot tubes, shown in figure 3.4, were manufactured at the University of Cape Town and consisted of a tapered glass tube fitted into a stainless steel tube (outer diameter of 6.35 mm and inner diameter (ID) of 4.57 mm), using a PVC collar.

Bailey (2015) used silicone gel when fitting the glass tube into the PVC collar to create a water tight seal. The tapered end of the glass tube (i.e. the tip of the Pitot tube) reduced to an ID of 0.5 mm, which was small enough to prevent a significant portion of the granular medium from entering the Pitot tube and large enough to obtain readings with the least amount of disturbance to the flow dynamics in the bed. A flexible transparent pipe connected the Pitot tube being used to a glass sight tube/piezometer from which readings within the fluidised bed were read and recorded.

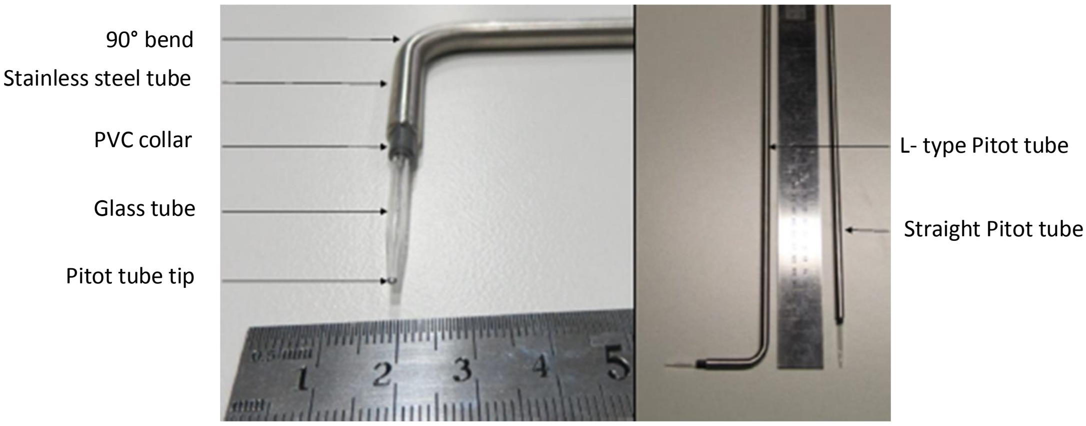

Figure 3.4: L and straight type Pitot tubes

(Bailey, 2015)

3.1.4 Pitot tube positing system

The main function of the Pitot tube positioning system was to secure and allow three dimensional positioning of the Pitot tube inside the tank. The components of the Pitot tube positioning system including arrows that show the movement of the system are given in figure 3.5.

The system operated by first fastening the Pitot tube in the bracing unit then, by moving the mounting platform the Pitot tube tip could be positioned in the X and Y plane. Thereafter, the Pitot tube is loosened in the bracing unit and is raised or lowered by hand to the required height in the Z plane. The Pitot tube is refastened in the bracing unit once its tip is at the desired point. Using steel rulers the Pitot tube positioning system is calibrated to allow positioning of the Pitot tube at known points in the tank.

Needle bearings (eight in total) fixed on the ends of the two aluminium blocks and on each corner of the square mounting platform were in contact with primary and secondary tubes respectively to facilitate movement in the X and Y plane.

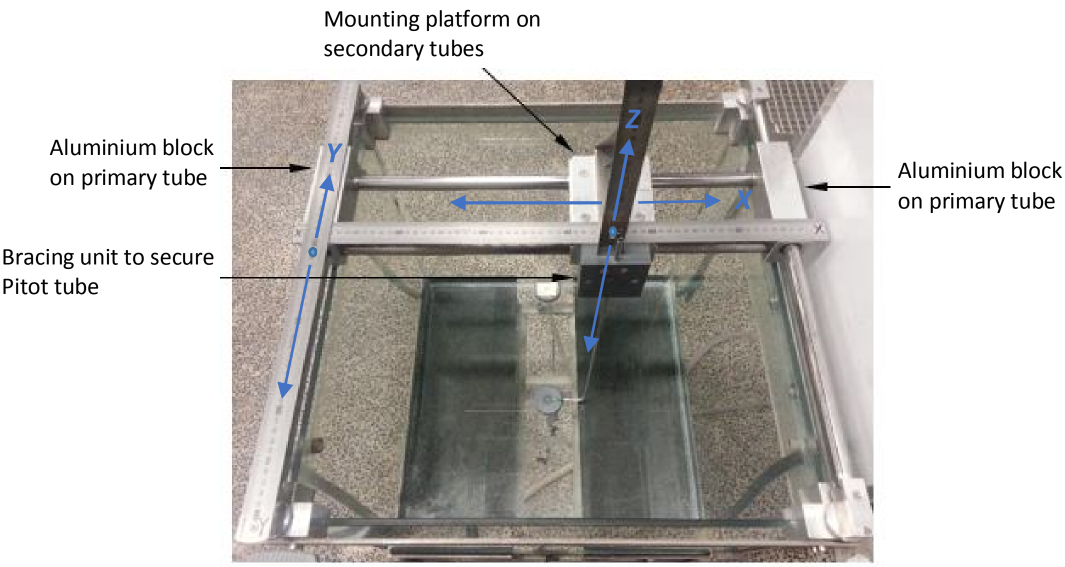

Figure 3.5: Image showing components of the Pitot positioning system including arrows that illustrate movement of the system.

3.2 Modifications made to the experimental setup

Various difficulties were anticipated with the experimental setup, which were addressed before any tests were conducted. This was based on Bailey's (2015) assessment on the functioning of the experimental setup. Details of the modifications that were made are given below.

3.2.1 Blockage of the water supply system

To avoid the tedious and time consuming task of locating the orifice with the narrow wire and to prevent disturbing the packing arrangement of the granular bed, the water supply system was modified to solve the blockage problem. The modifications to the inlet system, illustrated with a photograph in figure 3.6, was the addition of a short perpendicular branch that ended with a ball valve (No. 3) and another ball valve (No. 4) downstream of the new branch. The branch was added approximately 160 mm from the attachment point between the orifice and the supply hose.

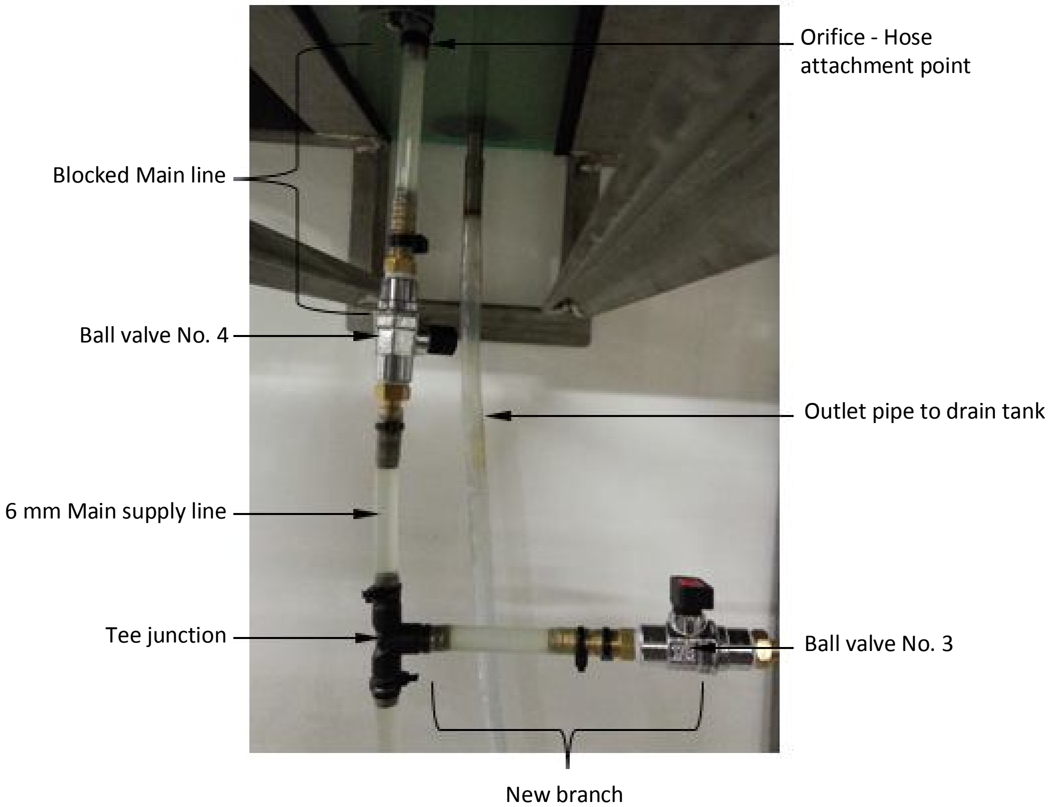

Figure 3.6: Photograph of the modifications made to unblock the water supply system.

In operation, valve No. 2 was left closed while valve No. 4 was opened. This allowed the ballotini particles in the pipe to fall and when they reached the tee junction, the main line was tilted such that the particles filled the new branch. When the main line was sufficiently emptied of the particles, valve No. 2 was opened for water to flow into the bed. Once there was flow in the main supply line, the free end of the branch containing the ballotini particles was lifted to allow the particles to slowly re-enter the main line so that it could be deposited into the bed.

A final modification made to the water supply line was the replacement of the ball valve (No. 1) on the 20 mm line with a needle valve, see figure 3.7. Needle valves are designed specifically to allow for precise and easy regulation of flow in systems that have relatively low flow rates. Thus, the needle valve was installed to take over the previous flow rate fine tuning function required of ball valve No. 2.

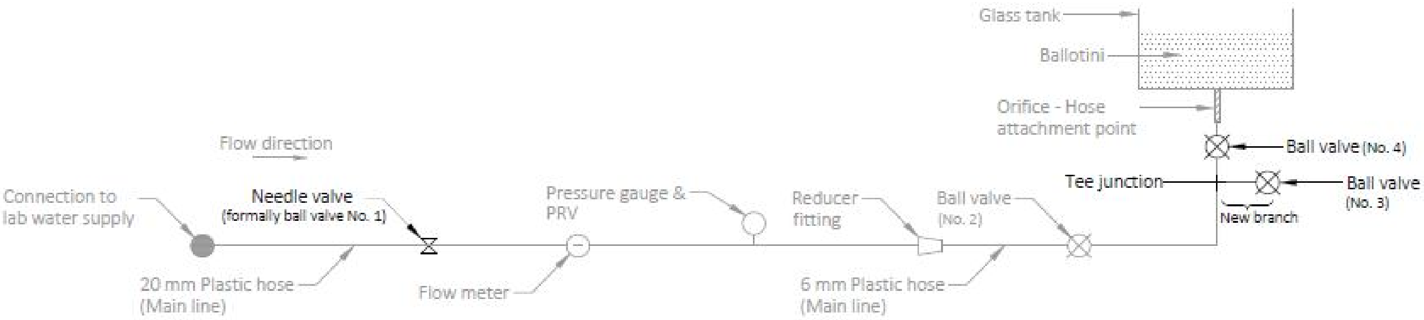

Figure 3.7: A Schematic drawing showing all modifications made to the water supply system.

3.2.2 Pitot tubes

During the current study, the glass tubes were found to be fragile and required great care to prevent the tips from breaking. The Pitot tubes were modified by replacing the glass tubes with hypodermic needles, as shown in figure 3.8.

The hypodermic needles were more durable and had a smaller wall thickness, which further reduced any disturbances the tip could have caused to the flow dynamics when taking readings. To increase the rigidity of the needles, the steel portion was cut to a length of 10 mm using power tools. The total length of the hypodermic needles (plastic fitting plus steel component) were 30 mm.

As shown in figure 3.9, the ID of the tip opening was roughly 0.60 mm after cutting and smoothening the exterior surface. Hypodermic needles with smaller ID's were tested but it was found that sight tube readings took in excess of 5 min to stabilise. Therefore, they were not practical to use during the experiments.

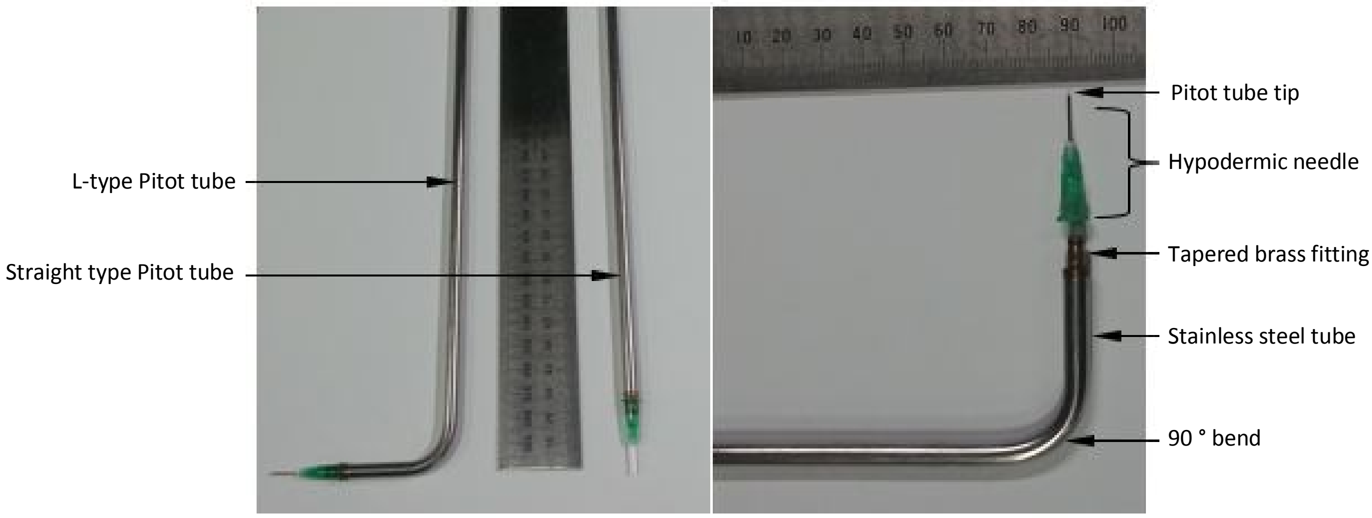

Figure 3.8: Modified straight and L- type Pitot tubes.

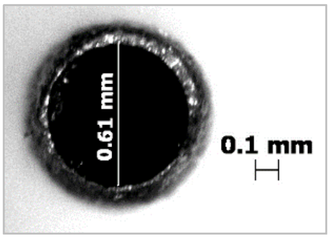

Figure 3.9: A microscopic view of the tip opening of a modified Pitot tube.

3.2.3 Pitot tube positioning system

The needle bearings located in the aluminium block and mounting platform are typically used for rotational movement around the longitudinal axis of a tube and not for sliding along the tubes exterior, as required. Thus, the needle bearings were not suited for its intended use, which impeded smooth functioning of the system. To improve the sliding ability of the positioning system whilst maintaining sufficient friction to prevent uncontrolled movement, the needle bearings were replaced with cylindrical bushes.

3.3 Soil properties

The experiments carried out during the course of this study were done using three types of ballotini material, named material A, B and C. In general, the ballotini materials served as an idealised soil medium made up of glass particles that were roughly uniform in size and shape. It was used in the experiments instead of actual bedding material to prevent the results from being influenced by particle size, shape (angularity) and roughness. A microscopic image showing the shape and smooth surface of the ballotini material is presented in figure 3.10.

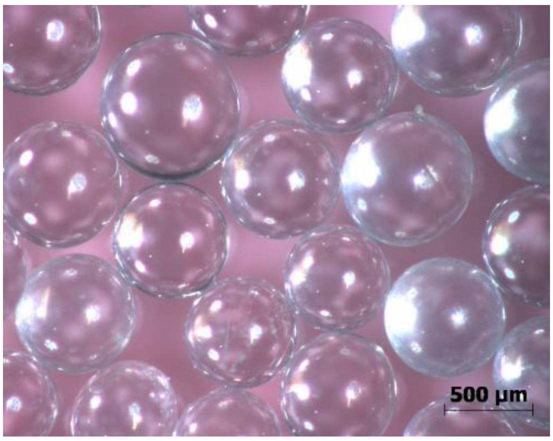

Figure 3.10: A typical microscopic view of the ballotini material used in the experiments.

Material type A was used in previous experiments conducted by Bailey (2015) and van Zyl et al. (2013). Therefore, it was adopted as the standard material type and was used in the flow rate and bed height sensitivity tests. The distribution of particle sizes was the main difference between material type A, B and C, which made the materials suitable to use when studying the influence of particle size on the fluidisation mechanism. The particle distribution for each material is shown in figure 3.11.

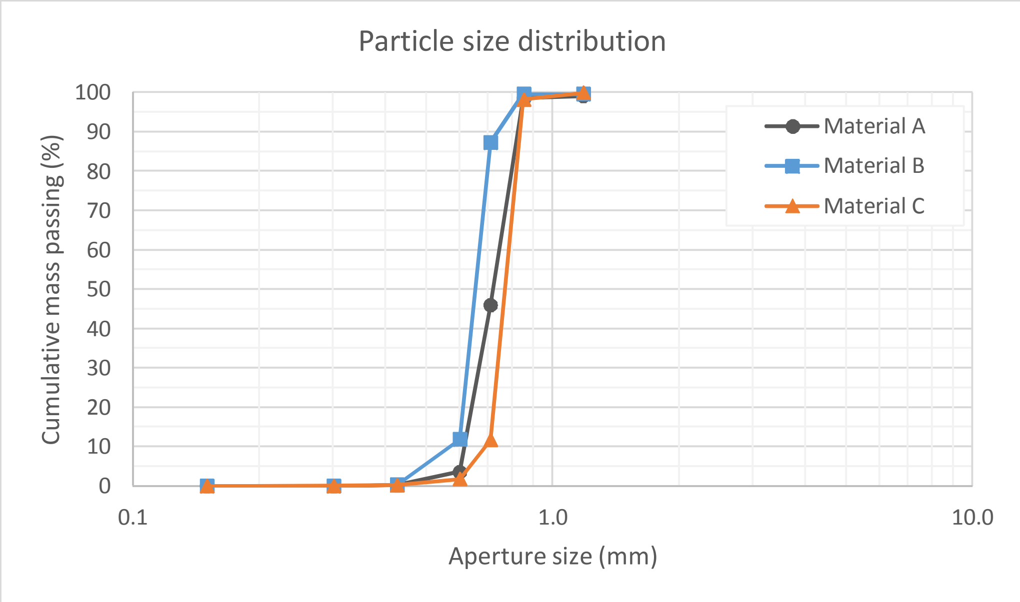

Figure 3.11: Particle size distribution of the ballotini materials used in the experiments.

Material type A had 96 % of its particles between the sieve range 0.600 and 0.850 mm, material type B had 87 % of its particles between the range 0.425 and 0.710 mm and material type C had 88 % of its particles between the range 0.710 and 0.850 mm. Other essential properties (including densities, void ratio, porosity ratio and permeability) of the ballotini materials are given in tables 3.1 and 3.2. The material properties were determined according to the standards set by the American Society for testing and Materials (ASTM) in the geotechnical laboratory at UCT. Particle sphericity was based on the SEES method described in section 2.4.7.3. The magnitude of L and S required to measure sphericity were determined using image analysis. The raw data from the geotechnical tests are given in appendix A.

Table 3.1: Particle density, permeability and sphericity of the ballotini materials used in the experiments.

Ballotini material	Particle density (Mg/m^3)	Permeability (cm/s)	Particle sphericity
A	2.484	0.288	0.98
B	2.481	0.288	0.98
C	2.477	0.411	0.98

Table 3.2: Maximum and minimum densities, void ratios and porosity ratios of the ballotini materials used in the experiments.

Ballotini material	Dry density (ρ)			Void ratio (e)			Porosity ratio (ϕ)		
	ρ_{max} (Mg/m^3)	ρ_{min} (Mg/m^3)	$\rho_{max} - \rho_{min}$ (Mg/m^3)	e_{max}	e_{min}	$e_{max} - e_{min}$	ϕ_{max}	ϕ_{min}	$\phi_{max} - \phi_{min}$
A	1.624	1.502	0.122	0.618	0.496	0.121	0.382	0.332	0.050
B	1.646	1.491	0.155	0.629	0.476	0.153	0.386	0.323	0.064
C	1.657	1.490	0.167	0.631	0.467	0.164	0.387	0.318	0.069

3.4 Experiment preparation and procedures

The preparatory steps and procedures used when carrying out the experiments were based on those developed by Bailey (2015); however, the measurement process was modified to suit this study. In this section the methods used to complete a standard experiment is given.

3.4.1 Standard experiment preparations

The procedures and techniques that were used to prepare the granular bed and apparatus for experimentation are described in the subsections that follow.

3.4.1.1. Plane used to take measurements

It was assumed that the geometry of the fluidised region was symmetrical about any vertical plane that passed through the origin (centre of the orifice) and that fluid did not flow perpendicularly on this vertical plane. The latter was experimentally determined in the study done by Bailey (2015). Thus, if the fluidised region was bisected by any vertical plane through the origin, the two halves would have identical characteristics (including shape, pore pressure, fluid velocity and energy) at corresponding points. Therefore, measurements of pore pressure and velocity head were only necessary on half of a plane that bisected the fluidised region. Due to spatial limitations of the Pitot placement system, the optimal plane for carrying out the experiments was on the negative Y and positive Z plane. An illustration of the measuring plane is shown in figure 3.12.

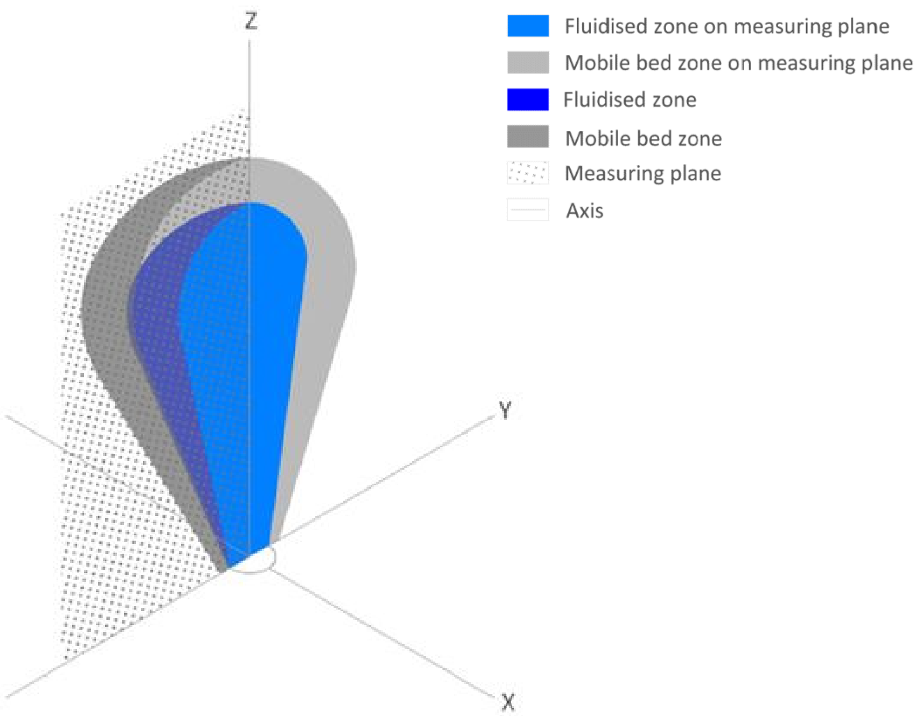

Figure 3.12: A schematic drawing of the fluidised region bisected by the measuring plane (-Y, Z).

3.4.1.2. Establishing datum co-ordinates for Pitot tubes

Determining the datum co-ordinates for both the straight and L-type Pitot tubes was a crucial step in achieving the ability to position the tip of the Pitot tubes at known points in the fluidised bed.

The centre orifice was used in the standard experiment. The centre point of the orifice was given the co-ordinates (0,0,0). This served as a reference point to which the Pitot tubes were calibrated.

The process of determining the datum co-ordinates was to position the tip of each Pitot tube at the reference point whilst the glass tank was empty. The readings on the X, Y and Z axis for the respective Pitot tubes were then recorded off the rulers to establish the datum co-ordinates. An example of this process is illustrated in figure 3.13. Two datum co-ordinates were required to conduct a standard experiment; they were as follows:

- The straight Pitot tube facing the negative Z axis to obtain the vertical velocity head readings.
- The L-type Pitot tube facing the negative X axis to obtain the surplus pore pressure head readings.

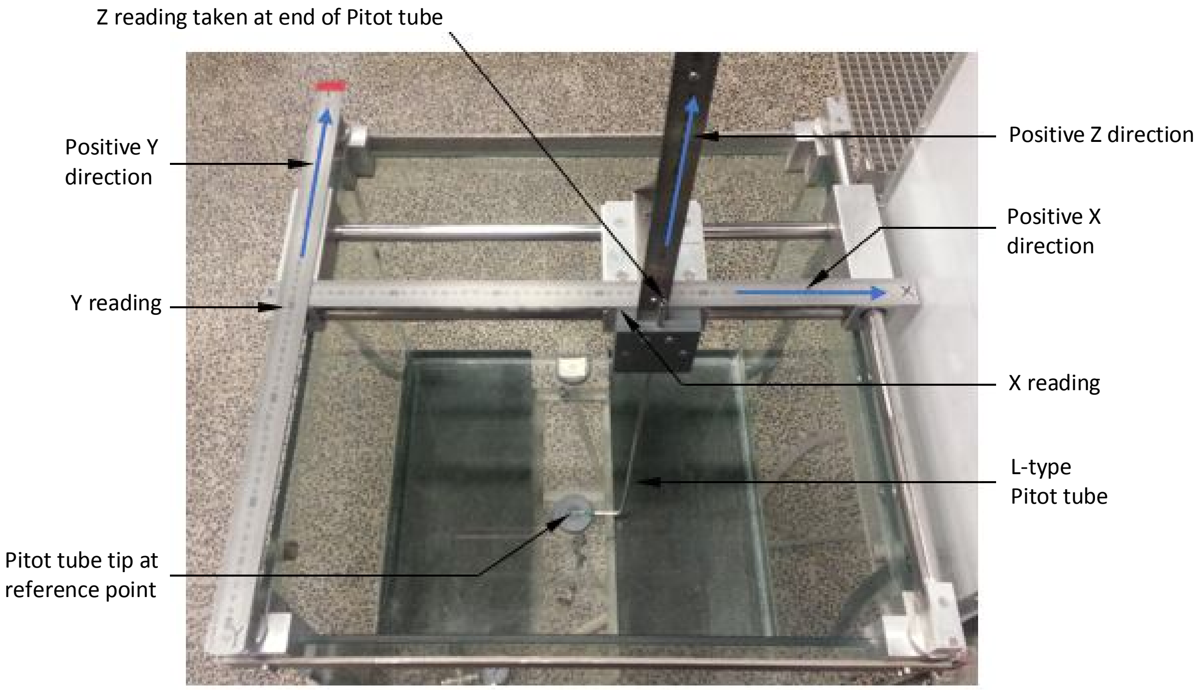

Figure 3.13: An illustration of how the datum co-ordinates were determined for the L-type Pitot tube facing the negative X direction.

During the course of the experimental phase there was need to compare readings taken at the side orifice and with the centre orifice. Hence the datum co-ordinates for the Pitot tubes at the side orifice was required. A process similar to the one described above was followed. The centre of the side orifice was made the reference point. However, due to spatial restrictions the Pitot positioning system could not align the straight Pitot tube directly above the side orifice reference point. The closest the tip could get was 7 mm away along the Y axis. Thus, datum co-ordinates for the Pitot tubes were determined at the side orifice for the point (Y= 7, Z= 0) and readings along the line Y=7 both orifices were compared.

It is important to mention that due to the tapering shape of the L- type Pitot tube (from steel tube to tip), the closest the tip could get to the reference points in the vertical direction was 2 mm above it. Therefore during the experiments, readings near the orifice using both the straight and L-type Pitot tubes were taken was at a height of 2 mm above and not at Z= 0 mm.

3.4.1.3. Bedding preparation

To obtain accurate and reliable results, the bed had to be prepared in a manner that was repeatable and with no air trapped between the particles. The following procedure was adopted:

- After closing the outlet, the tank was filled with water up to the overflow level.
- Using a scoop the moist ballotini was "rained" into the tank. Each scoop of ballotini was first submerged into the tank filled with water and then tilled such that the soil flowed over the longest edge of the scoop. This technique allowed the material to separate into individual particles and release the trapped air bubbles, which rose to the water surface.
- The soil was distributed in layers up to the required bed height to ensure uniform compression throughout the bed.
- Finally the bed surface was gently levelled using a ruler.

The bed was prepared daily at the start of an experiment and redone at the first signs of air bubbles during an experiment. The latter was observed when a submerged Pitot tube was removed from the bed creating a temporary channel, which was sufficient for air bubbles to flow through and reach the surface.

3.4.1.4. Priming the Pitot tubes

The following Pitot tube priming procedure was carried out before the prepared bed was fluidised:

- The Pitot tube together with its bracing unit was removed from the mounting platform.
- The Pitot tube was then detached from the flexible transparent hose that connected it to the sight tube.
- The free end of the flexible hose was raised and held parallel to the vertical sight tube.
- Using a squeeze bottle, de-aired water was injected into the open end of the hose until the maximum amount of water could be filled into the sight tube and hose.
- The water in the hose and sight glass was allowed to rest for a few seconds until all the air bubbles rose to the surface and burst.
- Keeping the flexible hose raised, the Pitot tube with its bracing unit was connected and then quickly lowered and attached to the mounting platform.
- The surplus water in the sight tube drained through the Pitot tube into the water layer above the bed surface until it finally stabilised.

- Any air bubbles that may have remained or formed in the hose was removed by tapping at its location and raising the hose so that the air bubbles would dislodge and rise until they reached the water surface in the sight tube.
- Finally, the stabilised water level reading in the sight tube was recorded after ensuring that the water in the tank was at the overflow level. This reading was a measure of the energy head in the tank under static conditions (i.e. before fluidisation) and regardless of the type of Pitot tube or its position in the tank this reading always remained constant. Therefore this reading was used as a datum for all measurements taken during the experimentation. From here on this reading will be referred to as the datum head.

3.4.2 Standard experiment procedures

Setting the flow rate to induce fluidisation in the bed marked the beginning of an experiment. Once this was achieved, the Pitot tubes were used to obtain surplus pressure and velocity head readings at various points within the bed. The methods that were used in carrying out these steps are described below.

3.4.2.1. Setting the flow rate

An important step before setting the flow rate was to ensure that all the air in the water supply line was removed. This step was done when the tank was filled with only water. The line was allowed to flow fully for a few seconds while ensuring that the only high point in the line was at the orifice attachment point.

The steps described below explains the procedure used to set the flow rate on a blocked main line:

- On the water supply line, valve no. 4 was opened whilst valve no. 2 was kept closed.
- The soil particles causing the blockage began to fall and when they reached the tee piece the main line was tilted to direct the soil particles into the branch.
- When the main line was free from the blockage, valve no. 2 was opened to allow water to flow into the bed.
- A few seconds later the free end of the branch containing the soil particles was raised. The soil in the branch slowly entered the main line and was deposited into the bed.
- Using the needle valve on the main line and the Senus Cosmos Data logger, which was attached to the flow meter, the flow rate in the supply line was fine-tuned to obtain the required flow rate.
- To stop the flow at the end of the experiment, valve no. 4 was closed first followed by valve no. 2.

3.4.2.2. Standard measurement process

The standard measuring process involved taking readings at predetermined points on the measuring plane (-Y, Z), where the centre of the orifice in use (centre or side orifice) and was the origin with the co-ordinates (0,0).

Using the centre orifice, surplus pore pressure and vertical velocity was measured at points along the central vertical axis (Y= 0, which was a line directly above the orifice). The points were spaced at 5 mm intervals to a height of Z= 90 mm. Thereafter, the interval increased to 10 mm to a height of Z= 130 and finally to a 20 mm interval to a height Z= 190 mm, with the last reading taken at Z= 200 mm. Readings were taken first at points closer to the bottom of the tank. The surplus pore pressure was measured first for each point followed by vertical velocity measurements. Bailey (2015) showed experimentally that flow in the horizontal direction along the central vertical axis was zero, therefore it was not measured.

Based on Baileys (2015) work the surplus pore pressure along the central vertical axis was expected to reach a peak, which could have occurred between the predetermined points. This reading was obtained by slowly raising the L-type Pitot tube to higher points until the water level in the sight tube peaked. Once this point was obtained the height of the Pitot tube and the magnitude of the pore pressure reading was recorded.

Readings were also taken on lines parallel to the central vertical axis, spaced at 5 mm intervals (i.e. at -Y= 5, 10, 15 mm etc.). However, on these measurement lines only surplus pore pressure was measured. Readings were taken at two points for each parallel line. The first reading was taken at the intersection with the horizontal line Z= 2 mm and the second reading was taken at the point of maximum surplus pore pressure. Measurements taken away from the orifice in the horizontal direction was stopped when no peak pore pressure head was observed along the parallel line.

Each reading taken during the experiment was recorded to the closest millimetre below the meniscus, which formed after the water level in the sight tube was allowed to stabilise i.e. no flow in the Pitot tube. Thus a time averaged reading was taken for each measurement.

3.4.2.3. <u>Measuring surplus pore pressure, velocity and energy using the Pitot tubes</u>

The first measurement was taken using the L-type Pitot tube before setting the flow rate. The Pitot tube was inserted into the water layer above the surface of the granular bed to obtain the datum head reading. Thereafter, the required flow rate was set and the bed was allowed to fluidise.

<u>Surplus pore pressure measurement</u>

The surplus pore pressure was measured at points in the bed and is defined as the pressure that formed after fluidisation i.e. the pore pressure that formed above that of the datum head.

Consider any point on the measuring plane. To measure the surplus pore pressure at this point, the surplus pore pressure head is required. To obtain this, the L-type Pitot tube was inserted into the bed such that it was perpendicular to the measuring plane and the tip of the Pitot tube was on the point. During the experiments the surplus pore pressure head was measured with the Pitot tube facing the direction of the negative X axis, see figure 3.14.

Since there was no radial flow about the vertical axis (i.e. perpendicular to the measurement plane) the sight tube reading was the datum head plus the surplus pore pressure head. Thus, to obtain the surplus pore pressure head at the point, the datum head was subtracted from the sight tube reading. The surplus pore pressure head (h_{sp}) can be converted into a pressure (p) reading using the equation [$p = \rho_f g h_{sp}$], but, in this study the use surplus pore pressure in terms of its head measurement was preferred.

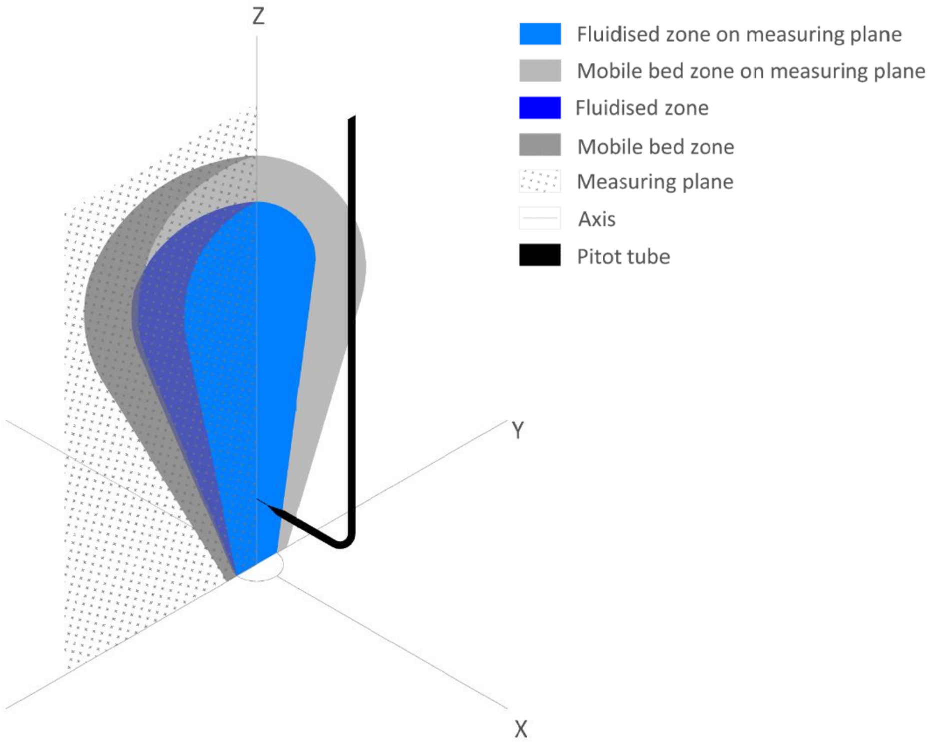

Figure 3.14: An illustration of how the L-type Pitot tube was positioned to measure surplus pressure head.

Velocity measurement

Equation (21) shows the relationship between the velocity head and the velocity of a flowing fluid:

$$h_v = \frac{u^2}{2g} \tag{21}$$

Where: h_v is the velocity head

To measure the velocity of the fluid at the point of interest the straight Pitot tube was inserted into the bed such that it faced the negative Z axis with its tip on the point (see figure 3.15). The reading on the sight tube represented the sum of the datum head, surplus pore pressure head and the velocity head of the vertical velocity component ($h_{v(v)}$). $h_{v(v)}$ was of importance and was calculated by subtracting the datum head and surplus pore pressure head from this sight tube reading.

By positioning the L-type Pitot tube such that it was parallel to the measuring plane, facing the positive Y axis and its tip on the point, the horizontal velocity head component ($h_{v(h)}$) can be measured. However, as mentioned previously the velocity for flow in the horizontal direction was not measured since velocity readings were taken along the central vertical axis only.

Therefore, having measured $h_{v(v)}$ of the fluids velocity at the point, equation (21) was used to convert the head measurement to velocity.

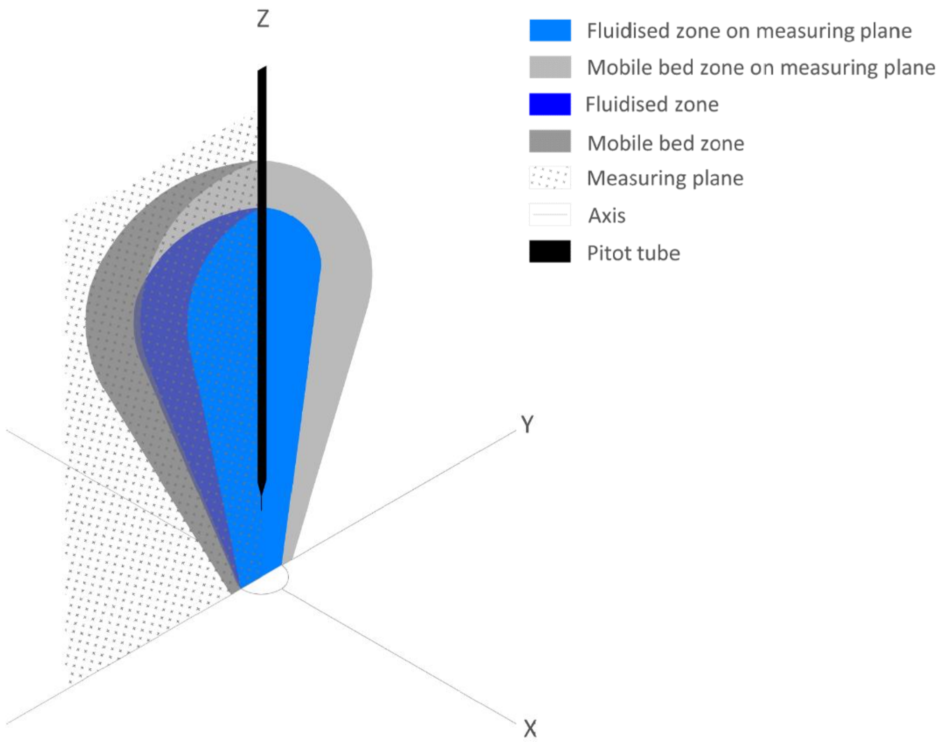

Figure 3.15: An illustration of how the straight Pitot tube was positioned to measure velocity in the vertical direction.

Energy head calculation

The energy head at the point was calculated by adding the surplus pore pressure head (h_{sp}) to the vertical velocity head:

$$H = h_{sp} + h_{v(v)} \tag{22}$$

Where: H is the energy head

h_{sp} is the surplus pore pressure head

$h_{v(v)}$ is the velocity head

3.4.2.4. Sample calculation

The sample calculation given below is a step-by-step process of how the individual components obtained from the measurement process described in section 3.3.2.2 was used to determine the surplus pore pressure, velocity and surplus energy head at a point. A point on the central vertical axis is considered in the example below.

Consider the following sight tube readings taken at the same point on the central vertical axis:

Datum head = 13 mm	*(Reading taken before fluidisation)*
L-type Pitot tube facing the neg. X axis = 71 mm	*(see figure 3.14)*
Straight type Pitot tube facing the neg. Z axis = 80 mm	*(see figure 3.15)*

Determine surplus pore pressure head:
Surplus pore pressure head = 71 - 13 = 58 mm

Determine velocity:
Velocity head (vert. direction) = 80 - 13 - 58 = 9 mm
Velocity head (Hori. Direction) = 0 mm

Velocity (vert. direction) = $\sqrt{2 \text{ x } 9.81 \text{ x } (9/1000)}$ *= 0.42 m/s*
Velocity (Hori. direction) = 0 m/s

Resultant velocity = $\sqrt{(0.42)^2 + (0)^2}$ *= 0.42 m/s*

(NB: The resultant velocity head will equal the velocity head in the vertical direction since there is no horizontal flow)

Determine surplus energy head:
Surplus energy head = 58 + 9 = 67 mm

3.4.2.5. Determining fluidisation height

The fluidisation height was determined by listening for a "scrambling noise" as the primed straight Pitot tube was inserted into the bed along the central vertical axis of the fluidised region. The scrambling noise described by Bailey (2015) occurred when the particles in motion in the head suspended zone made contract with the Pitot tube tip. The difference between the height of the Pitot tube when the "scrambling noise" was first heard and the vertical datum co-ordinate gave the fluidisation height.

This technique was carried out at both the centre and side orifice for the relevant experiments (see section 3.7). However, due to spatial limitations, the Pitot positioning system could not be used to determine the fluidisation height at the side orifice. To obtain those readings, the Pitot tube was inserted into the bed (against the tank wall), guided by a vertical line drawn on the glass wall. The line was parallel to the central vertical axis and was drawn directly above the orifice opening.

3.4.2.6. Determining fluidisation area and volume at the side orifice

The area and volume of the fluidised region was computed at the side orifice for leaks that had a flow rate of 2,3,4,5 and 6 l/min. The computation process involved taking photographs of the geometry of the fluidised regions that were in contact with the glass wall for each flow rate.

The extent of the suspended zone was identified by a V-shape made up of upward moving particles whilst the extent of the mobile bed zone was distinguishable by downward and slower moving particles. Each zone was outlined on the glass wall using dots made with white board markers, see figure 3.16. The dots were made such that edge and not the centre marked the point of interest. This was done to prevent the dots from blocking portions of the fluidised regions, so that a final check of the position of the dots could be done after the areas were marked.

The images were then imported into AutoCAD and scaled according to a ruler that was included in each image. Polylines were used in AutoCAD to define closed boundaries of the fluidised and mobile beds zone from which the areas for the respective zones that were in contact with the glass wall were determined.

The volume of the entire fluidised region that was in motion was estimated first, by dividing the outlined geometry into horizontal rectangles that had a width of 2 mm, as shown in figure 3.16. Each rectangular strip represented the summation of the area (in contact with the glass wall) of the fluidised and mobile bed portions. Thereafter, the length of the horizontal centre line for each rectangle, bound by the outer edge of the mobile bed zone was determined.

Two assumptions were made in order to estimate the volume of the fluidised regions. The first assumption was that each 2 mm horizontal strip was a plane (i.e. section) through the centre point of a circular disc and the second assumption was that the horizontal centre line was the diameter of the disc.

The individual diameters were used to calculate the area of each disc. The areas were then multiplied by the width (2mm) to obtain volume. A summation of the volume for each strip represented the total volume of the fluidised region (i.e. the fluidised zone plus the mobile bed zone). The process was repeated to determine the volume for the fluidised zone only. Finally, the volume of the mobile bed zone was obtained by subtracting the volume of the fluidised zone from the total volume of the fluidised region.

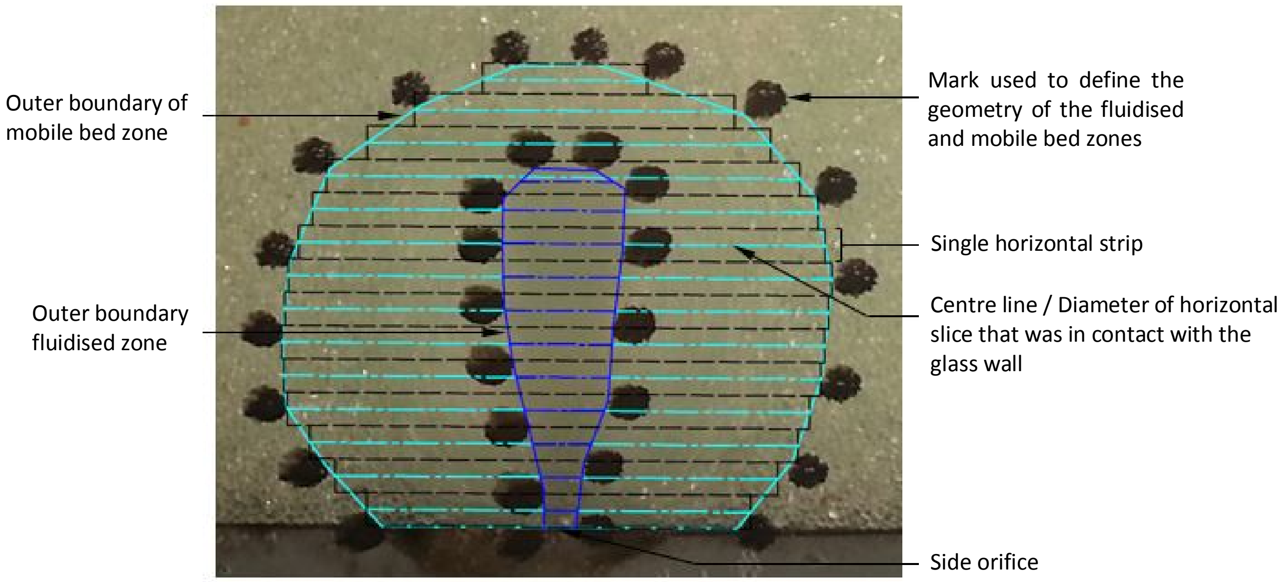

Figure 3.16: An example of how the geometry of the fluidised region against the side wall was divided into horizontal strips to determine the volume of the fluidised and mobile bed zones.

3.5 Preliminary experiments

A validation process was required before commencing with the experiments necessary to meet the goal of this study. The aim of this was to ensure that the experimental equipment and techniques that were employed were used correctly to give results that were reliable. A description of each validation test and the outcomes are discussed herein.

3.5.1 Validation of modified Pitot tube

Given that the Pitot tubes were modified as described in section 3.2.2, a test was designed to establish whether the modifications would lead to readings being unreliable. The nature of the test was to compare readings taken at the same points using the modified straight type Pitot tube (steel needle tip) and the original straight type Pitot tube (glass tip). A microscopic view of the original Pitot tube tip is given in figure 3.17.

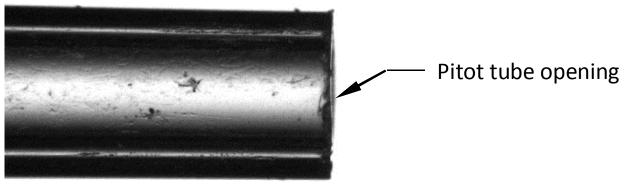

Figure 3.17: Microscopic view of the original Pitot tube tip.

To perform the experiment the tank was filled till the overflow level with only water. A flow rate of 1.5 l/min was allowed to flow into the tank through the centre orifice. Readings of velocity head was taken along the Y axis 1 mm below the orifice opening at the centre and adjacent to the left and right boundaries, see figure 3.18. This sequence was repeated five times for each Pitot tube.

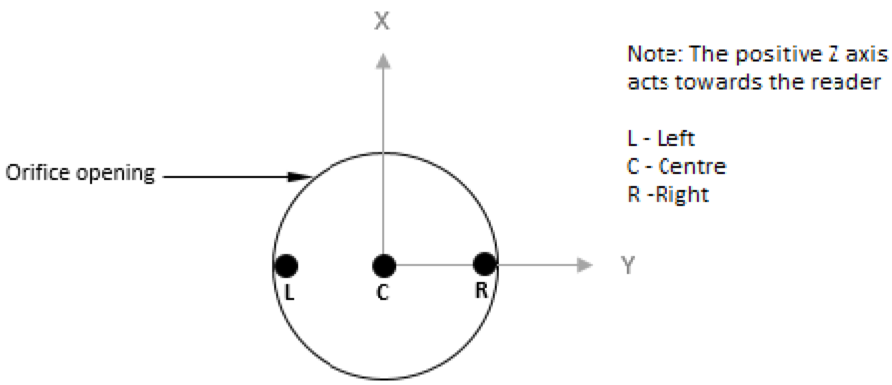

Figure 3.18: Schematic drawing of the orifice showing the points where readings were taken during the validation test for the modified Pitot tubes.

The measurements between the Pitot tubes were compared by looking at the difference between the average velocity head and the standard deviation of the readings taken at each point. The results from the experiment are given in table 3.3.

Table 3.3: Comparison of results for the old and modified straight type Pitot tubes

Position	Original Pitot tube		Modified Pitot tube		Velocity head difference (%)
	Average velocity head (mm)	Std. dev.	Average velocity head (mm)	Std. dev.	
left	870	3.4	871	1.8	0
centre	1070	4.3	1068	2.5	0.1
right	826	3.3	824	1.9	0.2
Average/Across orifice	922	3.7	921	2.0	0.1

When considering the average velocity head measurements taken at the left, centre and right positions, the values between the two Pitot tubes differed by 0, 0.1 and 0.2 % respectively. This amounts to an overall average difference of 0.1 %, which was sufficiently low to conclude that the modifications made to the Pitot tube did not affect the readings and therefore can be used in the main experiment.

Additionally, the modified Pitot tube gave results that were more accurate since the readings taken at the respective points varied the least with an overall average standard deviation of almost less than twice that of the original Pitot tube.

It is noticeable that the average velocity head measured at the boundaries of the orifice for the respective Pitot tubes were closely matched, varying by roughly 5.5 % for both Pitot tubes. However, the velocity head measured at the centre points for each Pitot tube was significantly higher than the boundary readings. This finding confirms the explanation Bailey (2015) used to justify why in his experiment the average velocity determined using the orifice equation (equation (3)) was lower than the point velocity measured just above the centre of the orifice.

Upon further investigation it was found that the shape of the Pitot tube tip was capable of influencing readings. This led to the test described above being repeated for a glass tip that was similar to the original Pitot tube but the tip opening had an irregular shape (see figure 3.19) and for the modified Pitot tube tip but in a slightly rotated (about the z axis) position. The latter was investigated since the tip of the modified Pitot tube was tailored by hand and although close it was not exactly symmetrical.

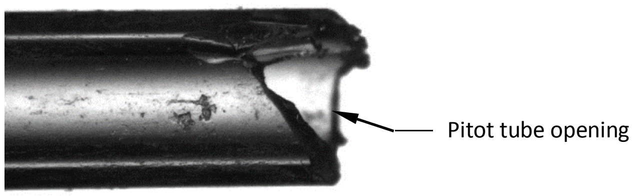

Figure 3.19: Microscopic view of the irregular glass Pitot tube tip

The results from these tests are shown in figure 20. For comparison reasons figure 20 also includes the readings that were previously obtained in the validation test.

The measurements gained with the irregular glass tip at the left and right positions were significantly lower and higher than the other corresponding readings, respectively. Interestingly, at the centre all readings were relatively closely matched, with the irregular glass tip reading falling only 2.4 % lower than the original Pitot tube tip reading. Therefore, the results indicated that only measurements adjacent to the orifice boundaries were significantly affected by the Pitot tube having an irregular shaped tip opening.

Lastly, one can notice from the plot that rotation of the modified needle tip resulted in measurements differing from the original needle position by 3.2, 0.4 and 1.1 % at the left, centre and right positions, respectively. These differences although significantly small did occur and to prevent them from influencing the results obtained in the main experiment, the hypodermic needles were marked so that they could always be fitted in the same position on the brass fitting of the Pitot tubes.

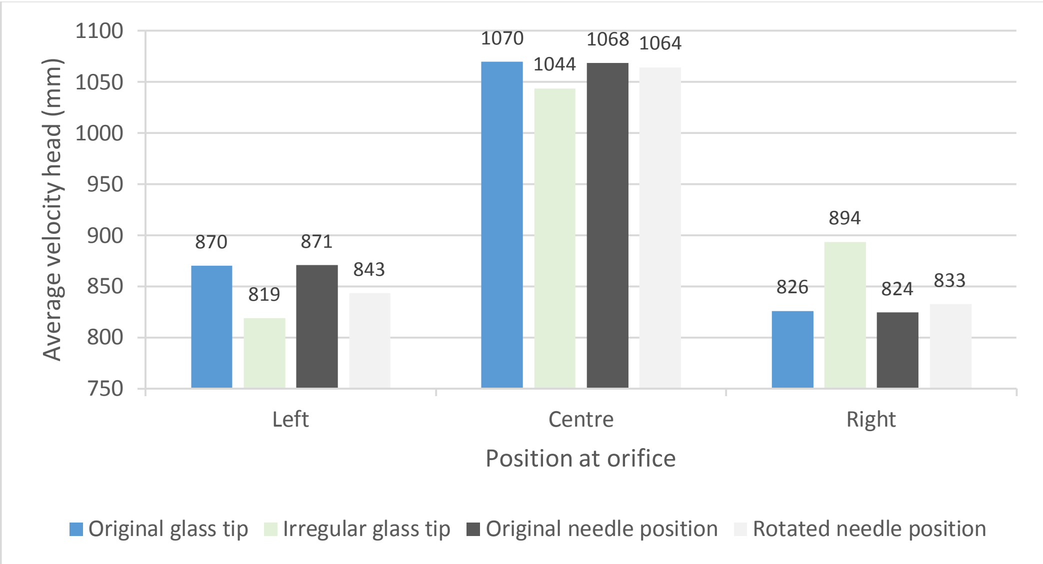

Figure 3.20: Comparison of results obtained in the investigation of the influence of Pitot tube tip geometry.

3.5.2 Validation of technique used to determine fluidisation height

The method (as described in section 3.4.2.5) used to determine the height of the fluidised region was to essentially insert the straight type Pitot tube along the line directly above the orifice until a scrambling noise was heard. When this noise was heard, it was assumed that the Pitot tube had its tip at the top of the internally fluidised region. Since this process could not be observed due to it occurring inside the granular bed, it gives rise to a level of uncertainty as to the location of the Pitot tube tip when the scrambling noise was heard.

Therefore, to observe the location of the tip of the Pitot tube when the scrambling noise was heard, the method of determining the height of the fluidised zone was repeated at the side orifice using the flow rates 2, 3, 4, 5 and 6 l/min. In this test, material type A and a bed height of 300 mm was used. The results from this validation process are given below and takes the form of a description of the observations made during the experiment.

3.5.2.1. Description of observations

The experiment began by simulating a 2 l/min leak using the side orifice. Fluidisation formed immediately, with the fluidised, mobile and static bed zones easily identifiably through the glass wall of the tank.

The scrambling noise was heard and was identified to occur due to the suspended ballotini particles striking the steel Pitot tube tip. The noise was first head when the tip was at the boundary between the static and mobile bed zones and was loudest, when it was at the head of the fluidised zone.

Upon slow removal of the Pitot tube it was noticed that the fluidised region stretched and reached a significantly greater height where it stabilised. It was further noticed that the scrambling noise was last heard at the boundary of the static and mobile bed zones as the Pitot tube was removed from the bed.

A photo of the enlarged fluidised region and the point where the scrambling noise was last heard is given in figure 3.21. In the photo, the tip of the Pitot tube is not visible but its location can be determined since the length of the steel portion of the hypodermic needle was 10 mm and the point where it was joined to the green plastic fitting was marked with the red dot in the image.

The process was repeated for the flow rates of 3, 4, 5 and 6 l/min without stopping the water jet or resetting the bed. It was found that the enlarged fluidised zone grew larger for the higher flow rates and responded in a similar manner as before when the Pitot tube was removed from the bed. Furthermore, even though the size of the fluidised regions were significantly affected by the Pitot tube, the tip was always located at the boundary between the mobile bed and the static bed when the scrambling noise was first and last heard.

Therefore, it can concluded that when determining the fluidisation height using the technique as per section 3.4.2.5, the tip of the Pitot tube when the scrambling noise is first heard is located at the boundary between the mobile bed and static bed zone and that the size of the fluidised region was significantly affected when the Pitot tube was in the process of being removed. Regarding the later, since the side orifice was used during this experiment the observations made are vulnerable to interference from the tank wall. Therefore, it is unknown whether the fluidised region is affected by the Pitot tube in the same manner when the leak is simulated in an unbound surrounding i.e. at the centre orifice.

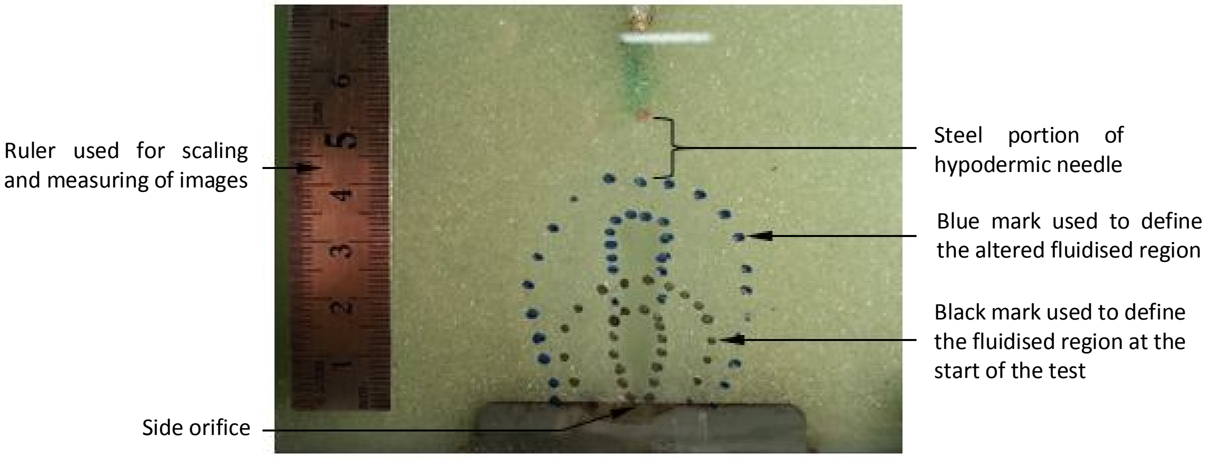

Figure 3.21: Image of a 2 l/min leak simulated at the side orifice before and after measuring the fluidisation height with the straight type Pitot tube.

3.5.3 Validation of experimental procedures and processes

A validation process was required to determine if the procedures and processes developed to conduct the experiments were performed correctly. The validation process involved repeating a previous experiment to which the outcomes could be compared. In this case the results obtained from Bailey's (2015) experiment (described in section 2.5) gave such a benchmark.

The validation test was performed using the same test parameters that Bailey (2015) used, which consisted of a flow rate of 2 l/min, ballotini material type A and a bed height of 300 mm. Since the surplus pore pressure, velocity and surplus energy distributions along the central vertical axis (Y= 0 mm) was of interest in the current study, only the results from the validation test obtained along this line were compared. Analysis of the two sets of results is presented in the sections that follow. The raw data is given in appendix B.

3.5.3.1. <u>Surplus pore pressure distribution</u>

A plot of the surplus pore pressure distribution found in the validation test and the experiment conducted by Bailey (2015) is given in figure 3.22. Various similarities are noticed between the two pressure profiles. In each case, as the height above the orifice increased the surplus pore pressure increased, peaked and thereafter followed a non-linear decrease to a height of 100 mm. Beyond Z= 100 mm, the plots show that the change in surplus pressure in each experiment occurred linearly and at roughly the same rate.

The fluidisation heights fell in close proximity to each other at 24 and 27 mm for the benchmark and validation tests respectively and is illustrated in the graphs with the horizontal dotted lines.

There were, however, some difference between the two distributions. For example, between the height range 2 to 24 mm, the validation test began with a decrease in surplus pore pressure before it increased. This trend cannot be dismissed even though it was not observed in the benchmark profile, since, a Computational Fluid Dynamic (CFD) model based on Bailey's (2015) results developed by

Meire (2014) found that a localised pressure peak could occur immediately outside the orifice opening.

A complete profile in this region was not obtained during the experiment due to limitations of the experimental equipment. However, the initial decrease in pore pressure observed in figure 3.22 could be the backend of the localised pore pressure peak and could therefore point to greater accuracy achieved with the modified Pitot tubes and testing methods. Meire (2014) explained that the impact of the ballotini particles entering the water jet from the mobile bed may be the reason for the pressure increase at the orifice.

Furthermore, between the height range the 2 to 24 mm the surplus pore pressure obtained in the validation test was consistently lower by roughly 15 mm, except for the first reading. Conversely, above 24 mm a change occurred where the surplus pore pressure in the validation test was slightly higher than the benchmark values by an average 8 mm.

Another difference one may notice is that the pore pressures at the turning points (peaks) did not match in location and magnitude but they were not far removed. In the validation test the pore pressure peaked at an elevation of 30 mm above the orifice with a value of 101 mm, whilst, in Bailey's (2015) test the comparative location and magnitude was 20 and 110.6 mm, respectively.

It is important to note that in this experiment readings were taken at preselected points, therefore the pore pressure measured at the turning points may not resemble the maximum pore pressures. The maximum pore pressures may in fact occur slightly higher or lower than the peak heights observed in plot. The standard measurement method used for the sensitivity tests, as described in section 3.4.2.2, was modified to find the exact height at which the maximum pore pressure occurred.

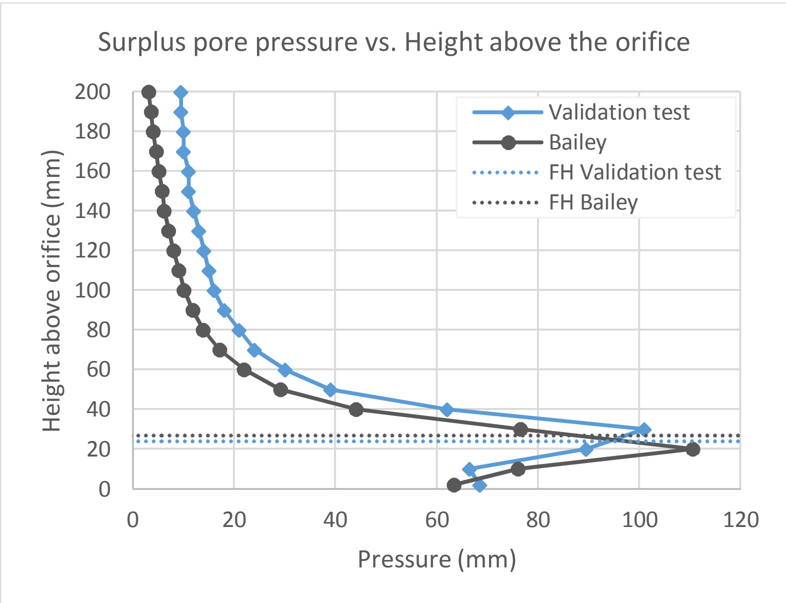

Figure 3.22 A comparative plot of the surplus pore pressure at heights along the vertical line of symmetry determined by Bailey (2015) and the validation test.

3.5.3.2. Velocity distribution

A plot of the vertical velocity at heights above the orifice determined by Bailey (2015) and the results from the validation test is given in figure 3.23. Both plots show a trend where the velocity was highest immediately above the orifice opening and then rapidly decreases at roughly the same rate with almost identical measures of velocity as the height above the office increases to 30 mm.

Between the heights of 30 and 50 mm, just above the fluidisation heights, the velocities from both plots are weak and show a sudden drop followed by an increase. In the validation test the drop was relatively larger resulting in temporary negative velocities. The presence of negative velocities symbolises fluid flow in the downward direction (towards the base of the tank) and although not present in the same regions, Bailey (2015) also obtained negative velocities, particularly at the 150 mm height.

At heights above 50 mm, the velocity in both plots are relatively low and gradually approaches zero. However, a notable difference in this region between the two plots is that, the velocities obtained in the validation test are consistently higher by an average 0.2 m/s.

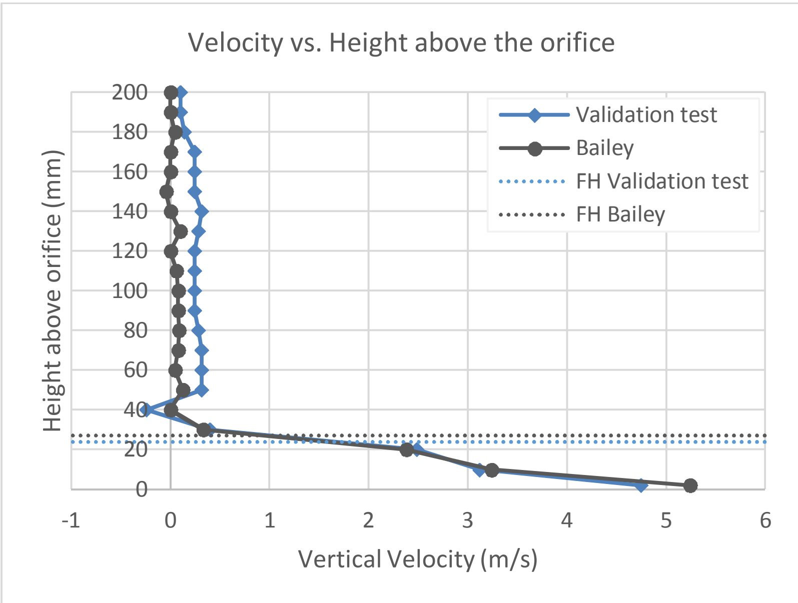

Figure 3.23: A comparative plot of the vertical velocity at heights along the vertical line of symmetry determined by Bailey (2015) and the validation test.

3.5.3.3. Energy distribution

The distribution of the surplus energy for both, the validation test and Bailey's (2015) experiment is given in figure 3.24. Analysis of these results show that both plots had almost identical trends.

In each case the surplus energy was highest immediately above the orifice opening and then rapidly decreased at roughly the same rate as the height above the orifice increased to an elevation of 30 mm. Interestingly, this height was just above the respective fluidisation heights, which implies that bulk of that region fell in the internally fluidised zone.

An assessment of energy loss in the 2 to 30 mm height region indicates that 91 % of the available energy was dissipated in the verification test. This is close to the comparative 94 % energy loss obtained in Bailey's (2015) experiment. Furthermore in this region, both experiments show that majority of the surplus energy head comes from the velocity head component, which explains the significant difference between the first readings (the points immediately above the orifice). Finally the plot shows that, at levels above the fluidisation heights, each distribution gradually decreases to negligible amounts of surplus energy.

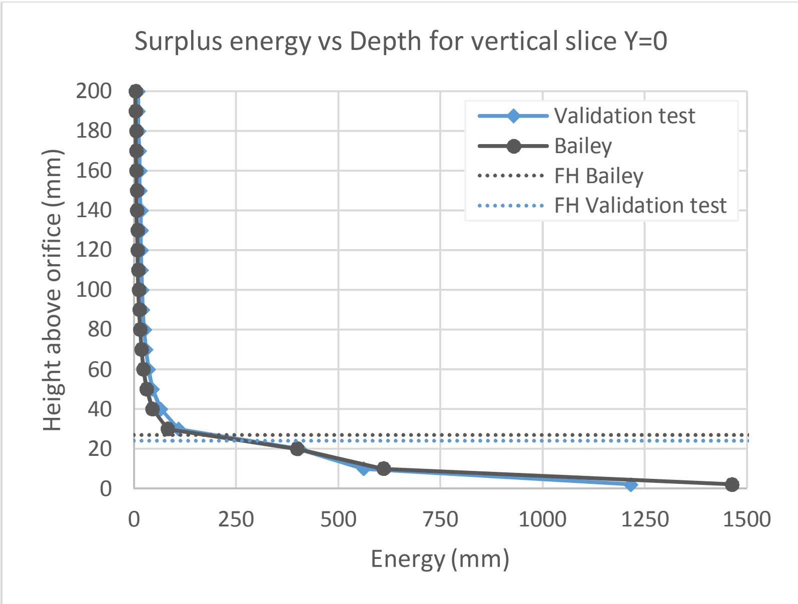

Figure 3.24: A comparative plot of the surplus energy head at heights along the vertical line of symmetry determined by Bailey (2015) and the validation test.

3.5.3.4. <u>Discussion</u>

In general, both sets of data compared well with the exception of the variations that were highlighted in the previous sections. A probable cause for the variation in the results could be linked to the packing structure of the granular beds. It has been shown in previous studies (Ma, 2011 and van Zyl et al., 2013) that the size and geometry of a fluidised region is greatly influenced by the packing structure of the bed.

Ma (2011) explained that the geometry of the fluidisation zone is influenced by the path that the flow takes. Even though the method used to prepare the granular beds was the same, it is likely that the packing structure of the beds were not identical. Thus, it is possible that the different packing structure between the beds led to channels of flow that differed from each other, which resulted in the formation of fluidised regions with slightly dissimilar geometries and sizes. This outcome would have a direct effect on the surplus pore pressures and velocities measured in the fluidised zone, since, at the measurement points the relative positions of the Pitot tube tips within the respective zones would not be the same.

Additionally, the method which Bailey (2015) used to unblock the supply line to initiate fluidisation was to insert a thin metal wire from the bed surface into the orifice. This practise would have further altered the bed structure, especially above the orifice, by creating spots of varying density as well as by creating a temporary channel for fluid to flow through when the wire was pulled out of the bed. In comparison, the supply line in the validation test was modified such that it could be unblocked without effecting the packing structure of the bed.

Another element that may have contributed to the differences observed between the two tests is related to the accuracy of jet flow rate during the tests. Bailey (2015) was able to achieve a flow rate with an accuracy that ranged 2 ± 0.03 l/min and described that when the flow rate fluctuated it would return to the desired magnitude but there were times when the flow rate had to be adjusted manually.

In the validation test, the flow rate fluctuated periodically but with a lower range of 2 ± 0.01 l/min. This was due to the modifications made to the supply line described in section 3.2.1. Thus, it is possible that readings at comparable points were taken when the flow rate between the tests were not exactly the same, which effectively would lead to results that vary from each other. However, this type of variation of the results between the tests would have had a small contribution to overall differences observed at the various points.

Therefore, the differences noticed between the two tests were relatively small and within reason, which allowed for the conclusion that the experimental techniques and equipment were used correctly.

3.5.4 Measurement errors

As mentioned previously, the flow meter used during the experiment read within the manufactured accuracy and periodically fluctuated by ± 0.01 l/min. This fluctuation range was too small to create significant variation in the measured readings.

The accuracy of positioning the tip of the Pitot tube at a required point in the tank was a factor that required investigation. To perform this a 10 cm long nail which was hammered through a 2 cm thick block was placed in the tank with the sharp end of the nail pointing vertically upward. The tips of both, the straight and L- type Pitot tubes were then positioned at the tip of the nail. The datum coordinates for each Pitot tube were recorded.

Thereafter, the Pitot tubes were moved away (in the X, Y and Z direction) and while trying not to look at the nail the Pitot tubes were repositioned to the datum coordinates. This process was repeated twice for each Pitot tube at two positions in the tank. The purpose of this exercise was to measure how far (distance in all three direction) the tip of the Pitot tubes were from the tip of the nail.

It was observed that the Pitot tube positioning system was able to place the tip of Pitot tubes within less than a millimetre away of the tip of the nail (in each direction) for each trail. It was not possible to take measurements of the differences with a vernier calliper due to the offset distance being too small. A specially constructed measuring device would be required to accurately measure such small readings. Therefore, it was concluded that the Pitot tube positioning system was sufficiently accurate at positioning the pitot tube at a desired point without creating significant variation in the measured readings.

However, variation of the measured readings are still possible even through flow rate, position of points and experiment parameters between tests are kept constant. This is due to the effect of the beds having different packing structure, which causes the shape, size and possibly trajectory of the particles in motion of the soil-leak interaction to vary.

3.6 Description of main experiment

The goal of this study was to develop an understanding of how soil-leak interaction resulting from a pipe leak is influenced by the jet flow rate and various bedding characteristics (including bed height and particle size). To achieve this, the experimental setup together with a bed consisting of an idealised soil medium (ballotini) were used to simulate a pipe leak under controlled conditions in a laboratory.

A standard experiment consisting of the use of a 2 l/min flow rate, 300 mm bed height and ballotini material type A was conducted to serve as a benchmark to which the results from sensitivity tests could be compared and analysed. The design of each sensitivity test is given in table 3.4. Each test was conducted only once.

The effects of the jet flow rate was investigated by varying only the flow rate using 3 and 4 l/min whist a bed height of 300 mm and ballotini type A was used and kept constant. The flow rate was varied with increasing flow rate since decreasing the flow rate may not have led to the bed becoming internally fluidised. A difference of 1 l/min between the flow rates was selected since it was high enough for the effects of changing the flow rate to be observed in the results.

The effects of bed height was investigated by varying only the bed height using 200 and 150 mm whist a flow rate of 2 l/min and ballotini type A was used and kept constant. The bed was varied with decreasing height because the amount of ballotini material for all three types was sufficient to prepare a bed with the maximum height of 300 mm. A difference of 100 mm between the bed heights was initially preferred so that distinct differences could be observed in the results. This would have resulted in the lowest bed height being 100 mm instead of 150 mm. The 100 mm bed height was initially used during the experiment but the fluidised region broken through the bed surface, which led to a bed height of 150 mm being used.

Lastly, the effects of particle size was investigated by varying only the ballotini material, using type B and C whist a flow rate of 2 l/min and bed height of 300 mm was used and kept constant. The test was limited to these particle distribution of these material types since it was difficult to obtain ballotini of various sizes that had the same particle density as the standard experiment.

Table 3.4: Parameters used for the sensitivity tests.

Sensitivity factor	Material Type	Flow rate (l/min)	Bed height (mm)	Comment
Standard experiment	A	2	300	Standard experimental preparation and procedures were used in each test, as detailed in section 3.4 The fluidisation height, surplus pore pressure, velocity and surplus energy distributions were determined directly above the orifice. Maximum pore pressures were determined along vertical slices in the horizontal direction.
Flow rate	A	3	300	
	A	4	300	
Bed height	A	2	250	
	A	2	150	
Particle size	B	2	300	
	C	2	300	

3.7 Comparison of leakage conditions between the centre and side orifice

An additional investigation was conducted that was aimed at examining leakage conditions between the centre and side orifice, for the reason that, should the results be similar the side orifice would be more advantageous to conduct future experiments since it offers the opportunity to visualise the fluidisation mechanism and assess how it responds to various situations.

3.7.1 Description of experiment

The first part of this experiment consisted of comparing fluidisation heights measured using the side orifice with those determined at the centre orifice in the previous flow rate experiments.

In this experiment the fluidisation height at the side orifice was measured for the flow rates of 2, 3, 4, 5 and 6 l/min from images that captured the geometry of the fluidised region that was in contact with the glass wall. Before each image was taken, the geometry of each zone (mobile and suspended zone) for each flow rate were marked on the tank wall using white board markers. A ruler was placed beside (parallel to the central vertical axis) the fluidised region to assist in scaling and making measurements from the images.

Once the image was captured for the desired flow rate, the flow rate was increased without stopping the flow or resetting the bed. The height of the various fluidised region was measured off the images at the boundary between the mobile and static bed along the line directly above the orifice. During the test a bed height of 300 mm and ballotini material type A was used and was kept constant.

The second part of this experiment was aimed at comparing the surplus pore pressure, velocity and surplus energy distributions measured at the centre and side orifice. This was the first experiment where these reading were required at the side orifice and therefore the datum co-ordinates for the Pitot tubes at the side orifice was necessary.

A process similar to the one used at the centre orifice was followed (see section 3.4.1.2). The centre of the side orifice was made the reference point. However, due to spatial restrictions the Pitot positioning system could not align the straight Pitot tube directly above the side orifice reference point. The closest the tip could get was 7 mm away along the Y axis. Therefore in order to obtain readings that were closest to the orifice the datum co-ordinates for the Pitot tubes were determined at the side orifice for the point (Y= 7, Z= 0) and readings along the vertical line Y=7 mm at both orifices were compared, see figure 3.25. Lastly, in this test a flow rate of 2 l/min, bed height of 300 mm and material type A was used and kept constant.

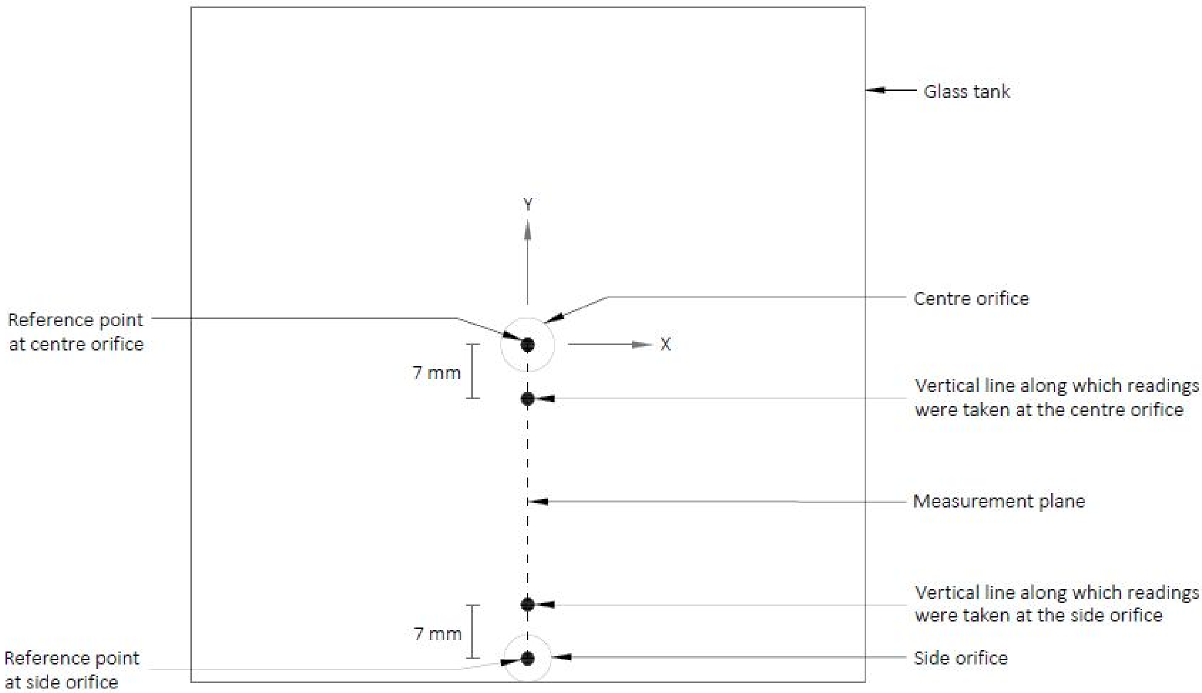

Figure 3.25: Schematic plan view of the experimental setup showing the relative reference points and the location of the lines along which readings at the centre and side orifice were compared.

4. Results and discussion

Results obtained during the experimental phase of the study is presented in this chapter. The results are accompanied with detailed description and discussion of the trends and relationships established through analysis.

First, attention is given to findings from the standard experiment. Focus then shifts to the results from the sensitivity experiments, which is followed by the findings from the additional tests that investigated leakage conditions between the centre and side orifice.

4.1 Standard experiment

The standard experiment was conducted to serve as a benchmark to which the results from the sensitivity experiments could be compared. The test comprised of an upright fluidised region initiated beneath an idealised soil bed using the 3 mm (diameter) centre orifice. A flow rate of 2 l/min, bed height of 300 mm and material type A was used. Measurements of surplus pore pressure, velocity and surplus energy were obtained in the bed along the line directly above the orifice. Additionally, maximum surplus pore pressure readings along vertical slices was also determined for horizontal distances (along the Y axis) spaced at 5 mm intervals away from the orifice.

The results from the experiment including interpretation is given in the sub sections that follow. The raw data obtained during the experiment is given in appendix C.

4.1.1 Surplus pore pressure distribution

The readings of surplus pore pressure was plotted on a graph, the result yielded the distribution shown in figure 4.1. In this experiment the fluidisation height was 23 mm.

The distribution shows that the surplus pore pressure in the bed immediately above the orifice experienced a decrease before increasing to reach a maximum pore pressure. The magnitude of the maximum surplus pore pressure was 96 mm and occurred at a height of 30 mm, just above the fluidisation height. At heights beyond the maximum pore pressure point, the surplus pore pressure initially decreases at a relatively rapid rate and then slows down to a point where the surplus pore pressure change can be seen to take on a linear trend. The linear trend, which begins at roughly 90 mm indicates that seepage in the bed in this region follows Darcy's law, which in turn suggests that flow was laminar. At points lower than 90 mm, the change in pressure loss is non-linear, which implies a deviation from Darcy flow.

The fluidisation height can be seen to occur at a height slightly below the maximum surplus pore pressure. There is a possibility that they both occurred at the same height but is not evident in the results due to interference to the fluidised region caused by the probing action of the Pitot tubes. For example, regardless of the type of the Pitot tube, when it was inserted into the bed the granular ballotini particles would have parted to make way for the instrument. This would have altered the packing structure of the bed (by creating channels, loosening the bed or conversely creating higher compaction points in the bed), which as a result would have changed the pattern of fluid flow, thus affecting characteristics of the fluidised region.

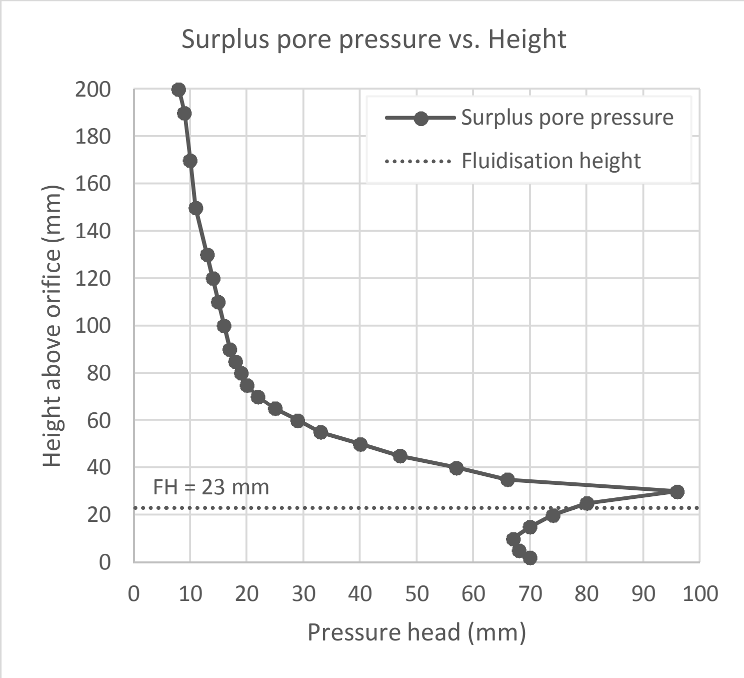

Figure 4.1 Surplus pore pressure distribution along the vertical line directly above the orifice for the standard experiment.

A plot of the maximum surplus pore pressure found along vertical slices for distances in the horizontal direction is given in Figure 4.2. The plot shows that the highest maximum surplus pore pressure occurred directly above the orifice. As the distance from the orifice increased the pressure readings decreased at a decreasing rate. An exponential trend line was used and match the data well, with an R^2 value of 0.97.

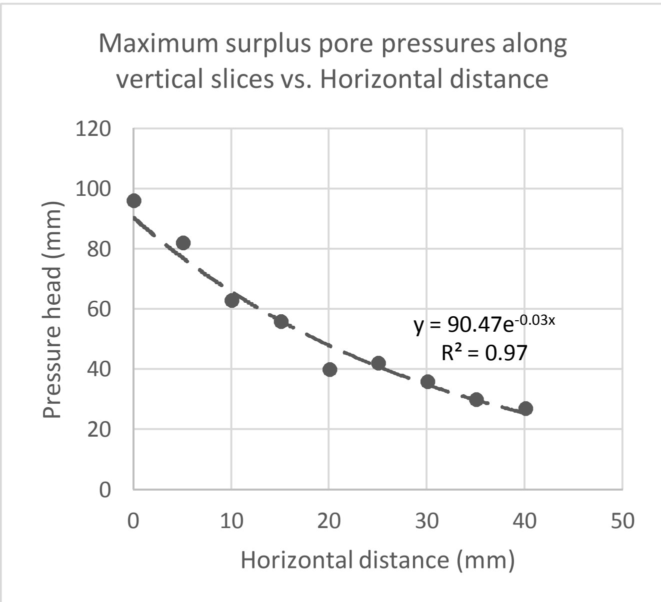

Figure 4.2 A plot of the maximum surplus pore pressure measured along vertical slices against horizontal distance for the standard experiment.

The heights at which the maximum surplus pore pressures where measured is presented graphically in figure 4.3. As explained, the highest pore pressure occurred directly above the orifice. Thus, the reading on the extreme right (corresponding to a surplus pore pressure head of 96 mm and height of 30 mm) reflects the position above the orifice. Moving left from this position are the measurements taken along the vertical slices, which were spaced at increments of 5 mm.

The data was scattered. A logarithmic trend line gave the highest R^2 value of 0.67 and highlighted a general pattern where the height of the maximum surplus pore pressures occurred closer to the base of the tank as the horizontal distance from the orifice increased.

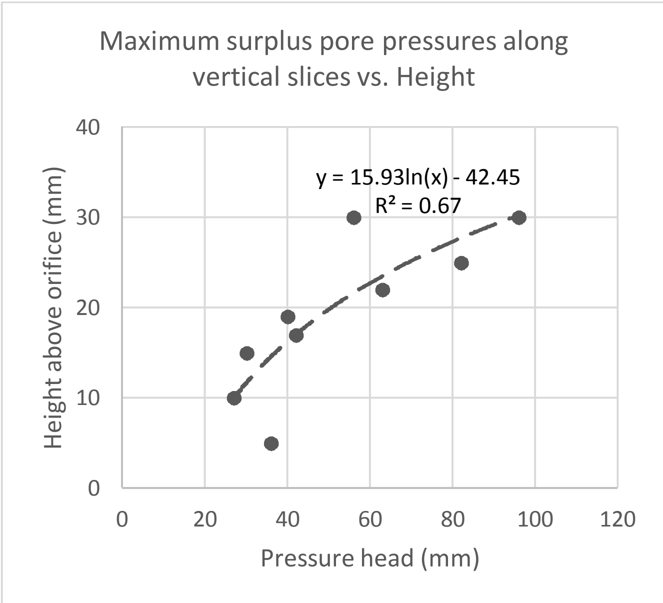

Figure 4.3 A plot of the maximum surplus pore pressure along vertical slices against height for the standard experiment.

4.1.2 Velocity distribution

The velocity distribution above the orifice is given in figure 4.4. The plot shows that the highest recording of velocity occurred in the regions closest to the orifice, with the highest value of roughly 4.74 m/s just above the orifice. The velocity rapidly decreased with increasing height and reached a value of negative 0.52 m/s at a height of 40 mm.

In the literature review in section 2.3.2, turbulent flow regime in a packed bed was estimated to begin at $Re_{inter} \geq 500$. At this benchmark the velocity of the fluid is approximately 0.8 m/s (based on equation (7)). Interestly, in figure 4.4 this velocity was achieved a few millimeters above the fluidisation height wich suggests that fluid flow in the fluidised region was turbulent. Transitional flow occurs between $1 < Re_{inter} < 500$, which equates to an approximate velocity range of 0.002 to 0.8 m/s. Laminar flow is present when $Re_{inter} \leq 1$ equating to a velocity less than and equal to 0.002 m/s. Those velocities were observed in the bed at increasing heights beyond the fluidised region, first with flow in the transional and then liminar regime. Therefore based on this finding, the deviation from the Darcian flow observed in figure 4.1 could have been a result of turbulent and transitional flow.

According to figure 4.4, the velocity at points greater than 40 mm begins to decrease and approach zero. The velocity in its approach to zero is shown to be constant before suddenly dropping to zero. That portion of the graph (beginning at roughly 90 mm) correlates to the linear pressure loss in figure 4.1, which suggested laminar flow (i.e. low fluid velocity). Thus, that segment of the velocity distribution may not be accurate and may have occurred due to limitations of the experimental equipment (Pitot tube) in being able to read low velocities. A more realistic trend would be for the velocity to show a more gradual decrease as it approached zero.

The presence of the negative velocities in the distribution is an indication of backflow. The results show that the velocity in the bed became and remained negative shortly after the fluidisation height. This indicates that at a macroscopic level the flow in the bed above the fluidised region followed a circulating pattern that resulted in the fluid being drawn toward the base of the tank along the centre line. It is unknown why this flow pattern developed, however though speculation one might consider that the unstable vortices at the head of the fluidised zone was responsible or the impact of the intrusive nature of the Pitot tubes may have led to this outcome.

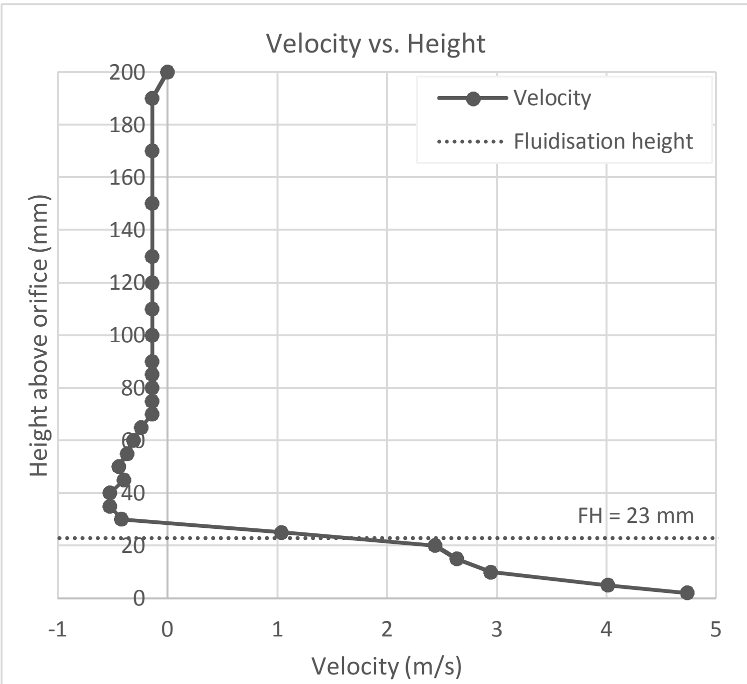

Figure 4.4 Velocity distribution along the vertical line directly above the orifice for the standard experiment.

4.1.3 Surplus energy distribution

The distribution of surplus energy measured in the bed is given in figure 4.5. The results show that the surplus energy was highest immediately above the orifice opening, with a value of 1214 mm. The energy rapidly decreased as height above the orifice increased. At heights beyond 60 mm the energy reduced to negligible amounts.

Surplus pore pressure and velocity readings were not measured at the fluidisation height but by assuming a linear relation for the closest energy readings above and below the fluidisation height, it can be shown that roughly 81 % of the available energy (based on the energy reading taken immediately above the orifice) was lost in the fluidised region. This result is consistent with the finding made by van Zyl et al. (2013) that the fluidised zone, which develops during a pipe leak acts as an energy dissipation mechanism that assists in preventing the leak from reaching the ground surface. In this test the leak was directed vertically toward the bed surface and it still did not penetrate the surface.

Interestingly, at the height at which the maximum pressure occurred (30 mm) the energy reduced to a value of 87 mm, which equates to an energy loss of roughly 93 %.

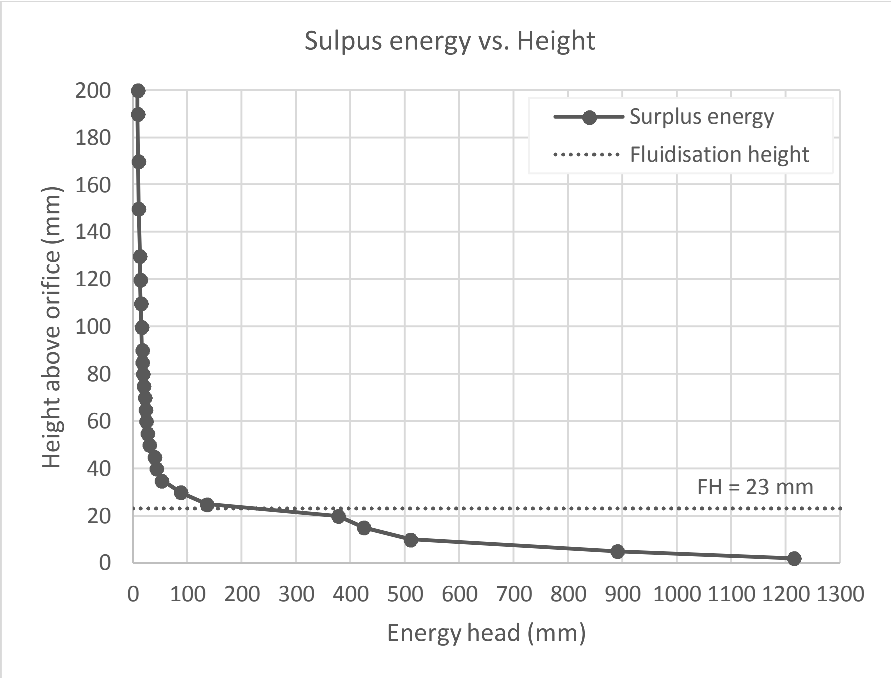

Figure 4.5 Surplus energy distribution along the vertical line directly above the orifice for the standard experiment.

A combined plot of the surplus pore pressure, velocity and surplus energy is presented in figure 4.6. Each element in the plot is represented in terms of its head reading. A clear distinction can be seen at the maximum pore pressure level. Below this height the surplus energy was mostly made up of the velocity head component, while, above it the surplus energy consisted mainly of the pore pressure component. Furthermore, the plot shows that as the pore pressure increased the velocity rapidly decreased. At the point where pore pressure was the highest the velocity was at its lowest value. This suggests that majority of the energy in the bed closer to the orifice was in the form of kinetic energy. As height above the orifice increased the kinetic energy was rapidly converted into potential pressure energy.

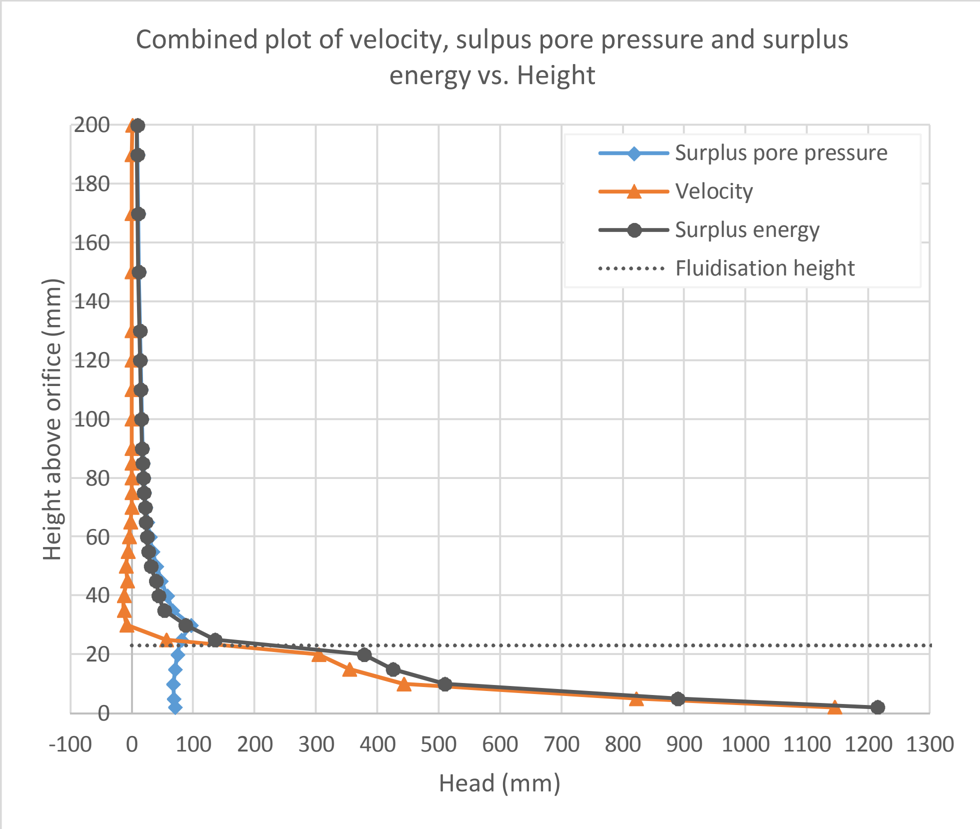

Figure 4.6 Combined plot of velocity, surplus pore pressure and surplus energy distribution along the vertical line directly above the orifice for the standard experiment.

4.2 Sensitivity analysis of factors that affect soil-leak interaction

The sensitivity tests that were conducted were aimed at investigating three sets of factors known to have an influence on the fluidised region, which occurs during a pipe leak. The factors that were investigated included the effects of the jet flow rate, bed height and particle size of the bedding material.

In all tests, an upright fluidised region was initiated in an idealised soil bed using the 3 mm (diameter) centre orifice. In each test the surplus pore pressure, velocity and surplus energy head was measured at points in the bed along a line directly above the orifice. The maximum surplus pore pressure along vertical slices was also determined for horizontal distances (along the Y axis) spaced at 5 mm intervals away from the orifice.

The results from the experiments is given and discussed in the sub sections that follow. As mentioned previously, the results from the standard experiment served as a benchmark to which the sensitivity analysis was conducted. Therefore, the results from the standard experiment was included in the graphs and is presented consistently in black with round markers. The raw data obtained from the experiments is given in appendix C.

4.2.1 Effects of the jet flow rate

The effect of the jet flow rate was investigated in separate tests where conditions in the bed were measured for 2, 3 and 4 l/min. A bed height of 300 mm and material type A was used in each test.

4.2.1.1. Fluidisation height

The fluidisation heights measured for the various flow rates were 23, 27 and 41 mm in order of increasing flow rate. This is illustrated graphically in figure 4.7. The results indicate that the height of the fluidised region increased at an increasing rate with increasing flow rate. Thus the data was fitted with an exponential trend line, which gave the highest R^2 value of 0.94.

A possible explanation for the result seen in figure 4.7 could come from analysing the forces that acted on the soil particles. It is known that the particles in the fluidised zone becomes suspended and is projected upwards when the upward drag force on the particles induced by the water jet overcomes the bulk weight of the bed (in a fully saturated condition). During this test, the flow rate of the fluidising water jet was increased whilst the height of the bed was kept constant. Thus increasing the flow rate increased the drag forces on the particles and since the opposing force from the weight of the bed remained constant, the suspended particles were able to reach greater heights.

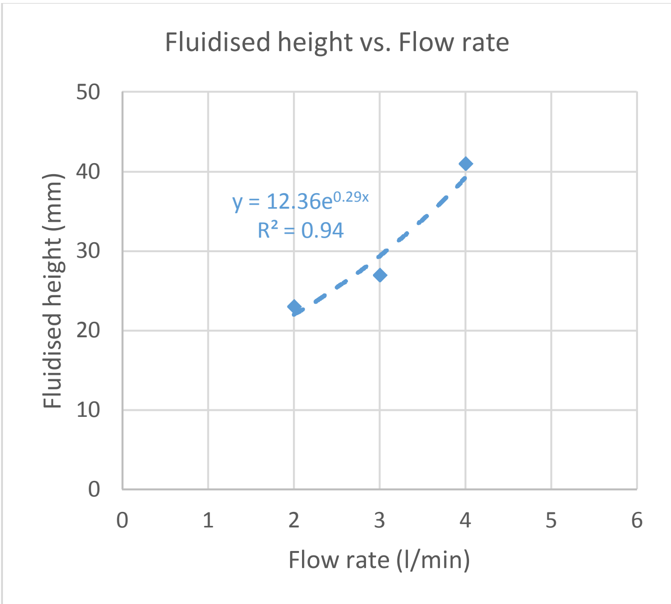

Figure 4.7: Fluidised heights measured for various flow rates.

4.2.1.2. Surplus pore pressure distribution

A plot of the surplus pore pressure distribution for each flow rate is given in figure 4.8. Qualitatively, the 3 and 4 l/min jets have similar pore pressure distributions when compared to the standard experiment but they were somewhat "exaggerated".

The magnitude and height of the maximum surplus pore pressure reached in each experiment increased with increasing flow rate and remained consistently higher than the corresponding fluidisation heights. The magnitude of the maximum surplus pore pressures with respect to the flow rate of 3 and 4 l/min was 164 and 294 mm, which occurred at a height of 40 and 61 mm above the orifice. A linear trend line fitted through these points provides some evidence that the maximum surplus pore pressures increased linearly. This is illustrated in figure 4.8 using the red dashed trend line, which had a R^2 value of 1.

The linear change in surplus pore pressure for the 3 and 4 l/min profiles, can be seen to begin higher up in the bed at roughly 100 and 120 mm above the orifice respectively, compared to 90 mm seen in the standard experiment. Lastly, the distributions show that at heights immediately above the orifice a lower pressure was reached for higher flow rates.

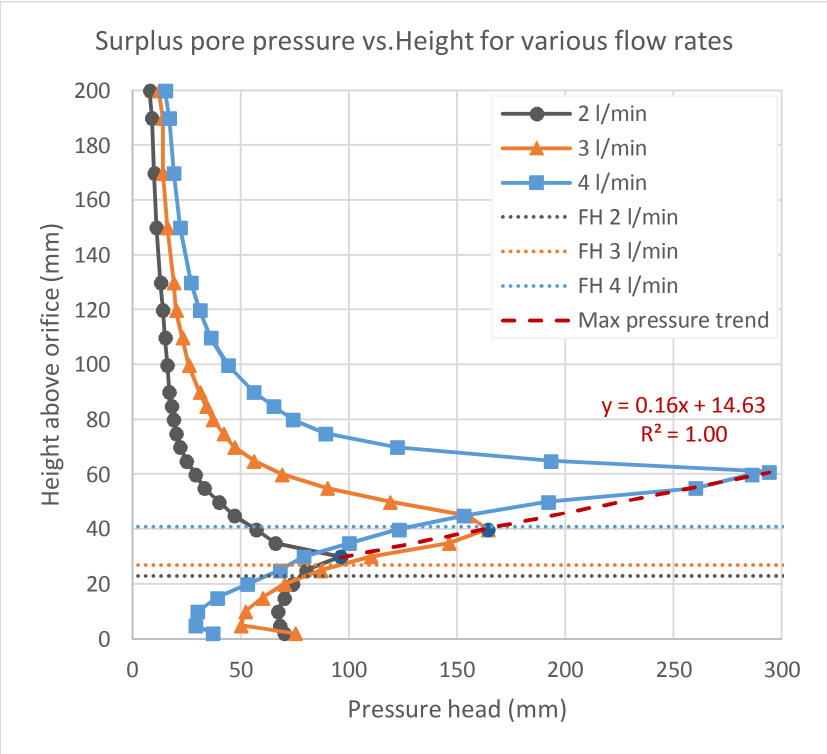

Figure 4.8: Distribution of surplus pore pressure along a vertical line directly above the orifice for various flow rates.

A plot of the maximum surplus pore pressures found along vertical slices in the horizontal direction for the various flow rates is shown in Figure 4.9. The graph shows that the distribution obtained for the increased flow rates were similar to the standard experiment, however, higher flow rates resulted in higher surplus pore pressures. This indicates that surplus pore pressures resulting from higher flow rates will diminish further away from the orifice in the horizontal direction.

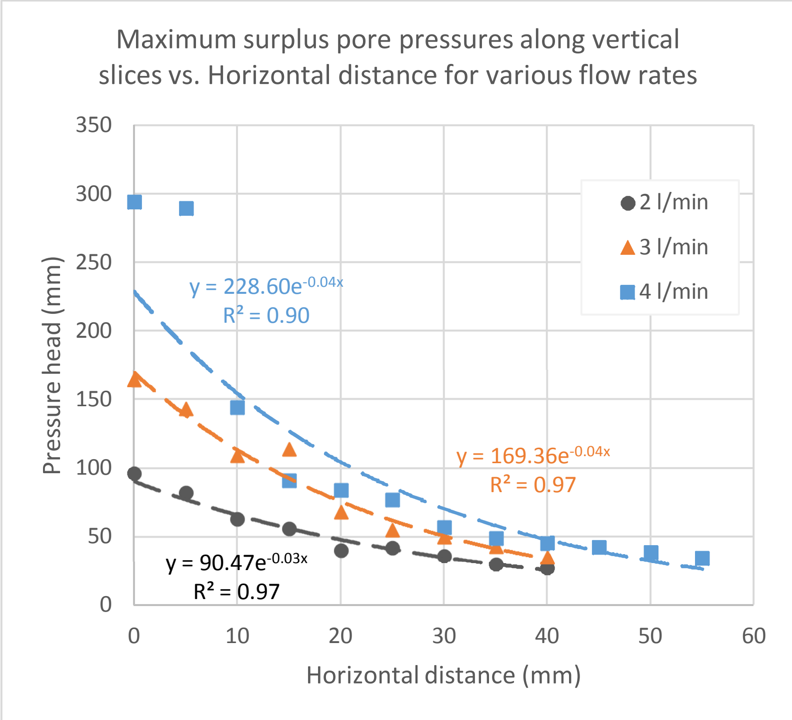

Figure 4.9: A plot of the maximum surplus pore pressure measured along vertical slices against horizontal distance for various flow rates.

A plot of the maximum surplus pore pressures and the height above the orifice at which they occurred for the various flow rates is given Figure 4.10. Again similar distributions can be see between the higher flow rates and the standard experiment with the exception that higher flow rates caused the maximum surplus pore pressures to occur higher up in the bed.

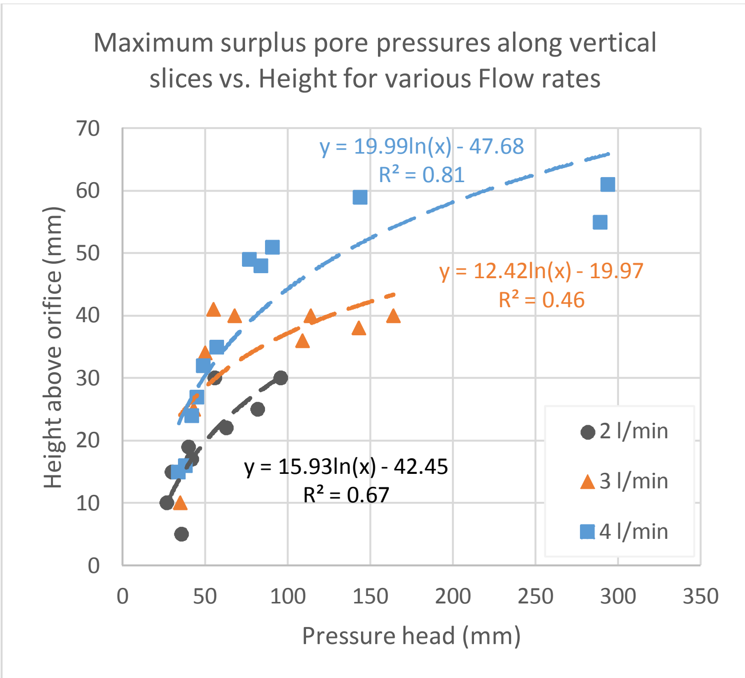

Figure 4.10: A plot of the maximum surplus pore pressure measured along vertical slices against height for various flow rates.

4.2.1.3. Velocity distribution

The velocity distribution for each flow rate is given in figure 4.11. During the 4 l/min test repeated blockage of the straight type Pitot tube prevented readings from being obtained immediately above the orifice and between the height range 10 to 45 mm. Thus, for those heights the velocity distribution was predicted based on the data obtained during the test as well as the trends that were observed in the 3 l/min test.

The results show that the velocity distribution obtained for the 3 and 4 l/min flow rate was similar to the standard experiment however, higher flow rates gave higher velocities and correspond with greater negative velocities, which occurred higher up in the bed.

Additionally, the results indicate that the velocity in the regions below the fluidisation height for the 3 and 4 l/min flow rate tests exceeded 0.8 m/s, which as seen in the standard experiment identifies turbulent flow in that region.

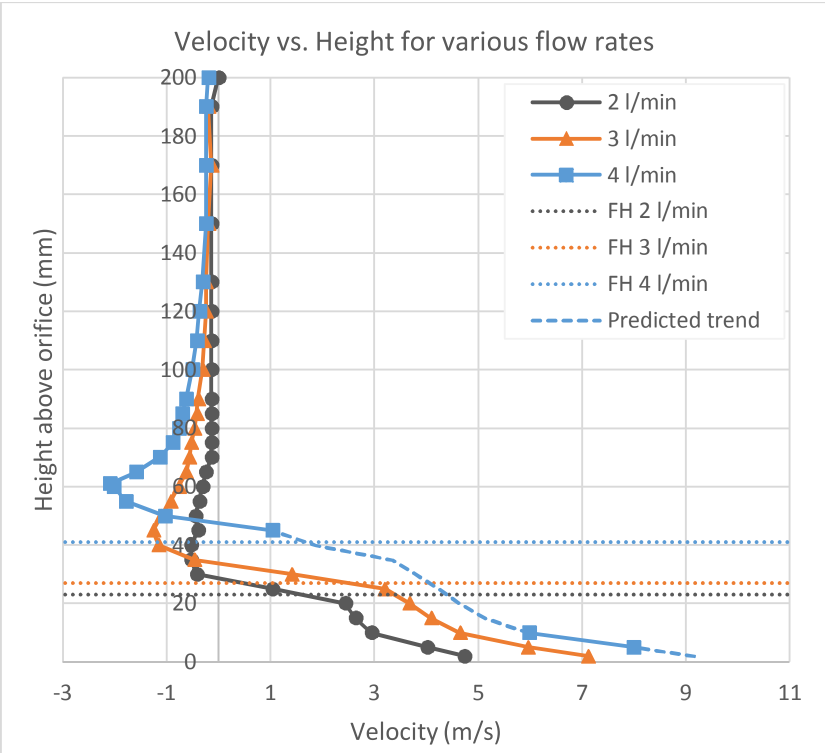

Figure 4.11: Distribution of velocity along a vertical slice directly above the orifice for various flow rates.

4.2.1.4. Surplus energy distribution

The distribution of surplus energy determined for the various flow rates is given in figure 4.12. The surplus energy distribution for 3 and 4 l/min followed a trend similar to the standard experiment, where energy was highest immediately above the orifice opening and rapidly decreased with increasing height. However between the height range 2 to 60 mm, higher flow rates gave significantly higher energies and beyond the 60 mm level the surplus energy in the bed for all cases was considerably low.

An assessment of the energy loss in the standard experiment revealed that the fluidised region acted as an energy dissipation mechanism where roughly 81 % of the available energy was lost. The same can be seen for the flow rates of 3 and 4 l/min, however, the energy loss in the fluidised regions increased to roughly 83 and 93 % respectively. Thus, larger amounts of the available energy was lost in the fluidised and mobile bed zones as the flow rate of the water jet was increased.

Therefore the sensitivity analysis revealed that by increasing the leakage rate, the surplus energy in regions closer to the orifice increased and as seen in the standard experiment, bulk of the available energy in the bed was dissipated in the fluidised regions.

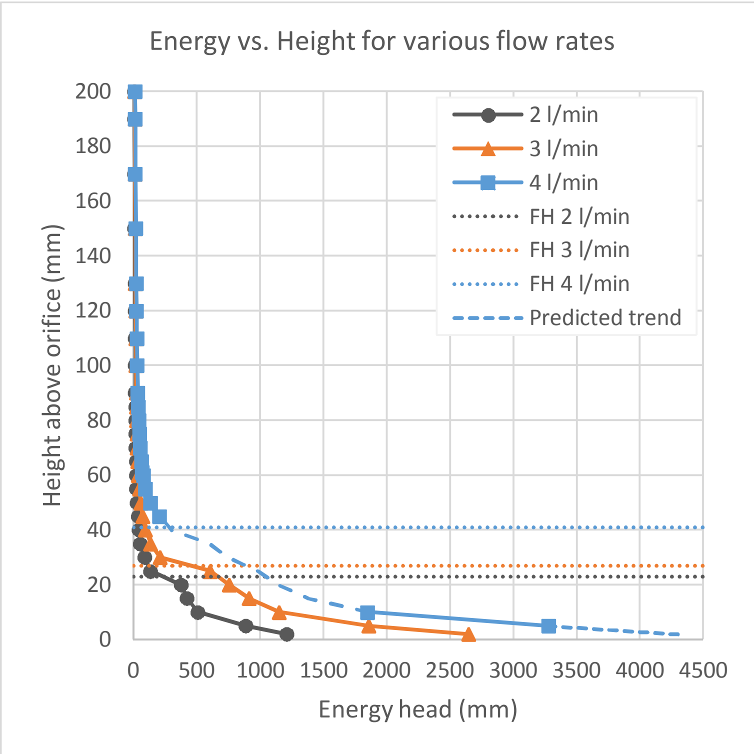

Figure 4.12: Distribution of surplus energy along a vertical slice directly above the orifice for various flow rates.

4.2.2 Effects of bed height

The effects of the bed height was investigated in individual tests where conditions in the bed were measured for the heights of 150, 200 and 300 mm. A flow rate of 2 l/min and material type A was used in each test.

4.2.2.1. <u>Fluidisation height</u>

The fluidisation heights measured for the various bed heights were 23, 38 and 43 mm in order of decreasing bed height. This is illustrated graphically in figure 4.13. The results indicate that the height of the fluidised region increased at an almost steady rate with decreasing bed height. This describes a linear relationship between fluidisation height and bed height. Thus, the data was fitted with a linear trend line, which gave the highest R^2 value of roughly 1.

When analysing the forces that acted on the particles, this type of result is expected since the mechanism that occurred during the flow rate sensitivity experiment was reversed. In this experiment the flow rate of the fluidising water jet was kept constant whilst the height of the bed varied. By decreasing the bed height the weight of the bed, which opposes the constant upward drag force was decreased. Thus, the suspended particles were able to reach greater heights.

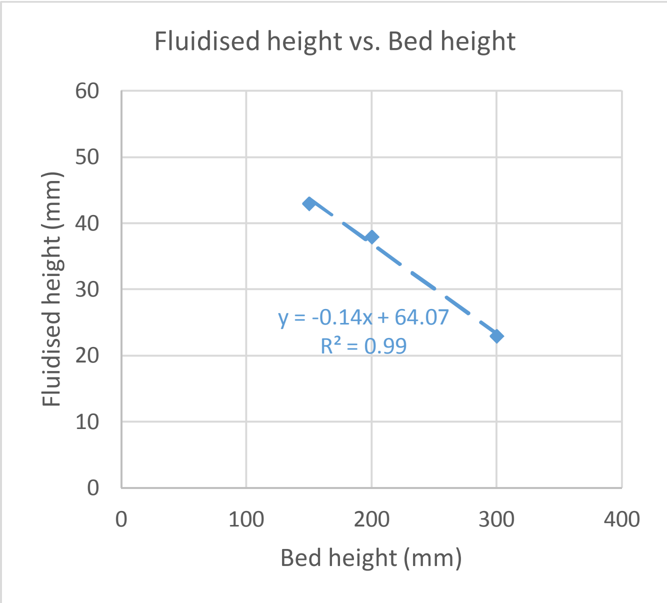

Figure 4.13: Fluidised heights measured for various bed heights.

4.2.2.2. <u>Surplus pore pressure distribution</u>

The surplus pore pressure distribution obtained for the various bed heights is presented in figure 4.14. One may notice that the surplus pore pressures although similar in distribution have been significantly altered by the changes in bed height. Evidence of this is seen in the deviations of the distributions from the standard experiment. The maximum surplus pore pressure in lower bed heights reached higher heights above the orifice and were greater in magnitude. The exact measures of maximum surplus pore pressure in the 200 and 150 mm bed were 115 and 113 mm and occurred at a height of 38 and 37 mm, respectively. Interestingly those points are not far removed from each other even though the bed height differed by 50 mm. This shows that, for considerable variation to occur a larger difference in bed height is required.

Additionally, it can be seen that the maximum surplus pore pressures did not occur consistently above the respective fluidisation heights as found in the flow rate sensitivity tests. Instead a dynamic response is observed where, as the bed height decreased the distance between the fluidisation height and maximum pore pressure also decreased resulting in the fluidisation height surpassing the height of the maximum pore pressure. Nevertheless, the two heights (fluidisation height and maximum surplus pore pressure) remained in close proximity to each other and therefore the possibility that they might occur at the same height cannot be dismissed.

The last significant deviation from the benchmark can be seen between 2 to 20 mm above the orifice where the surplus pore pressures in lower beds were consistently lower.

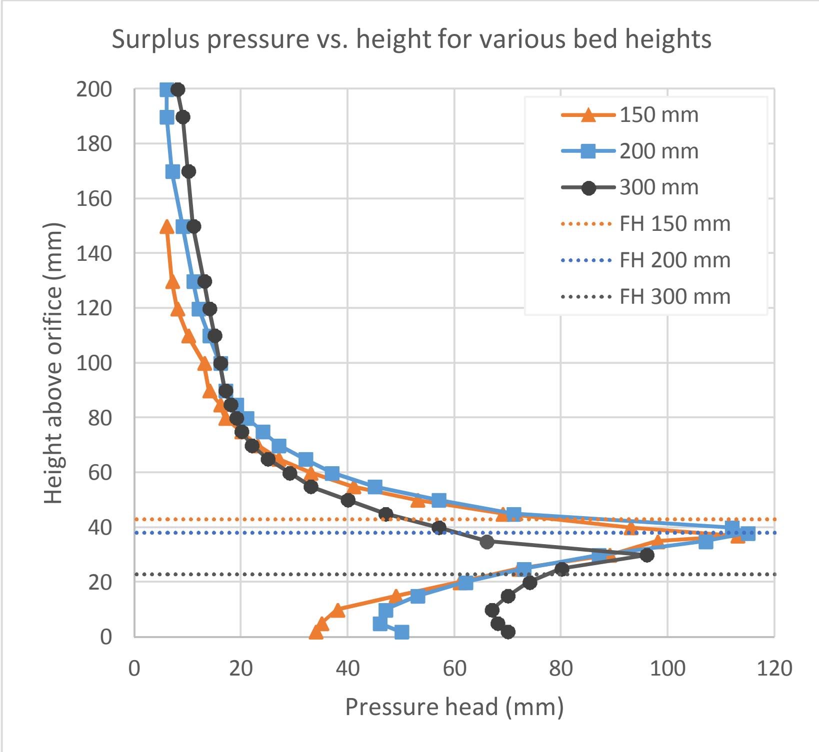

Figure 4.14: Distribution of surplus pore pressure along a vertical line directly above the orifice for various bed heights.

A plot of the maximum surplus pore pressures found along vertical slices in the horizontal direction for the various bed heights is shown in figure 4.15. The graph shows (as seen above) that the maximum surplus pore pressures directly above the orifice increased with lower bed heights, however, as distance from the orifice increased the pressures in the shallower beds diminished considerably quicker. This finding suggests that the maximum surplus pore pressure in the bed will diminish further away from the orifice with increasing bed height. The plot also shows that the trend line for the 200 and 150 mm bed height were almost identical, again illustrating that the 50 mm difference in bed height was not sufficient to create a significant change.

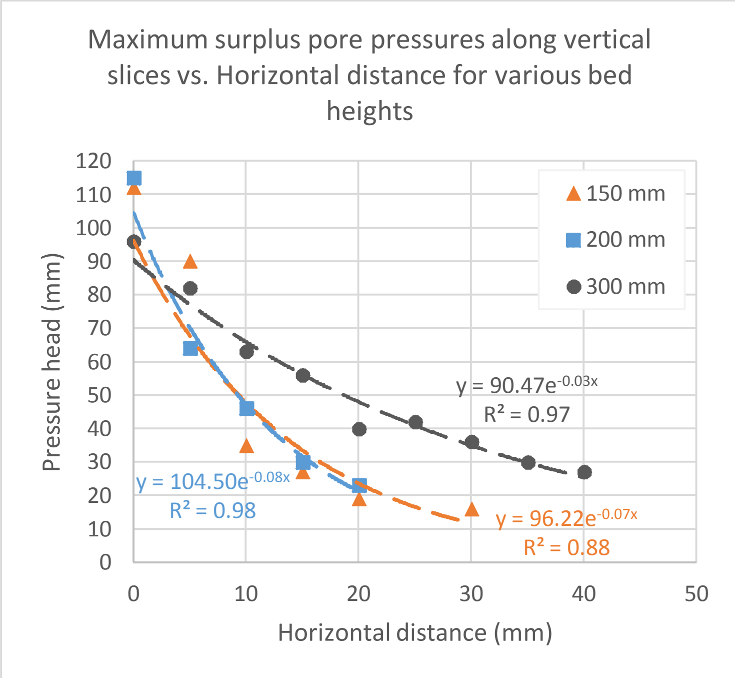

Figure 4.15: A plot of the maximum surplus pore pressure measured along vertical slices against horizontal distance for various bed heights.

The maximum surplus pore pressures and corresponding heights above the orifice measured in the various bed heights is given in figure 4.16. The data remained relatively scatted but with a general trend that showed that, the distributions occurred high up in the bed as the bed height decreased. A linear trend line was used for the 150 mm bed height since it gave the highest R^2 reading of 0.13.

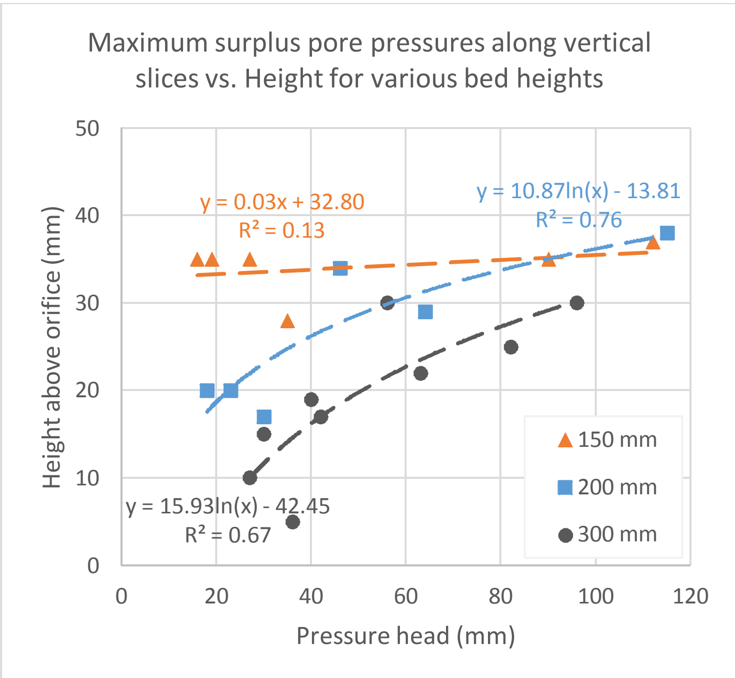

Figure 4.16: A plot of the maximum surplus pore pressure measured along vertical slices against height for various bed heights.

4.2.2.3. Velocity distribution

The velocity distribution obtained for the various bed heights is presented in figure 4.17. The results indicate that the velocity distribution in the 200 and 150 mm beds followed a pattern similar to that obtained in the standard experiment. However, larger negative velocities formed in the shallower beds at slightly higher heights.

Interestingly in the 200 and 150 mm beds, the height of the respective fluidised zones surpassed the height at which the turbulent flow regime ends (i.e. when velocity equals 0.8 m/s). Unlike before this suggests that flow in the 200 and 150 mm beds transitioned from turbulent to transitional in the fluidised region.

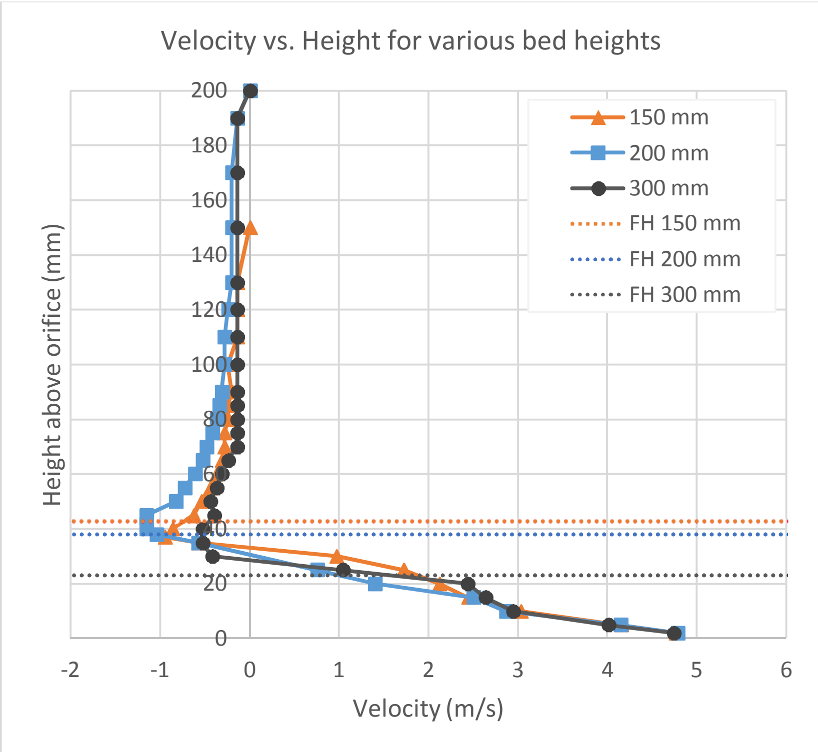

Figure 4.17: Distribution of velocity along a vertical slice directly above the orifice for various bed heights.

4.2.2.4. Surplus energy distribution

The distribution of surplus energy determined for the various bed heights is given in figure 4.18. Interestingly, even though the bed height was varied using 200 and 150 mm the energy distribution was remarkably similar to the energy distribution found in the standard experiment. A slight deviation from the standard experiment energy line can be seen between the height range 10 to 40 mm for both bed heights, however, no obvious trends can be seen across the tests. At heights greater than 40 mm the energy in the bed for all cases decreased to a negligible amount.

The energy loss in the fluidised region for the bed height of 200 and 150 mm amounted to roughly 96 % in both experiments. This indicates an increase of energy loss in the fluidised regions when compared to the 81 % established in the standard experiment. Therefore, varying the bed height did not significantly change the behaviour in which the surplus energy in the bed was distributed or dissipated.

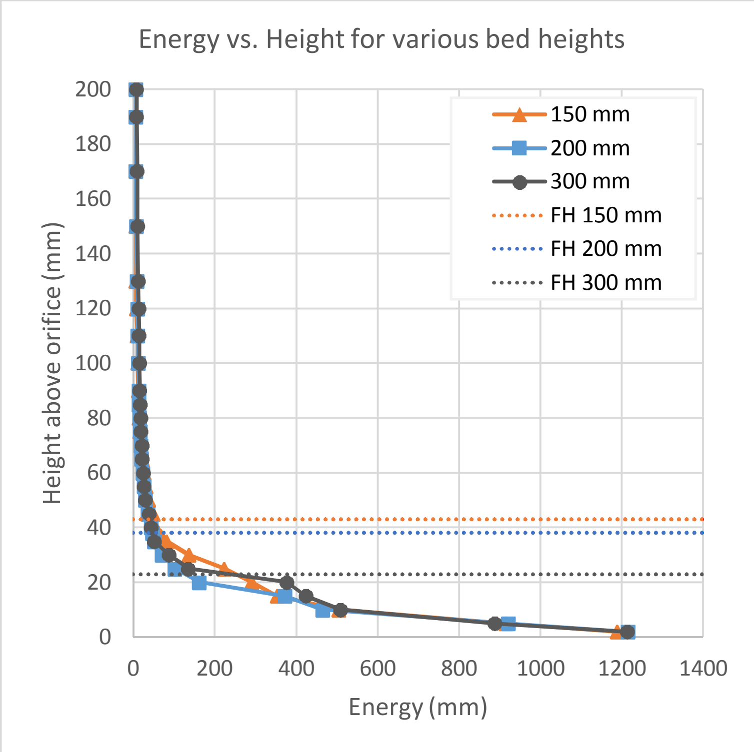

Figure 4.18: Distribution of surplus energy along a vertical slice directly above the orifice for various bed heights.

4.2.3 Effects of particle size

The effects of particle size was investigated by measuring conditions in separate beds consisting of material type A, B and C. A flow rate of 2 l/min and a bed height of 300 mm was used each test.

4.2.3.1. <u>Fluidisation height</u>

The fluidisation heights measured in material type A, B and C were 24, 23 and 19 mm respectively. This is illustrated graphically in figure 4.19 using the d_{50} particle size for each material type. The d_{50} for material A, B and C was 0.72, 0.66 and 0.77 mm, respectively. The results indicate a small increase in the height of the fluidised region before rapidly decreasing as the average particles size in the bed increased. The fluidisation height difference between material type A and B was just 1 mm. This points to the idea that there might be a minimum particle size below which the fluidised region is not influenced by particle size. However, further investigation will be required to confirm this.

Stokes' law (equation (16) discussed in section 2.4.7.2) could be used to explain the outcome of this experiment. According to stokes' law the drag force required to suspend a particle is directly proportional to the particle diameter. A larger particle would require a larger drag force for it to become suspended at a constant height. During the experiments the drag force induced on the particles did not vary. It remained constant since the flow rate of the fluidising jet used during the tests was kept constant. Thus, a small increase in particle size was sufficient for fluidisation to occur but at a relatively lower height.

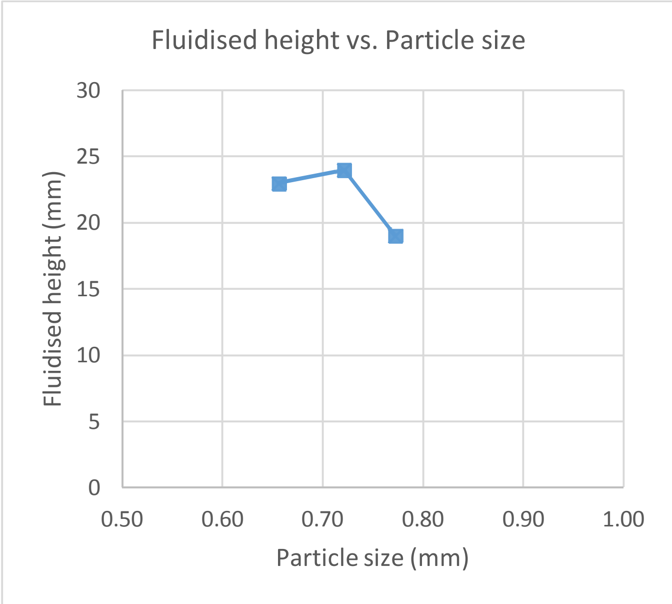

Figure 4.19: Fluidised heights measured for various particle sizes.

4.2.3.2. <u>Surplus pore pressure distribution</u>

The surplus pore pressure distribution obtained in the individual beds consisting of material type A, B and C is presented in figure 4.20. The surplus pore pressure distribution in the bed with the larger and smaller particles (material C and B respectively) produced the typical shape described for the standard experiment, however, some significant deviations and similarities are observed when compared to the standard experiment.

In material type C the surplus pore pressure distribution was consistently lower at corresponding heights above the orifice. Additionally, the magnitude of the maximum surplus pore pressure was considerably lower and occurred slightly closer to the orifice.

In material type B the surplus pore pressure distribution below the 30 mm height level resulted in higher pressures, while above this level the distribution between the standard experiment and in material B matched. The magnitude of the maximum surplus pore pressure in material type B was higher but occurred at almost the same height above the orifice as in the standard experiment.

Finally, figure 4.20 shows that the fluidisation heights occurred slightly below the maximum surplus pressure points and that the linear change in pressure began at approximately 90 mm above the orifice in all three material types.

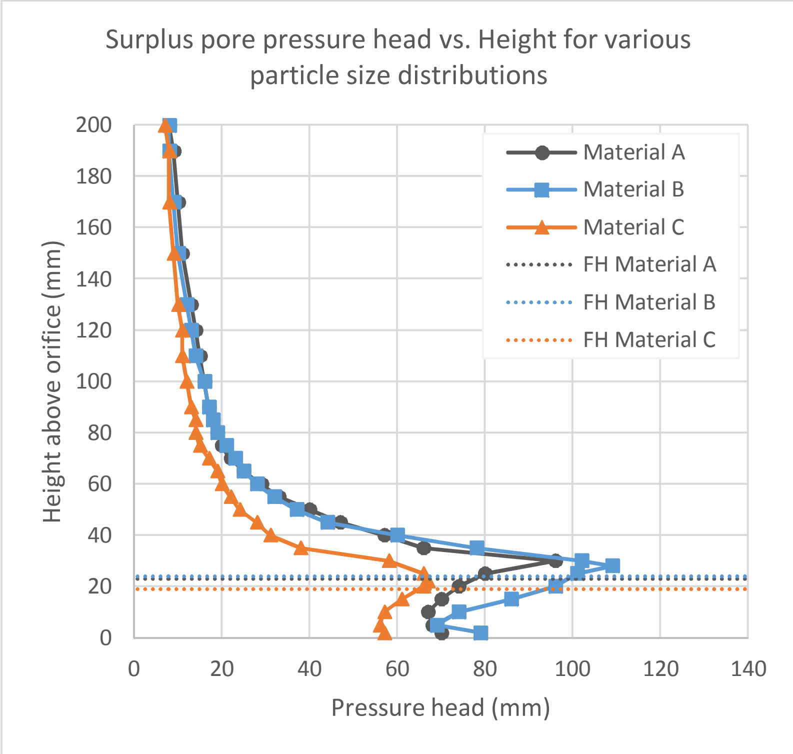

Figure 4.20: Distribution of surplus pore pressure along a vertical line directly above the orifice for various particle sizes.

A plot of the maximum surplus pore pressures found along vertical slices spaced in the horizontal direction for the various material types is shown in figure 4.21. The graph shows that the distribution obtained in Material type C was constantly lower than the benchmark curve. In material type B the distribution began higher than the benchmark curve but decreased to meet the distribution obtained in material type C as the distance in the horizontal direction increased.

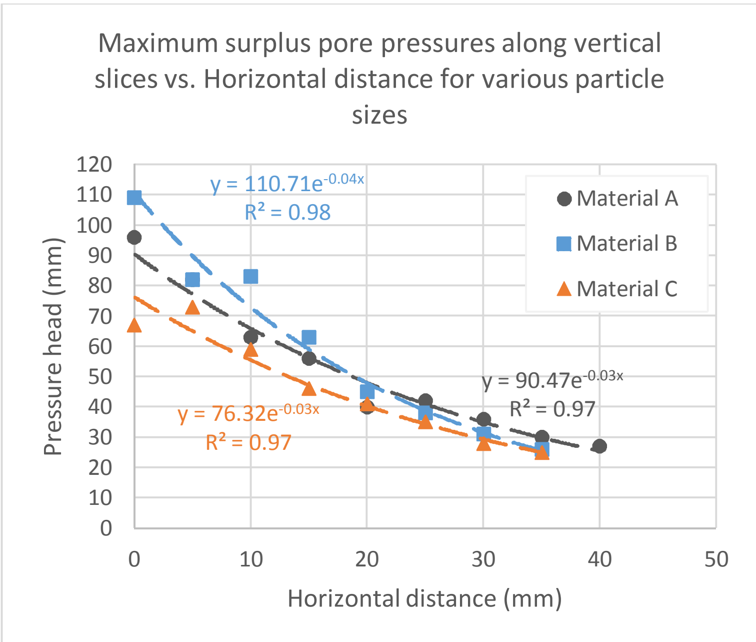

Figure 4.21: A plot of the maximum surplus pore pressure measured along vertical slices against horizontal distance for various particle sizes.

The maximum surplus pore pressures and corresponding heights above the orifice measured in the various material types is given in figure 4.22. As before, the data remained relatively scatted but general trends were observable. The distributions between the standard experiment and Material type B was almost the same while the distribution in material type C differed significantly with the maximum surplus pore pressures occurring higher up in the bed as distance away from the orifice increased.

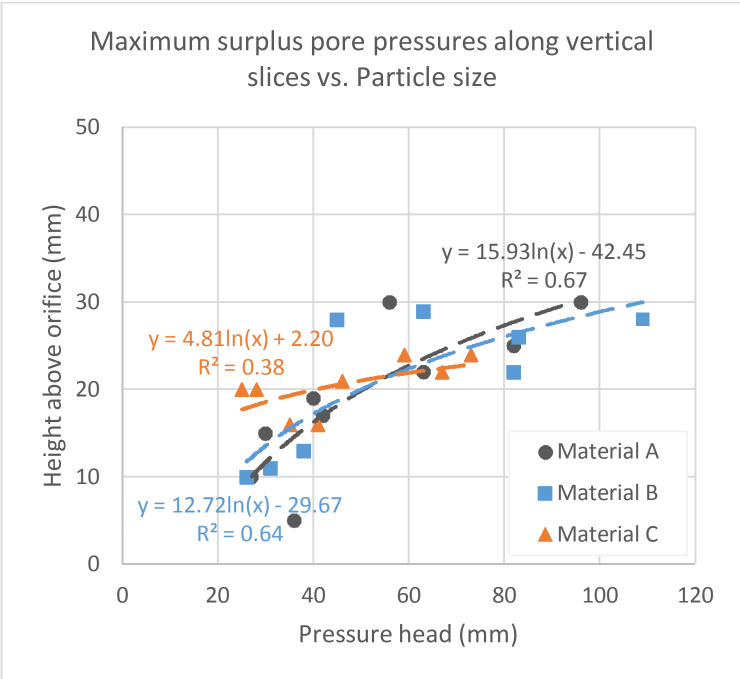

Figure 4.22: A plot of the maximum surplus pore pressure measured along vertical slices against height for various particle sizes.

4.2.3.3. Velocity distribution

The velocity distribution determined in the various material types is given in figure 4.23. According to the results the velocity distribution in material type B was almost identical to the distribution found in material type A, which was used in the standard experiment. Unlike in material type A and B, no negative velocities developed in the bed consisting of material type C. Instead, the distribution in material type C remained positive suggesting that the fluid was consistently in the upward direction along the centre line (Y = 0 mm) of the fluidised region.

Interestingly, the beds consisting of material type A and B had a permeability of 0.288 cm/s whilst the bed made up of material type C had a higher permeability of 0.411. This implies that the permeability of the beds could be the cause for the similarities and differences noticed between the velocity distributions as well as the pore pressure distributions (figure 4.20).

The reason for material type A and B having the same permeability even though the particle distribution and average particle size of the two materials differed can be understood by analysing the d_{10} particle size for each material. According to equation (5) (in section 2.3.1) the permeability of a soil bed is greatly influenced by the d_{10} particle size of the soil and since both material types had almost equal d_{10} particle sizes (shown in figure 3.8) the permeability of the materials were the same. Material type C had a higher d_{10}, which resulted in a higher permeability in the bed. Therefore, in addition to the size of the particles in the bed affecting the fluidised region the fines in the bedding material may also have a significance influence, which should not be ignored.

Lastly, it is noticeable that in each velocity distribution the flow in the fluidised region was greater than the corresponding benchmark velocities that identifies turbulent flow. The turbulent benchmark velocity for material A, B and C were approximately 0.8, 0.9 and 0.7 m/s respectively. This outcome is consistent with the findings in flow rate sensitivity tests.

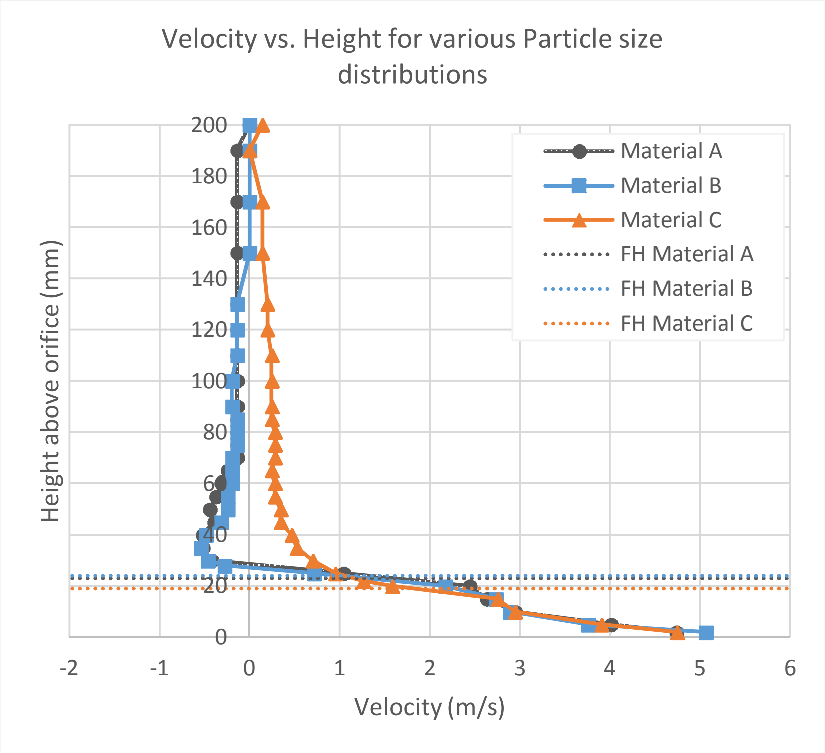

Figure 4.23: Distribution of velocity along a vertical slice directly above the orifice for various particle sizes.

4.2.3.4. Surplus energy distribution

The distribution of surplus energy determined in the separate beds consisting of material type A, B and C is shown in figure 4.24. According to the results the energy distribution attained in material B and C closely matched the distribution obtained in the standard experiment, except for small deviations observed between the height range 10 to 30 mm and immediately above the orifice. In the height range 10 to 30 mm the energy distribution for material B was identical to the standard experiment whereas the distribution for material C was lower.

In the region above the orifice, the distribution for the standard experiment and material type C were similar but material type B experienced higher energies closer to the orifice. The deviations from the standard experiment were significantly small and no obvious trend in the variations can be identified across the tests. At heights beyond the 30 mm level the energy in the bed in each experiment decreases to negligible amounts.

The magnitude of energy loss in the fluidised region for material B and C amounted to roughly 86 and 80 % respectively. This indicates a slight decrease of the bulk energy loss occurred in the fluidised regions for increasing particle sizes. Nevertheless, the sensitivity analysis revealed that varying the size of the particles in the bed did not significantly affect the surplus energy distribution and the dissipation mechanism.

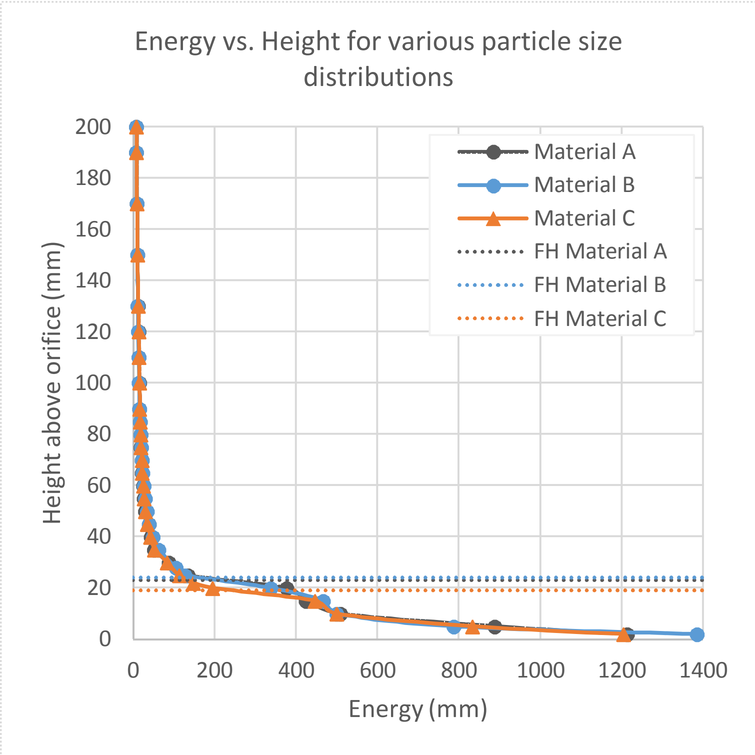

Figure 4.24: Distribution of surplus energy along a vertical slice directly above the orifice for various particle sizes.

4.3 Discussion of results regarding leak discovery

The outcome of the sensitivity analysis illustrated that elements such as the leakage flow rate, pipe cover depth and the size of the particles in the bedding material when altered brought about varying degrees of changes, which could influence leak discovery.

In the leakage flow rate study, the height of the fluidised region, which occurs during the soil-leak interaction grew exponentially by increasing the leakage rate. It could be deduced that should a sufficiently high flow rate be applied to a leak, it could grow to become visible on the ground surface. Conversely, for smaller leaks (low leakage rate) the fluidisation height will be relatively small resulting in the leak being concealed beneath the bed, making it substantially more difficult to detect.

In the study that investigated the influence of bed height, it was found that the height of the fluidised region decreased linearly with increasing cover depth. Thus, pipes with large cover depths will result in greater difficulty of locating leaks.

The results from the experiments that examined the effect particle size revealed that if larger particles are used to form the bedding material, the height of the fluidised region for an upright vertical leak will reduce. This in turn will reduce the possibility of locating and repairing the leak.

When the results from all three soil-leak parameters are considered, the leakage flow rate had the greatest impact on the fluidised zone, with bed height and particle size playing lesser roles. However, the bed heights used in this study varied little, and may have a greater impact in practice. Therefore based on the findings from the experiments conducted in this study, the possibility of finding a leak will increase for higher leakages rates, lower cover depths and smaller diameter particles in the bedding material.

4.4 Comparison of leakage conditions between side and centre orifice

An additional investigation was conducted to establish whether leakage conditions such as fluidisation height, surplus pore pressure, vertical velocity and surplus energy distributions gave similar readings at the centre and side orifice. The results are given below.

4.4.1 Fluidisation height

A plot of the fluidisation heights measured at the side and centre orifice is shown in figure 4.25. The plot shows that the fluidisation height at both orifices increased at an increasing rate as the flow rate increased. This describes an exponential relationship. Additionally, the results shows that the fluidisation height measured at each orifice was the same for the flow rate of 2 and 3 l/min but began to deviate for flow rates greater than 3 l/min, with the fluidisation heights at side orifice being significantly lower.

The fluidisation heights at the side orifice during this investigation were measured using image analysis whereas the fluidisation heights at the centre orifice were measured by adopting the method of listening for the scrambling noise as the straight type Pitot tube was inserted into the bed directly above the orifice. Therefore, it is possible that for the flow rate of 4 l/min the Pitot tube may have influenced the fluidisation height measured at the centre orifice by loosening the bedding material above the fluidised region, which caused it to rise higher and vary considerably from the fluidisation height obtained at the side orifice. Moreover, readings of fluidisation height for each flow rate was measured once at each orifice hence, the results may show significant deviations should outliers exist in the measured data. A more accurate approach would have been to find an average of at least three readings for each flow rate at each orifice.

In a related experiment, Bailey (2015) determined the fluidisation height and properties such as area and volume of the fluidised and mobile zones for the flow rates of 1, 2 and 4 l/min at the side orifice by also adopting the image analysis method. The fluidisation heights obtained in that experiment are included in figure 4.25.

When compared to the results attained in this study, it is noticeable that the fluidisation heights found for the flow rates of 1 and 2 l/min seem to match closely but once again the fluidisation heights measured for 4 l/min does not. In Bailey's (2015) experiment the fluidisation height measured at the 4 l/min flow rate was lower by 8 mm, which equates to a fluidised region that was approximately 27 % smaller in height. This finding highlights the possibility for properties of the fluidised region to vary even though the parameters such as soil type, bed height and leakage flow rate remained constant, which reiterates the need for average readings to be used.

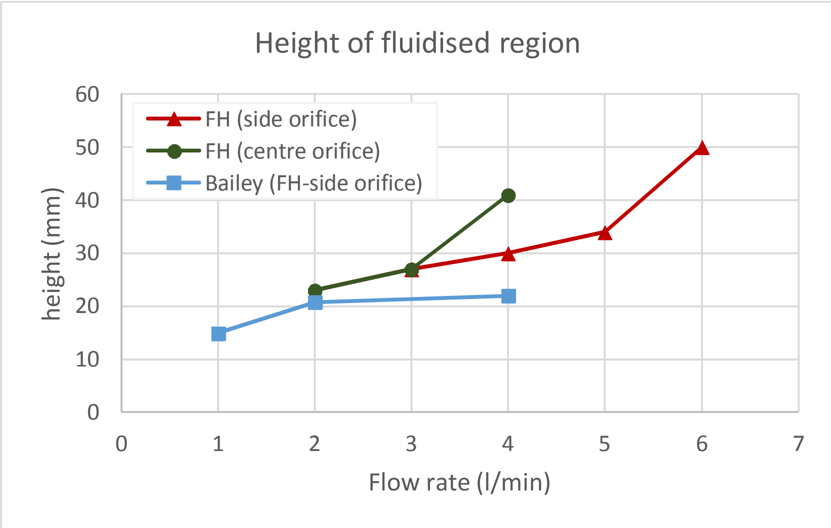

Figure 4.25: Comparison of fluidisation heights between the centre and side orifice.

4.4.1.1. Measurement of fluidisation geometry at the side orifice

Data regarding the area and volume of the fluidised region could be extrapolated from the images that were taken at the side orifice, using the extrapolation methods that were described in section 3.4.2.6. The results for the area of the fluidised and mobile bed zones that were in contact with the tank wall for increasing flow rates is given in Figure 4.26. Bailey's (2015) results from a similar experiment are also included for comparison purposes.

The results obtained in the current study shows good agreement with Bailey's (2015) findings, which described a linear relation between the area of the fluidised and mobile bed zone and flow rate. However, this relationship can be seen to be true only for flow rates less than 4 l/min. At higher flow rates the area of the fluidised and mobile bed zone begin to increase exponentially.

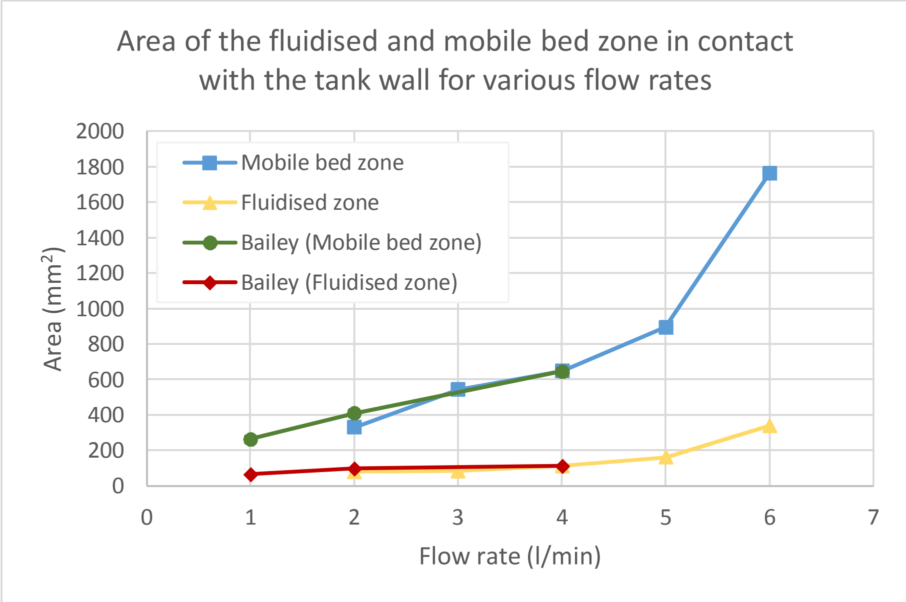

Figure 4.26: A plot of the area of the fluidised and mobile bed zone in contact with the tank wall for various flow rate.

Concerning the results for volume of the fluidised and mobile bed zone for increasing flow rates (given in figure 4.27 and figure 4.28 respectively), there lies a relatively large discrepancy between the results obtained in the current study and Bailey's (2015) findings. The results from the current study shows higher values for the fluidised and mobile bed zones as the flow rate increased. The reason for this is unknown. Furthermore as seen above, in the current study an exponential relationship begins to develop between the volumes of the respective zones and flow rate when the flow rate exceeds 4 l/min.

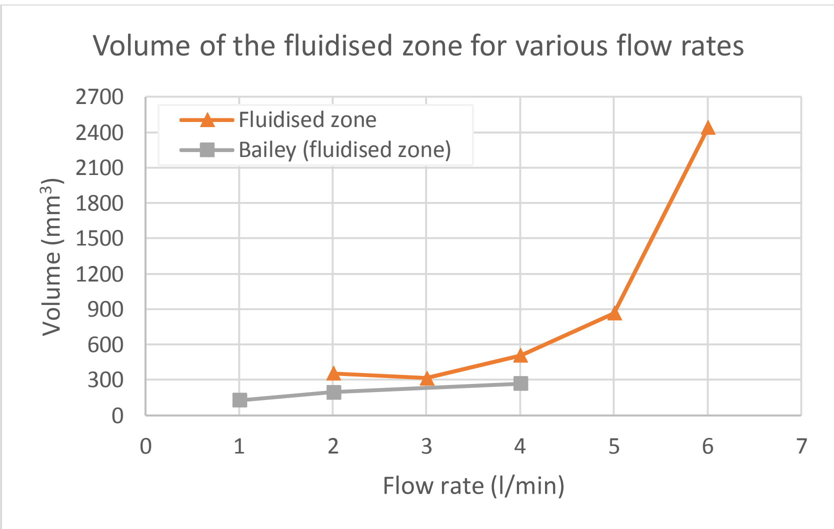

Figure 4.27: A plot of the area of the fluidised and mobile bed zone in contact with the tank wall for various flow rate.

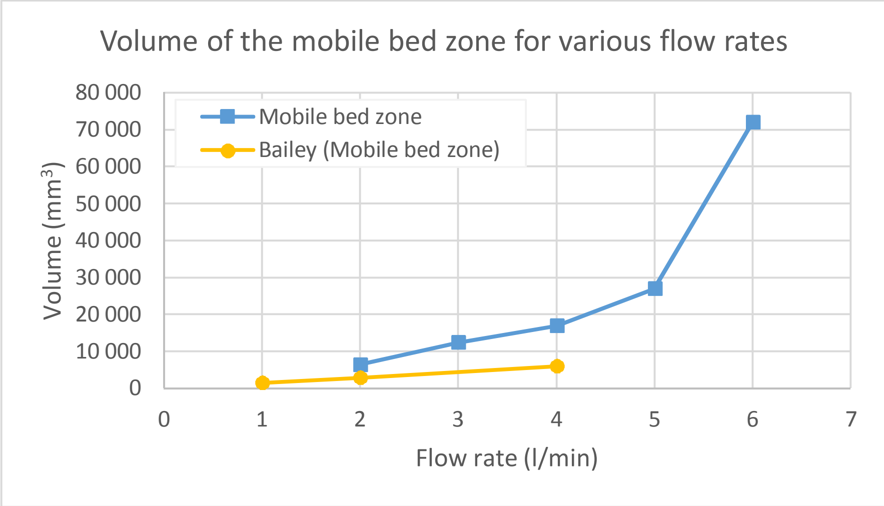

Figure 4.28: A plot of the area of the mobile bed zone in contact with the tank wall for various flow rate.

4.4.2 Pore pressure, velocity and energy distributions

Surplus pore pressure distributions determined at the centre and side orifice is given in figure 4.29. The trend of both distributions have are similar to the standard experiment, however, the surplus pore pressures measured at the side orifice up to a height of roughly 130 mm above the orifice were significantly higher than the surplus pore pressures measured at the centre orifice. Beyond this height the distributions seem to come together.

Fluidisation at the side orifice formed against the tank wall, it is believed that the wall may have been responsible for the higher surplus pore pressures measured at the side orifice. The wall restricted the fluidised region from reaching its full geometric form. Consequently, when the fluid and ballotini particles were project toward or onto the glass wall they were forced to decelerate and/or take a path that deviated from its original trajectory. This process in turn would have caused the pore pressure surrounding the fluidised region to increase, which was recorded during the experiment.

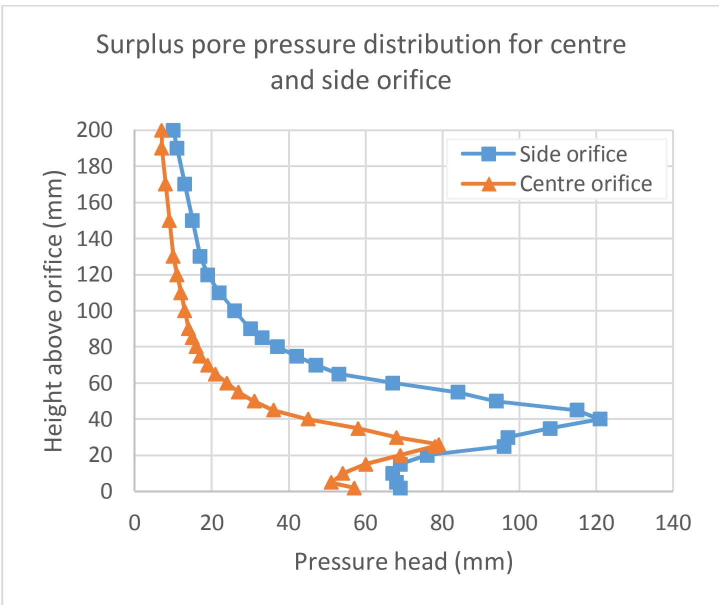

Figure 4.29: Comparison of surplus pore pressure distribution between the centre and side orifice.

The distributions for vertical velocity is shown in figure 4.30. It can be seen from the plot that the two distributions do not match. The only similarity between the distributions can be seen just above the orifice where the readings for vertical velocity was the highest and were almost equal in magnitude.

It is noticeable that the velocities in each test were low, ranging between negative 0.5 and positive 0.78 m/s. It was previously pointed out that, the Pitot tubes may not have been able to accurately measure low velocity heads. This could explain why the two distributions in figure 4.30 show large variations from each other. The interference of the tank wall on the fluidised region as described above may also have had an influence in causing the disparities between the velocity distributions.

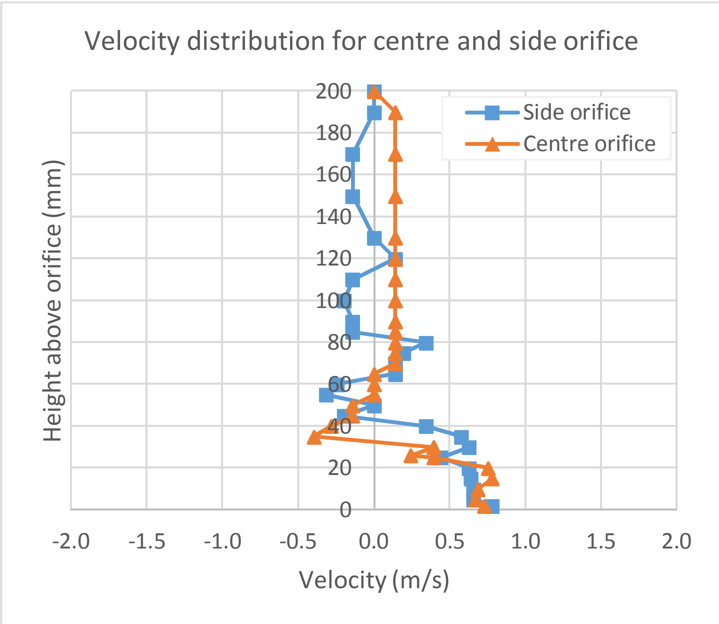

Figure 4.30: Comparison of velocity distribution between the centre and side orifice.

The surplus energy distributions found for each orifice is shown in figure 4.31. It is important to note that the energy determined in the graph consists only of the vertical velocity component. Since measurements were taken along the vertical line 7 mm from each orifice, flow in the horizontal direction should not have been ignored. The resultant velocity between the vertical and horizontal components should have been used to determine the energy at each point to form the distributions.

Nevertheless, the pattern of the energy distributions are similar to the pore pressure distribution, which suggests that the velocity component was significantly small to have a considerable impact on the distributions. Furthermore, since the pore pressures measured at the side orifice were generally higher than the centre orifice, the energy distributions show the same trend.

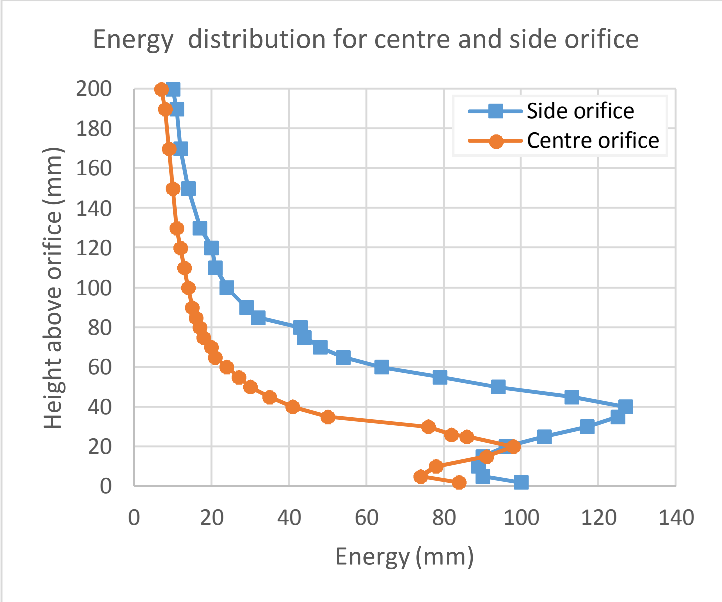

Figure 4.31: Comparison of surplus energy distribution between the centre and side orifice.

5. Conclusion and recommendations

This chapter summarises the main findings of the investigation and discusses recommendations for improving the experimental equipment as well as future research.

5.1 Summary of study

In this study, experimental research was conducted on unbound soil-leak interaction from a point source. This was achieved by injecting a centrally located jet of water in a fully saturated bed of idealised granular particles (ballotini) that was housed in a custom built glass tank.

A standard method of investigation was used, where an experimental setup including straight and L-type Pitot tubes were utilized to obtain readings of surplus pore pressure, velocity and surplus energy in the ballotini bed. Readings were taken at points directly above the orifice through which the water jet entered the tank. Measurement of fluidisation height and maximum surplus pore pressure along vertical slices that increased in the horizontal direction from the orifice were also taken. The measured readings were used to develop distributions, which were utilised to perform a sensitivity analysis of how leakage conditions (i.e. surplus pore pressure, velocity and energy) in the bed changed when soil-leak parameters including the jet flow rate, bed height and particle size were varied.

Modifications were made to some of the equipment. Therefore, the modified equipment and the techniques that were used to conduct the experiments were subjected a validation process before the main experiments were conducted. This was done to ensure that the results that were obtained were accurate and reliable. The validation process was carried out by means of repeatability analysis. The results showed that the modified equipment was competent and the experimental techniques were implemented correctly.

In addition to the main experiment another investigation was conducted to determine whether leakage conditions at the centrally located orifice were the same as a second orifice on the tank base, which was located adjacent to a tank wall. The second orifice was termed "side orifice".

5.2 Summary of findings

5.2.1 Standard experiment

A standard experiment was conducted to serve as a benchmark to which the results from the sensitivity experiments could be compared. The distributions found in the standard experiment can also be seen as typical curves, since similar trends were seen in the sensitivity experiments. The typical distribution found for the surplus pore pressure, velocity and surplus energy is described in this section. A graph for each of the trends is given to support the descriptions.

Typical surplus pore pressure distributions

The typical pore pressure distribution along the line above the orifice is illustrated in figure 5.1. It shows that the surplus pore pressure in the bed, immediately above the orifice, experiences a decrease before increasing to reach a maximum surplus pore pressure. At heights beyond the maximum point, the surplus pore pressure initially decreases at a relatively rapid rate and then slows down to a point where the pressure change can be seen to take on a linear trend. The linear trend indicates Darcy flow.

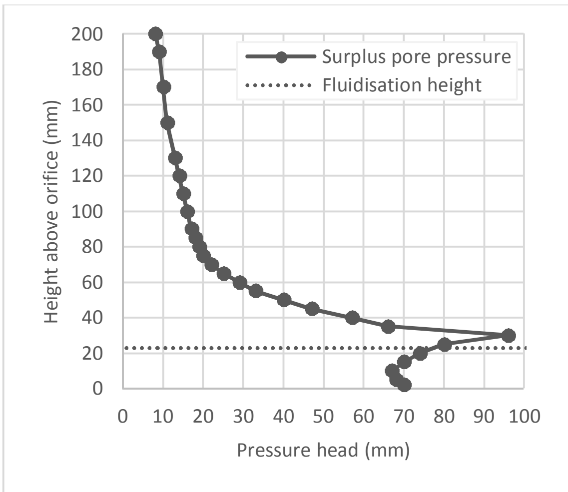

Figure 5.1: Typical surplus pore pressure distribution.

The typical distribution for maximum surplus pore pressure found along vertical slices for distances in the horizontal direction is given in figure 5.2. The plot shows that the highest maximum pore pressure occurs directly above the orifice and as distance from the orifice increased the maximum surplus pore pressures decreased at a decreasing rate. This describes an exponential trend.

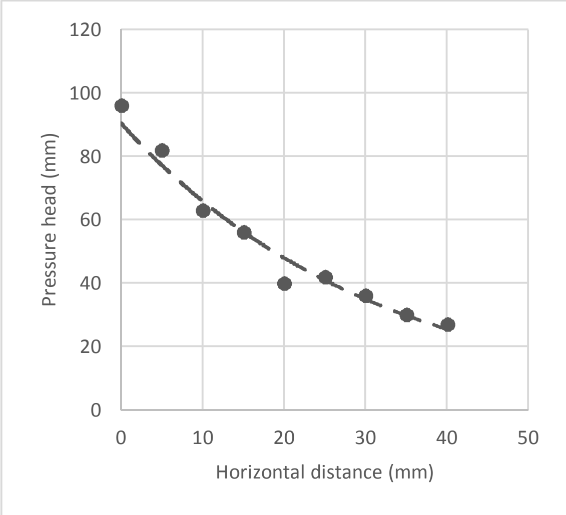

Figure 5.2: Typical distribution for maximum surplus pore pressures along vertical slices in the horizontal direction.

Typical velocity distribution

The typical velocity distribution along the line above the orifice illustrated in figure 5.3 shows that the highest recording of velocity occurs in the regions closest to the orifice. The velocity rapidly decreases with increasing height above the orifice and reaches negative values in regions just above the fluidisation height, where it peaks before decreasing to zero. The presence of the negative velocities in the distribution is an indication of backflow (i.e. flow toward the orifice).

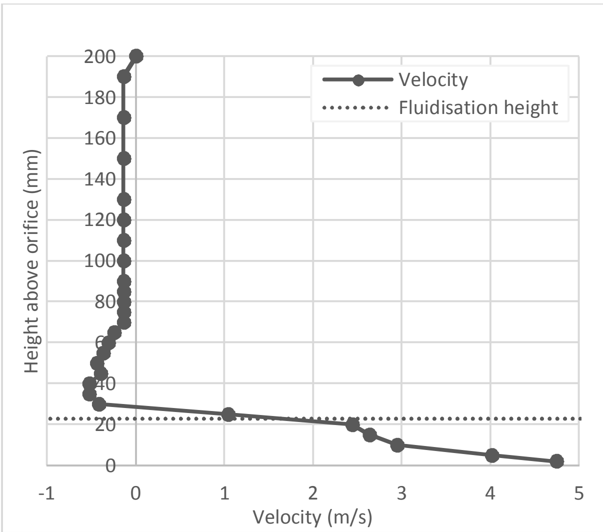

Figure 5.3: Typical velocity distribution.

Typical surplus energy distribution

The typical surplus energy distribution along the line above the orifice illustrated in figure 5.4 shows that the surplus energy was highest immediately above the orifice opening. The energy rapidly decreased as height above the orifice increased. At heights beyond a certain point, the energy reduces to negligible amounts. In figure 5.4 this occurred at 60 mm above the orifice. Furthermore, the distribution shows that majority of the available energy was dissipated in the fluidised zone i.e. below the fluidisation height.

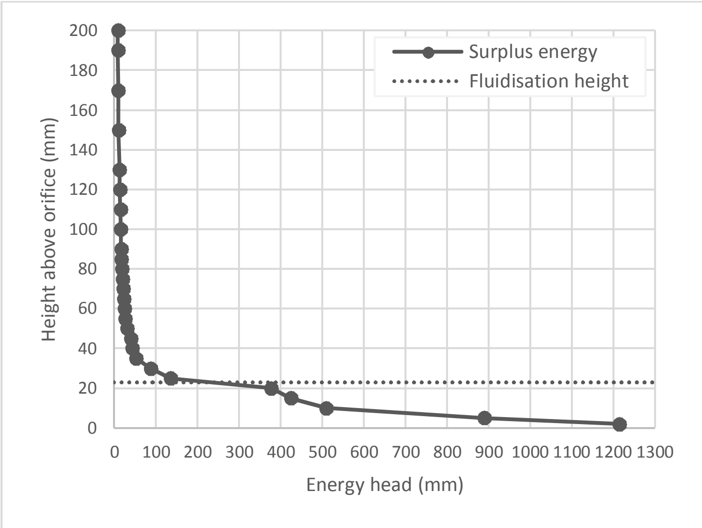

Figure 5.4: Typical surplus energy distribution.

5.2.2 Sensitivity experiments

The effects of increasing the jet flow rate resulted in the following findings:

- The height of the fluidised region increased.
- Both the magnitude and height (above the orifice) of the maximum surplus pore pressure reached higher values.
- The position of maximum surplus pore pressures were consistently higher than corresponding fluidisation heights.
- Darcy flow began higher up in the bed.
- The maximum surplus pore pressures in the horizontal direction diminished further away from the orifice.
- Larger velocities were measured at the injection point.
- Larger negative velocities were measured, which occurred higher up in the bed.
- Flow in the fluidised regions corresponded with turbulent flow, according to Re_{inte}.
- Higher readings of surplus energy occurred in regions closer to the injection point.
- Majority of the measured energy was lost in the fluidised zone.
- Percent of energy dissipation in the fluidised zone increased.

The effects of decreasing the bed height resulted in the following findings:

- The height of the fluidised region increased.
- Both the magnitude and height (above the orifice) of the maximum surplus pore pressure reached higher values.
- The fluidisation height surpassed the height of the maximum surplus pore pressure but both elements remained in close proximity to each other.
- The maximum surplus pore pressures in the horizontal direction diminished closer to the orifice.
- For considerable pore pressure variation to occur, a significant difference in bed height is required. The bed heights of 200 and 150 mm gave similar results.

- Larger negative velocities formed in the beds at slightly higher heights.
- Unlike in other tests turbulent and transitional flow occurred in the fluidised region.
- Majority of the measured energy was lost in the fluidised zone.
- Percent of energy dissipation in the fluidised zone increased.

The effects of increasing the particle size in the bed resulted in the following findings:

- The height of the fluidised region decreased.
- The maximum surplus pore pressures occurred closer to the orifice and were lower in magnitude.
- The position of maximum surplus pore pressures were consistently higher than corresponding fluidisation heights.
- The maximum surplus pore pressures in the horizontal direction diminished at roughly the same distance from the orifice.
- Large negative velocities did not occur in the bed.
- Flow in the fluidised regions corresponded with turbulent flow, according to Re_{inte}.
- Majority of the measured energy was lost in the fluidised zone.
- Percent of energy dissipated in the fluidised zone remained almost the same.

5.2.3 Comparison of leakage conditions between centre and side orifice

Based on the results obtained from the test that compared fluidisation heights, it can be concluded that the results gave evidence that the height of the fluidised regions for corresponding flow rates obtained at the centre and side orifice could be the same.

Analysis of the surplus pore pressure, vertical velocity and surplus energy distributions found at centre and side orifice reviled large disparities between corresponding distributions, which suggested that leakage conditions at the two locations are not the same. Therefore, interchanging measurements of surplus pore pressure, velocity and surplus energy between the orifices would be misleading. Interference of the tank wall and limitations with the Pitot tubes of accurately measuring low pore pressure and velocity heads was thought to be factors that caused the disparities of the results between the two orifices.

5.2.4 Main Conclusions

- It was found that the flow rate of the jet that fluidised the bed had considerable influence on the distribution of surplus pore pressure, velocity and surplus energy along the line directly above the orifice. Larger pore pressures, velocities, energies and fluidisation heights were measured for jets with larger flow rates.
- The distribution of surplus pore pressure directly above the orifice and the height of the fluidised region was mostly affected during the bed height sensitivity tests. Larger surplus pore pressures and fluidisation heights were measured in beds that were shallower.
- Soil particle size was found to have a significant effect on the distribution of pore pressure, velocity and fluidisation height measured above the orifice but almost no influence on the energy distribution. Beds that contained larger particles experienced lower fluidisation heights and maximum pore pressures, and did not experience negative velocities.
- Based on the findings from the sensitivity experiments the possibility of finding a leak will increase for higher leakages rates, lower cover depths and smaller diameter particles in the bedding material.
- All surplus pore pressure distributions found during the study showed a decrease in surplus pore pressure immediately downstream of the orifice before reaching the maximum surplus pore pressure higher up in the bed.
- The fluidised region in all experiments can be seen as an energy dissipation mechanism, which restricted the water jet from penetrating deeper into the bed.
- The fluidisation height and the height of the surplus maximum pore pressure was seen to occur in close proximity to each other. In most cases the maximum surplus pore pressure occurred slightly above the fluidisation height.
- Flow in the fluidised region measured using Re_{inter} corresponded with turbulent and transitional flow. Turbulence in this region increased closer to the orifice and decreased as height above the orifice increased.
- In the method used to determine the fluidisation height, the tip of the Pitot tube when the scrambling noise was first heard was located at the boundary between the mobile bed and static bed zone and was loudest when the tip was at the head of the fluidised zone i.e. at the vortices.
- Measurements of surplus pore pressure, velocity and energy distribution at the centre and side orifice did not match. Therefore results from the respective orifices cannot be used interchangeably.

5.3 Recommendations

5.2.5 Recommendations on improving the experimental setup

- Pitot tubes

The Pitot tubes were modified such that the uniform plastic portion of any hypodermic needle can be fitted onto the brass push fit type fitting that connects the needle to the stainless steel tubing. It was noticed that the plastic portion of the needle although tappers to a point, has indentations and pieces of plastic that slightly protrude. It is proposed that the plastic fitting be tailored to be made more streamlined or smooth. This will reduce any disturbances the Pitot tube shape may have on the particles in the bed as well as on the fluid flow around the Pitot tube.

- Pitot tube brace

The Pitot tube brace is a component in the Pitot tube positioning system. Its main function is to hold the Pitot tube in place once it has been set to the point a reading is required. It would be advantageous to extend the bottom of Pitot tube brace along the Z plane (i.e. its height), so that it can offer more support to the Pitot tube especially when readings at the bottom of the tank or close to the orifice are required. Importantly, when determining the length to extend the brace, care must be taken to avoid the brace from interacting with bed surface. Therefore, the bottom of the brace must be extended such that it ends in the water layer that lies above the granular bed.

- De-aired water supply

The water supply system should be modified to allow for de-aired water to be used instead of ordinary tap water. Portable water from a municipal source can be de-aired in the lab either by boiling it or placing it in a tank under negative pressure for an appropriate amount of time. This improvement to the apparatus will eliminate air bubbles from forming in the tank, which will prevent the time consuming task of emptying and refill the tank during experiments.

5.2.6 Recommendations for further research

- Impact of the granular medium during soil-leak interaction

There is value in understanding the impact that the granular material has during a pipe leak. Readings of surplus pore pressure, vertical and horizontal velocity and surplus energy should be taken on a 5 mm grid above the centre orifice when flow enters the tank filled with only water and then when the tank has a layer of fully saturated ballotini. A dye can be used to observe the motion of the fluid when it enters the tank filled with water, which can be compared to the circular motion observed when a granular bed is fluidised. Any difference when the results are compared will be due to the soil particles interacting with the fluid in the bed.

- Effect of jet orientation on soil-leak interaction

In water distribution systems, water jets issuing from a leak opening can be orientated in any direction and angle. To understand the effects of this, leakage conditions can be compared for water jets that are horizontal, vertically upright and downward or directed at various angles.

- Effect of pipe slope on soil-leak interaction

Water distribution pipes are often laid parallel to the ground surface to keep a constant cover depth, which, in most cases are sloped for drainage purposes. Thus, the effects of soil-leak interaction initiated from a sloped pipe is a factor that can be investigated.

- Effect of bed compaction on soil-leak interaction

The bedding material of water pipes are often compacted according to construction standards. The aim of this practice is to strengthen the bed in order to protect the underlying pipe. A pipe leak should be simulated in beds where compaction is controlled to understand the effects it has on leakage conditions in the bed.

- Effects of a combination of bedding characteristics on soil-leak interaction

In this research leakage conditions were studied when single parameters were varied. A study can be conducted to assess how the soil-leak interaction behaves when multiple factors such as particle sphericity, roughness, size, and bed height have a combined influence.

- Testing of real world scenario

In a real world situation, fluidisation of the bedding material will begin before the soil is fully saturated and when air is trapped between the soil particles. This type of configuration can be simulated to analyse the influence it may have on soil-leak interaction.

References

Abbireddy, C.O.R., Schiebel, R., Clayton, C.R.I.R.I., To, A.Y. & It, I. 2009. A method of estimating the form of coarse particulates. *Géotechnique*. 59(6):493–501. DOI: 10.1680/geot.2007.00195.

Ahmed, N. & Sunada, D.K. 1969. Nonlinear Flow in Porous Media. *Journal of Hydraulics Division, ASCE,*. 95(6).

Alsaydalani, M.O.A. 2010. Internal fluidisation of granular material. *Ph.D. Thesis.University of Southampton*.

Alsaydalani, M.O.A. & Clayton, C.R.I. 2014. Internal Fluidization in Granular Soils. *Journal of Geotechnical and Geoenvironmental Engineering*. 140(3):1–10. DOI: 10.1061/(ASCE)GT.1943-5606.0001039.

Arnell, N.W. 2004. Climate change and global water resources: SRES emissions and socio-economic scenarios. *Global Environmental Change*. 14(1):31–52. DOI: 10.1016/j.gloenvcha.2003.10.006.

Bailey, N. 2015. Development and testing of experimental equipment to measure pore pressure and dynamic pressure at points outside a pipe leak. *MSc. Thesis. University of Cape Town*.

Bird, R.B., Stewart, W.E. & Lightfoot, E.N. 2002. *Transport Phenomena*. New York: John Wiley and Sons.

Chadwick, A., Morfett, J. & Borthwick, M. 2004. *Hydraulics in civil and environmental engineering*. London: Spon Press.

Chiesa, M., Mathiesen, V., Melheim, J.A. & Halvorsen, B. 2005. Numerical simulation of particulate flow by the Eulerian-Lagrangian and the Eulerian-Eulerian approach with application to a fluidized bed. *Computers and Chemical Engineering*. 29(2):291–304. DOI: 10.1016/j.compchemeng.2004.09.002.

Clayton, C.R.I. & van Zyl, J.E. 2007. The effect of pressure on leakage in water distribution systems. *Water Management*. 160(June):109–114. DOI: 10.1680/wama.2007.160.2.109.

Craig, R.F. 2004. *Craigs soil mechanics*. London: Spon Press.

Crawford, C. & Plumb, O.A. 1986. The Influence of Surface Roughness on Resistance to Flow Through Packed Beds. *Journal of Fluids Engineering*. 108(3):343–347.

Department of Water and Sanitation. 2000. Chapter One Overview of the South African Water Sector. *Governing Board Induction Manual*. Available: https://www.dwa.gov.za/IO/Docs/CMA/CMA GB Training Manuals/gbtrainingmanualchapter1.pdf.

Eastwood, J., Matzen, E.J. & Epstein, N. 1969. Random loose porosity of packed beds. *Br Chem Eng*. 14:1956–1972.

Ergun, S. 1952. Fluid flow through packed columns. *Chemical Engineering Progress*. 48(2):89–94.

Finnemore, J. & Franzini, J. 2002. *Fluid Mechanics with engineering applications*. McGraw Hill.

Foda, M.A., Hill, D.F., DeNealle, P.L. & Huang, C.M. 1997. Fluidisation response of sediment bed to rapidly falling water surface. *Journal of waterway, port,coastal and ocean engineering*. 123(5).

Forchheimer, P. 1901. Wasserbewegung Durch Boden. *Z Ver Deutsch Ing*. 45:1782–1788.

Greenkorn, R. a. 1981. Steady flow through porous media. *AIChE Journal*. 27(4):529–545. DOI: 10.1002/aic.690270402.

Harr, M.E. 1962. *Groundwater and Seepage*. New York: M.cGraw Hill.

Hlushkou, D. & Tallarek, U. 2006. Transition from creeping via viscous-inertial to turbulent flow in fixed beds. *Journal of Chromatography A*. 1126(1-2):70–85. DOI: 10.1016/j.chroma.2006.06.011.

Jordi, R.D., Young, B.D. & van Vliet, B. 1990. The effect of surface roughness on pressure drop in a packed bed. *Chemical Engineering Communications*. 89(1):137–146.

Kingdom, B., Liemberger, R. & Marin, P. 2006. The Challenge of Reducing Non-Revenue Water (NRW) in Developing Countries How the Private Sector Can Help : A Look at Performance-Based Service Contracting. *Watersupply and Sanitation Sector Board Discusion Paper Series*. (8). Available: http://siteresources.worldbank.org/INTWSS/Resources/WSS8fin4.pdf.

Krumbein, W.C. 1941. Measurement and geological significance of shape and roundness of sedimentary particles. *Journal of Sedimentary Research*. 11(2):64–72. DOI: 10.1306/d42690f3-2b26-11d7-8648000102c1865d.

Leva, M. 1959. *Fluidization*. New York: McGraw-Hill Book Co.

Ma, C.H. 2011. Internal Fluidisation due to Horizontal Seepage – A Laboratory Study. *MSc. Thesis. University of Southhampton*.

Meire, L. 2014. Numerical investigation of the interaction between a leak in a pressurised pipeline and the surrounding soil. *MSc Thesis. Imperial Colledge London*.

Niven, R.K. 2002. Physical insight into the Ergun and Wen and Yu equations for fluid flow in packed and fluidised beds. *Chemical Engineering Science*. 57(3):527–534. DOI: 10.1016/S0009-2509(01)00371-2.

Niven, R.K. & Khalili, N. 1998. In situ fluidisation by a single internal vertical jet. *Journal of Hydraulic Research*. 36(2):199–228. DOI: 10.1080/00221689809498633.

Ojha, R., Menon, N. & Durian, D.J. 2000. Hysteresis and packing in gas-fluidized beds. *Physical Review E - Statistical Physics, Plasmas, Fluids, and Related Interdisciplinary Topics*. 62(3 B):4442–4445. DOI: 10.1103/PhysRevE.62.4442.

Philippe, P. & Badiane, M. 2013. Localized fluidization in a granular medium. *Physical Review E - Statistical, Nonlinear, and Soft Matter Physics*. 87(4):31–33. DOI: 10.1103/PhysRevE.87.042206.

Powrie, W. 2004. *Soil Mechanics Concepts & Applications*. London and New York: Spon Press.

Sneed, E.D. & Folk, R.L. 1958. Pebbles in the Lower Colorado River, Texas a Study in Particle Morphogenesis. *The Journal of Geology*. 66(2):114–150. DOI: 10.1086/626490.

Venkataraman, P. & Rao, P.R.M. 1998. Darcian, Transitional, and Turbulent Flow through Porous Media. *Journal of Hydraulic Engineering*. 124(8):840–846. DOI: 10.1061/(ASCE)0733-9429(1998)124:8(840).

Wadell, H. 1933. Sphericity and Roundness of Rock Particles. *The Journal of Geology*. 41(3):310–331. DOI: 10.1086/624040.

Walski, T., Bezts, W., Posluszny, E.T., Weir, M. & Whitman, B.E. 2006. Modeling leakage reduction through pressure control. *Journal / American Water Works Association*. 98(4):147–155.

Ward, J.C. 1946. Turbulent Flow in Porous Media. *Journal of Hydraulics Division, ASCE,*. 90(5):421–439.

Weisman, B.R.N., Lennon, G.P. & Roberts, W. 1988. Experiment on Fluidization in Unbounded

Domains. *ASCEJ. Hydraulic Engineering*. 114(5):502–515.

Wen, C.Y. & Yu, Y.H. 1966. Mechanics of fluidization. *Chemical Engineering Progress Symposium*. 62(62):100–111.

Zoueshtiagh, F. & Merlen, A. 2007. Effect of a vertically flowing water jet underneath a granular bed. *Physical Review E - Statistical, Nonlinear, and Soft Matter Physics*. 75(5):1–12. DOI: 10.1103/PhysRevE.75.056313.

van Zyl, J.E., Alsaydalani, M.O.A., Clayton, C.R.I., Bird, T. & Dennis, A. 2013. Soil fluidisation outside leaks in water distribution pipes – preliminary observations. *Water Management*. 166(WM10):546–555. DOI: 10.1680/wama.11.00119.

(Weisman, Lennon & Roberts, 1988)(Weisman, Lennon & Roberts, 1988)(Weisman, Lennon & Roberts, 1988)

Appendix A – Raw data for geotechnical data

Sieve analysis

Soil Type: Material type A

Aperture size (mm)	Aperture mass (g)	Aperture + soil mass (g)	Mass of soil retained (g)	Mass of soil retained (%)	cumulative mass retained (%)	cumulative mass passing (%)
1.180	552.800	553.40	0.60	0.85	0.85	99.15
0.850	514.500	514.90	0.40	0.56	1.41	98.59
0.710	433.300	470.60	37.30	52.61	54.02	45.98
0.600	514.000	544.00	30.00	42.31	96.33	3.67
0.425	505.300	507.70	2.40	3.39	99.72	0.28
0.300	476.700	476.90	0.20	0.28	100.00	0.00
0.150	472.400	472.40	0.00	0.00	100.00	0.00
			70.90	**100.00**		

Soil Type: Material type B

Aperture size (mm)	Aperture mass (g)	Aperture + soil mass (g)	Mass of soil retained (g)	Mass of soil retained (%)	cumulative mass retained (%)	cumulative mass passing (%)
1.180	552.10	552.60	0.50	0.40	0.40	99.60
0.850	513.30	513.30	0.00	0.00	0.40	99.60
0.710	433.20	448.70	15.50	12.36	12.76	87.24
0.600	511.60	606.10	94.50	75.36	88.12	11.88
0.425	296.30	310.80	14.50	11.56	99.68	0.32
0.300	519.80	520.20	0.40	0.32	100.00	0.00
0.150	517.60	517.60	0.00	0.00	100.00	0.00
			125.40	**100.00**		

Soil Type: Materail type C

Aperture size (mm)	Aperture mass (g)	Aperture + soil mass (g)	Mass of soil retained (g)	Mass of soil retained (%)	cumulative mass retained (%)	cumulative mass passing (%)
1.180	552.40	552.50	0.10	0.08	0.08	99.92
0.850	513.50	515.70	2.20	1.68	1.75	98.25
0.710	432.60	546.10	113.50	86.58	88.33	11.67
0.600	512.20	525.20	13.00	9.92	98.25	1.75
0.425	296.20	298.20	2.00	1.53	99.77	0.23
0.300	520.00	520.20	0.20	0.15	99.92	0.08
0.150	517.40	517.50	0.10	0.08	100.00	0.00
			131.10	**100.00**		

Particle density

Soil type: Material type A

Description	Unit	Test 1	Test 2	Test 3
Mass of density bottle + stopper	g	37.38	36.71	34.53
Mass of density bottle + stopper + soil sample	g	45.55	45.08	42.71
Mass of density bottle + stopper + soil sample + air free liquid	g	93.40	93.11	89.06
Mass of density bottle + stopper + air free liquid	g	88.52	88.10	84.18
Density of liquid	Mg/m^3	1.00	1.00	1.00
Particle density	Mg/m^3	2.49	2.48	2.48
Average Particle density	Mg/m^3		**2.48**	

Soil type: Material type B

Description	Unit	Test 1	Test 2	Test 3
Mass of density bottle + stopper	g	33.99	34.99	33.69
Mass of density bottle + stopper + soil sample	g	42.28	43.80	42.12
Mass of density bottle + stopper + soil sample + air free liquid	g	89.60	92.70	88.24
Mass of density bottle + stopper + air free liquid	g	84.66	87.44	83.21
Density of liquid	Mg/m^3	1.00	1.00	1.00
Particle density	Mg/m^3	2.48	2.49	2.48
Average Particle density	Mg/m^3		**2.48**	

Soil type: Material type C

Description	Unit	Test 1	Test 2	Test 3
Mass of density bottle + stopper	g	35.44	34.66	34.77
Mass of density bottle + stopper + soil sample	g	44.09	43.20	43.25
Mass of density bottle + stopper + soil sample + air free liquid	g	89.03	89.78	89.68
Mass of density bottle + stopper + air free liquid	g	83.89	84.68	84.62
Density of liquid	Mg/m^3	1.00	1.00	1.00
Particle density	Mg/m^3	2.47	2.48	2.48
Average Particle density	Mg/m^3		**2.48**	

Permeability

Soil sample: Material Type A

Discription	Value	Units
Chamber Diameter	11.34	cm
Chamber area	101.11	cm
H1	98.50	cm
H2	71.70	cm
H3	41.60	cm
Height of P1	14.50	cm
Height of P2	24.50	cm
Height of P3	34.50	cm
L (p2-p1)	10.00	cm
L (p3-p1)	20.00	cm
L (p3-p2)	10.00	cm
delta h (p2-p1)	-26.80	cm
delta h (p3-p1)	-56.90	cm
delta h (p3-p2)	-30.10	cm
k (p2-p1)	-0.30	cm/s
k (p3-p1)	-0.29	cm/s
k (p3-p2)	-0.27	cm/s
Average K	**-0.29**	**cm/s**

Flow rate for Materail type A

Discription	Value
Mass of bucket (g)	284.50
Mass of bucket+ water (g)	1379.40
Mass of water (kg) or (l)	1.09
Time (s)	13.25
Q (l/s)	0.083
Q (cm^3/s)	82.63

Soil sample: Material Type B

Discription	Value	Units
Chamber Diameter	11.34	cm
Chamber area	101.11	cm
H1	58.50	cm
H2	38.10	cm
H3	14.70	cm
Height of P1	14.50	cm
Height of P2	24.50	cm
Height of P3	34.50	cm
L (p2-p1)	10.00	cm
L (p3-p1)	20.00	cm
L (p3-p2)	10.00	cm
delta h (p2-p1)	-20.40	cm
delta h (p3-p1)	-43.80	cm
delta h (p3-p2)	-23.40	cm
k (p2-p1)	-0.31	cm/s
k (p3-p1)	-0.29	cm/s
k (p3-p2)	-0.27	cm/s
Average K	**-0.29**	**cm/s**

Flow rate for Materail type B

Discription	Value
Mass of bucket (g)	284.60
Mass of bucket+ water (g)	2209.30
Mass of water (kg) or (l)	1.92
Time (s)	30.27
Q (l/s)	0.064
Q (cm^3/s)	63.58

Soil sample: Material Type C

Discription	Value	Units
Chamber Diameter	11.34	cm
Chamber area	101.11	cm
H1	60.30	cm
H2	39.00	cm
H3	17.80	cm
Height of P1	14.50	cm
Height of P2	24.50	cm
Height of P3	34.50	cm
L (p2-p1)	10.00	cm
L (p3-p1)	20.00	cm
L (p3-p2)	10.00	cm
delta h (p2-p1)	-21.30	cm
delta h (p3-p1)	-42.50	cm
delta h (p3-p2)	-21.20	cm
k (p2-p1)	-0.41	cm/s
k (p3-p1)	-0.41	cm/s
k (p3-p2)	-0.41	cm/s
Average K	**-0.41**	**cm/s**

Flow rate for Materail type C

Discription	Value
Mass of bucket (g)	284.30
Mass of bucket+ water (g)	2079.50
Mass of water (kg) or (l)	1.80
Time (s)	20.35
Q (l/s)	0.088
Q (cm^3/s)	88.22

Sphericity

Soil type: Material type A

Parameter	Particle specimen		
	1	2	3
S	0.60	0.62	0.72
L	0.62	0.64	0.73
Sphericity	0.98	0.97	0.99
Average		0.98	

Soil type: Material type B

Parameter	Particle specimen		
	1	2	3
S	0.74	0.71	0.69
L	0.75	0.73	0.70
Sphericity	0.99	0.97	0.99
Average		0.98	

Soil type: Material type C

Parameter	Particle specimen		
	1	2	3
S	0.75	0.74	0.77
L	0.75	0.77	0.78
Sphericity	0.99	0.96	0.99
Average		0.98	

Minimum bulk density

Mould properties

Description	Units	Value
Diameter	m	0.153
Length	m	0.156
Volume	m^3	0.0029

Soil type: Material type A

Description	Units	Test		
		No. 1	No. 2	No. 3
Mass of mould	kg	3.03	3.03	3.03
Mass of mould + soil	kg	7.32	7.32	7.32
Mass of soil	kg	4.29	4.29	4.29
Density	kg/m^3	1502.32	1501.27	1502.67
Average	kg/m^3		1502.1	

Soil type: Material type B

Description	Units	Test		
		No. 1	No. 2	No. 3
Mass of mould	kg	3.033	3.03	3.03
Mass of mould + soil	kg	7.28	7.30	7.28
Mass of soil	kg	4.25	4.27	4.25
Density	kg/m^3	1489.01	1494.96	1490.06
Average	kg/m^3		1491.3	

Soil type: Material type C

Description	Units	Test		
		No. 1	No. 2	No. 3
Mass of mould	kg	3.033	3.03	3.03
Mass of mould + soil	kg	7.28	7.28	7.30
Mass of soil	kg	4.24	4.25	4.27
Density	kg/m^3	1486.20	1488.66	1496.01
Average	kg/m^3		1490.3	

Appendix B – Raw data for validation test

Experiment: Validation test

Flow rate (l/min)	2
Bed height (mm)	300
Ballotini sample	A
FH (measured-mm)	24

Co-ordinates on ruler

90 Pitot tube (Facing neg X)

X	283.5
Y	308
Z	37

Straight Pitot tube

X	361
Y	305
Z	20

Static Pressure reading (mm) 13

Height on Ruler (mm)	Height above orifice (mm)	Y co-ordinate 0	
		S_R	H_P
39	2	81	68
47	10	79	66
57	20	103	90
67	30	115	102
77	40	75	62
87	50	52	39
97	60	43	30
107	70	37	24
117	80	34	21
127	90	31	18
137	100	29	16
147	110	28	15
157	120	27	14
167	130	26	13
177	140	25	12
187	150	24	11
197	160	24	11
207	170	23	10
217	180	23	10
227	190	22	9
237	200	22	9

Static Pressure reading (mm) 13

Height above orifice (mm)	Height on Ruler (mm)	Y co-ordinate 0		
		S_R	$H_{P(V)}$	$V_{V\,(m/s)}$
2	22	1228	1147	4.74
10	30	575	496	3.12
20	40	417	314	2.48
30	50	122	7	0.37
40	60	72	-3	-0.24
50	70	57	5	0.31
60	80	48	5	0.31
70	90	42	5	0.31
80	100	38	4	0.28
90	110	34	3	0.24
100	120	32	3	0.24
110	130	31	3	0.24
120	140	30	3	0.24
130	150	30	4	0.28
140	160	30	5	0.31
150	170	27	3	0.24
160	180	27	3	0.24
170	190	26	3	0.24
180	200	24	1	0.14
190	210	23	1	0.14
200	220	23	1	0.14

Y co-ordinate 0
Energy (mm)
1215
562
404
109
59
44
35
29
25
21
19
18
17
17
17
14
14
13
11
10
10

S_R	Sight tube reading
H_P	Pressure head
$H_{P(V)}$	Velocity head vertical component
V_V	Velocity Vertical component
FH	Fluidised height
	Input cell
	Predicted value (besed on trend)

Appendix C – Raw data for standard and sensitivity experiments

Experiment: Standard experiment

Flow rate (l/min)	2
Bed height (mm)	300
Ballotini sample	A
FH (measured)	23

Centre co-ordinates

90 Pitot tube (Facing neg X)

X	283.5	283.5	283.5	283.5	283.5	283.5	283.5	283.5	283.5
Y	301	306	311	316	321	326	331	336	341
Z	37								

Straight Pitot tube

X	361
Y	298
Z	20

Static Pressure reading (mm) 13

Height on Ruler (mm)	Height above orifice (mm)	Y co-ordinate																	
		0		5		10		15		20		25		30		35		40	
		S_R	H_P	S_R	H_P	S_R	H_P	S_R	H_P	S_R	H_P	S_R	H_P	S_R	H_P	S_R	H_P	S_R	H_P
39	2	83	70	77	64	68	55	52	39	49	36	42	29	47	34	44	31	40	27
42	5	81	68		0									49	36				
46	9																		
47	10	80	67		0											44	31	40	27
52	15	83	70		0											43	30	39	26
54	17											55	42						
56	19									53	40								
57	20	87	74		0											42	29	39	26
59	22					76	63												
62	25	93	80	95	82														
66	29																		
67	30	109	96		0			69	56										
72	35	79	66		0											41	27	38	25
77	40	70	57		0														
82	45	60	47		0														
87	50	53	40		0											36	23	35	22
92	55	46	33		0														
97	60	42	29		0														
102	65	38	25		0														
107	70	35	22		0														
112	75	33	20		0														
117	80	32	19		0														
122	85	31	18		0														
127	90	30	17		0														
137	100	29	16		0											29	16	29	16
147	110	28	15		0														
157	120	27	14		0														
167	130	26	13		0														
187	150	24	11		0														
207	170	23	10		0														
227	190	22	9		0														
237	200	21	8		0											22	9	22	9

Static Pressure reading (mm) 13

Height above orifice (mm)	Height on Ruler (mm)	Y co-ordinate		
		0		
		S_R	$H_{P(V)}$	$V_{V\,(m/s)}$
2	22	1227	1144	4.74
5	25	902	821	4.01
10	30	522	442	2.94
15	35	437	354	2.64
20	40	390	303	2.44
25	45	148	55	1.04
30	50	100	-9	-0.42
35	55	65	-14	-0.52
40	60	56	-14	-0.52
45	65	52	-8	-0.40
50	70	43	-10	-0.44
55	75	39	-7	-0.37
60	80	37	-5	-0.31
65	85	35	-3	-0.24
70	90	34	-1	-0.14
75	95	32	-1	-0.14
80	100	31	-1	-0.14
85	105	30	-1	-0.14
90	110	29	-1	-0.14
100	120	28	-1	-0.14
110	130	27	-1	-0.14
120	140	26	-1	-0.14
130	150	25	-1	-0.14
150	170	23	-1	-0.14
170	190	22	-1	-0.14
190	210	21	-1	-0.14
200	220	21	0	0.00

Height above orifice (mm)	Y co-ordinate
	0
	Energy (mm)
2	1214
5	889
10	509
15	424
20	377
25	135
30	87
35	52
40	43
45	39
50	30
55	26
60	24
65	22
70	21
75	19
80	18
85	17
90	16
100	15
110	14
120	13
130	12
150	10
170	9
190	8
200	8

S_R	Sight tube reading
H_P	Pressure head
$H_{P(V)}$	Velocity head vertical component
V_V	Velocity Vertical component
FH	Fluidised height
	Input cell

Experiment: Flow rate

Flow rate (l/min)	3
Bed height (mm)	300
Ballotini sample	A
FH (measured)	27

Co-ordinates on ruler

90 Pitot tube (Facing neg X)

X	283.5	283.5	283.5	283.5	283.5	283.5	283.5	283.5	283.5
Y	301	306	311	316	321	326	331	336	341
Z	37								

Straight Pitot tube

X	361
Y	298
Z	20

Static Pressure reading (mm) 13

Height on Ruler (mm)	Height above orifice (mm)	Y co-ordinate 0		5		10		15		20		25		30		35		40	
		S_R	H_P	S_R	H_P	S_R	H_P	S_R	H_P	S_R	H_P	S_R	H_P	S_R	H_P	S_R	H_P	S_R	H_P
39	2	88	75	80	67	72	59	75	62	57	44	55	42	41	28	52	39	51	38
42	5	63	50	71														49	36
47	10	65	52															48	35
52	15	73	60															46	33
57	20	83	70																
62	25	100	87													56	43		
67	30	123	110																
71	34													63	50				
72	35	159	146															46	33
73	36					122	109												
75	38			156	143														
77	40	177	164					127	114	81	68								
78	41											68	55						
82	45	168	155																
87	50	132	119															45	32
92	55	103	90																
97	60	82	69																
102	65	69	56																
107	70	60	47																
112	75	55	42																
117	80	50	37																
122	85	47	34																
127	90	44	31																
137	100	39	26															34	21
147	110	36	23																
157	120	33	20																
167	130	32	19																
187	150	29	16																
207	170	27	14																
227	190	27	14																
237	200	25	12															30	17

Static Pressure reading (mm) 13

Height above orifice (mm)	Height on Ruler (mm)	Y co-ordinate 0		
		S_R	$H_{P(V)}$	$V_{V\,(m/s)}$
2	22	2663	2575	7.11
5	25	1873	1810	5.96
10	30	1163	1098	4.64
15	35	926	853	4.09
20	40	769	686	3.67
25	45	620	520	3.19
30	50	224	101	1.41
35	55	148	-11	-0.46
40	60	109	-68	-1.16
45	65	87	-81	-1.26
50	70	70	-62	-1.10
55	75	60	-43	-0.92
60	80	52	-30	-0.77
65	85	49	-20	-0.63
70	90	44	-16	-0.56
75	95	41	-14	-0.52
80	100	39	-11	-0.46
85	105	38	-9	-0.42
90	110	36	-8	-0.40
100	120	34	-5	-0.31
110	130	32	-4	-0.28
120	140	30	-3	-0.24
130	150	29	-3	-0.24
150	170	27	-2	-0.20
170	190	26	-1	-0.14
190	210	25	-2	-0.20
200	220	24	-1	-0.14

Height above orifice (mm)	Y co-ordinate 0
	Energy (mm)
2	2650
5	1860
10	1150
15	913
20	756
25	607
30	211
35	135
40	96
45	74
50	57
55	47
60	39
65	36
70	31
75	28
80	26
85	25
90	23
100	21
110	19
120	17
130	16
150	14
170	13
190	12
200	11

S_R	Sight tube reading
H_P	Pressure head
$H_{P(V)}$	Velocity head vertical component
V_V	Velocity Vertical component
FH	Fluidised height
(shaded)	Input cell

Experiment: Flow rate

Flow rate (l/min)	4
Bed height (mm)	300
Ballotini sample	A
FH (measured)	41

Co-ordinates on ruler

90 Pitot tube (Facing neg X)

X	283.5	283.5	283.5	283.5	283.5	283.5	283.5	283.5	283.5	283.5	283.5	283.5
Y	301	306	311	316	321	326	331	336	341	346	351	356
Z	37											

Straight Pitot tube

X	361
Y	298
Z	20

Static Pressure reading (mm) 13

Height on Ruler (mm)	Height above orifice (mm)	Y co-ordinate																							
		0		5		10		15		20		25		30		35		40		45		50		55	
		S_R	H_P	S_R	H_P	S_R	H_P	S_R	H_P	S_R	H_P	S_R	H_P	S_R	H_P	S_R	H_P	S_R	H_P	S_R	H_P	S_R	H_P	S_R	H_P
39	2	50	37	52	39	47	34	50	37	50	37	49	36	54	41	54	41	54	41	53	40	48	35	47	34
42	5	42	29																					47	34
47	10	43	30																					47	34
52	15	52	39																					47	34
53	16																					51	38		
57	20	66	53																						
61	24																			55	42				
62	25	81	68																						
64	27																	58	45					47	33
65	28																								
67	30	92	79																						
69	32															62	49								
72	35	113	100											70	57										
77	40	136	123																						
82	45	166	153																					47	33
85	48									97	84														
86	49											90	77												
87	50	205	192																						
88	51							104	91																
92	55	273	260	302	289																				
96	59					157	144																		
97	60	299	286																						
98	61	307	294																						
102	65	206	193																					46	33
107	70	135	122																						
112	75	102	89																						
117	80	87	74																						
122	85	78	65																						
127	90	69	56																						
137	100	57	44																						
147	110	49	36																					39	26
157	120	44	31																						
167	130	40	27																						
187	150	35	22																						
207	170	32	19																						
227	190	30	17																						
237	200	28	15																					38	25

Static Pressure reading (mm) 13

Height above orifice (mm)	Height on Ruler (mm)	Y co-ordinate		
		0		
		S_R	$H_{P(V)}$	$V_{V\,(m/s)}$
2	22	4313	4263	9.15
5	25	3293	3251	7.99
10	30	1863	1820	5.98
15	35	1393	1341	5.13
20	40	1163	1097	4.64
25	45	993	912	4.23
30	50	823	731	3.79
35	55	683	570	3.34
40	60	313	177	1.86
45	65	221	55	1.04
50	70	150	-55	-1.04
55	75	110	-163	-1.79
60	80	91	-208	-2.02
61	81	84	-223	-2.09
65	85	78	-128	-1.58
70	90	69	-66	-1.14
75	95	62	-40	-0.89
80	100	57	-30	-0.77
85	105	53	-25	-0.70
90	110	49	-20	-0.63
100	120	44	-13	-0.51
110	130	40	-9	-0.42
120	140	37	-7	-0.37
130	150	35	-5	-0.31
150	170	32	-3	-0.24
170	190	29	-3	-0.24
190	210	27	-3	-0.24
200	220	26	-2	-0.20

Height above orifice (mm)	Y co-ordinate
	0
	Energy (mm)
2	4300
5	3280
10	1850
15	1380
20	1150
25	980
30	750
35	600
40	300
45	208
50	137
55	97
60	78
61	71
65	65
70	56
75	49
80	44
85	40
90	36
100	31
110	27
120	24
130	22
150	19
170	16
190	14
200	13

S_R	Sight tube reading
H_P	Pressure head
$H_{P(V)}$	Velocity head vertical component
V_V	Velocity Vertical component
FH	Fluidised height
	Input cell
	Predicted value

Experiment: Bed height

Flow rate (l/min)	2
Bed height (mm)	150
Ballotini sample	A
FH (measured)	43

Co-ordinates on ruler

90 Pitot tube (Facing neg X)

X	283.5	283.5	283.5	283.5	283.5	283.5
Y	301	311	321	331	341	351
Z	37					

Straight Pitot tube

X	361
Y	298
Z	20

Static Pressure reading (mm) 13

Height on Ruler (mm)	Height above orifice (mm)	Y co-ordinate											
		0		10		20		30		40		50	
		S_R	H_P	S_R	H_P	S_R	H_P	S_R	H_P	S_R	H_P	S_R	H_P
39	2	47	34	46	33	42	29	34	21	31	18	29	16
42	5	48	35										
47	10	51	38										
52	15	62	49										
55	18									32	19	29	16
57	20	74	61										
62	25	85	72										
65	28					48	35						
67	30	102	89										
72	35	111	98	103	90			40	27	32	19	29	16
74	37	126	113										
77	40	106	93										
82	45	82	69										
87	50	66	53							31	18	28	15
92	55	54	41										
97	60	46	33										
102	65	40	27										
107	70	36	23										
112	75	33	20										
117	80	30	17										
122	85	29	16										
127	90	27	14										
137	100	26	13							24	11	24	11
147	110	23	10										
157	120	21	8										
167	130	20	7										
187	150	19	6							19	6	19	6

Static Pressure reading (mm) 13

Height above orifice (mm)	Height on Ruler (mm)	Y co-ordinate		
		0		
		S_R	$H_{P(V)}$	$V_{V\,(m/s)}$
2	22	1202	1155	4.76
5	25	928	880	4.16
10	30	518	467	3.03
15	35	366	304	2.44
20	40	303	229	2.12
25	45	236	151	1.72
30	50	150	48	0.97
35	55	94	-17	-0.58
37	57	80	-46	-0.95
40	60	68	-38	-0.86
45	65	62	-20	-0.63
50	70	51	-15	-0.54
55	75	44	-10	-0.44
60	80	39	-7	-0.37
65	85	35	-5	-0.31
70	90	32	-4	-0.28
75	95	29	-4	-0.28
80	100	27	-3	-0.24
85	105	26	-3	-0.24
90	110	25	-2	-0.20
100	120	23	-3	-0.24
110	130	22	-1	-0.14
120	140	20	-1	-0.14
130	150	19	-1	-0.14
150	170	19	0	0.00

Height above orifice (mm)	Y co-ordinate
	0
	Energy (mm)
2	1189
5	915
10	505
15	353
20	290
25	223
30	137
35	81
37	67
40	55
45	49
50	38
55	31
60	26
65	22
70	19
75	16
80	14
85	13
90	12
100	10
110	9
120	7
130	6
150	6

S_R	Sight tube reading
H_P	Pressure head
$H_{P(V)}$	Velocity head vertical component
V_V	Velocity Vertical component
FH	Fluidised height
(shaded)	Input cell

Experiment: Bed height

Flow rate (l/min)	2
Bed height (mm)	200
Ballotini sample	A
FH (measured)	38

Co-ordinates on ruler

90 Pitot tube (Facing neg X)

X	283.5	283.5	283.5	283.5	283.5	283.5
Y	301	311	321	331	341	351
Z	37					

Straight Pitot tube

X	361
Y	298
Z	20

Static Pressure reading (mm) 13

Height on Ruler (mm)	Height above orifice (mm)	Y co-ordinate 0		10		20		30		40		50	
		S_R	H_P	S_R	H_P	S_R	H_P	S_R	H_P	S_R	H_P	S_R	H_P
39	2	63	50	55	42	52	39	40	27	36	23	32	19
42	5	59	46							36	23	32	19
47	10	60	47							36	23	31	18
52	15	66	53							36	23	31	18
54	17							43	30				
57	20	75	62							36	23	31	18
62	25	86	73										
66	29			77	64								
67	30	100	87										
71	34					59	46						
72	35	120	107							33	20	30	17
75	38	128	115										
77	40	125	112										
82	45	84	71										
87	50	70	57							32	19	28	15
92	55	58	45										
97	60	50	37										
102	65	45	32										
107	70	40	27										
112	75	37	24										
117	80	34	21										
122	85	32	19										
127	90	30	17										
137	100	29	16							25	12	24	11
147	110	27	14										
157	120	25	12										
167	130	24	11										
187	150	22	9										
207	170	20	7										
227	190	19	6										
237	200	19	6							19	6	19	6

Static Pressure reading (mm) 13

Height above orifice (mm)	Height on Pitot Tube	Y co-ordinate 0		
		S_R	$H_{P(V)}$	$V_{V\,(m/s)}$
2	22	1228	1165	4.78
5	25	934	875	4.14
10	30	478	418	2.86
15	35	385	319	2.50
20	40	175	100	1.40
25	45	115	29	0.75
30	50	83	-17	-0.58
35	55	65	-55	-1.04
38	58	60	-68	-1.16
40	60	57	-68	-1.16
45	65	49	-35	-0.83
50	70	43	-27	-0.73
55	75	39	-19	-0.61
60	80	36	-14	-0.52
65	85	33	-12	-0.49
70	90	31	-9	-0.42
75	95	30	-7	-0.37
80	100	28	-6	-0.34
85	105	27	-5	-0.31
90	110	26	-4	-0.28
100	120	25	-4	-0.28
110	130	24	-3	-0.24
120	140	23	-2	-0.20
130	150	22	-2	-0.20
150	170	20	-2	-0.20
170	190	19	-1	-0.14
190	210	19	0	0.00
200	220	19	0	0.00

Height above orifice (mm)	Y co-ordinate 0
	Energy (mm)
2	1215
5	921
10	465
15	372
20	162
25	102
30	70
35	52
38	47
40	44
45	36
50	30
55	26
60	23
65	20
70	18
75	17
80	15
85	14
90	13
100	12
110	11
120	10
130	9
150	7
170	6
190	6
200	6

S_R	Sight tube reading
H_P	Pressure head
$H_{P(V)}$	Velocity head vertical component
V_V	Velocity Vertical component
FH	Fluidised height
(shaded)	Input cell

Experiment: Particle size

Flow rate (l/min)	2
Bed height (mm)	300
Ballotini sample	B
FH (measured)	24

Co-ordinates on ruler

90 Pitot tube (Facing neg X)

X	283.5	283.5	283.5	283.5	283.5	283.5	283.5	283.5	283.5
Y	301	306	311	316	321	326	331	336	341
Z	37								

Straight Pitot tube

X	361
Y	298
Z	20

Static Pressure reading (mm) 13

Height on Ruler (mm)	Height above orifice (mm)	Y co-ordinate																	
		0		5		10		15		20		25		30		35		40	
		S_R	H_P	S_R	H_P	S_R	H_P	S_R	H_P	S_R	H_P	S_R	H_P	S_R	H_P	S_R	H_P	S_R	H_P
39	2	92	79	81	68	82	69	65	52	52	39	47	34	42	29	38	25	37	24
42	5	82	69																
47	10	87	74													39	26	37	24
48	11													44	31				
50	13											51	38						
52	15	99	86															37	24
57	20	109	96															37	24
59	22			95	82														
62	25	114	101																
63	26					96	83												
65	28	122	109							58	45								
66	29							76	63										
67	30	115	102																
72	35	91	78															36	23
77	40	73	60																
82	45	57	44																
87	50	50	37															34	21
92	55	45	32																
97	60	41	28																
102	65	38	25																
107	70	36	23																
112	75	34	21																
117	80	32	19																
122	85	31	18																
127	90	30	17																
137	100	29	16															28	15
147	110	27	14																
157	120	26	13																
167	130	25	12																
187	150	23	10																
207	170	22	9																
227	190	21	8																
237	200	21	8															23	10

Static Pressure reading (mm) 13

Height above orifice (mm)	Height on Ruler (mm)	Y co-ordinate		
		0		
		S_R	$H_{P(V)}$	$V_{V\,(m/s)}$
2	22	1399	1307	5.06
5	25	800	718	3.75
10	30	513	426	2.89
15	35	480	381	2.73
20	40	350	241	2.17
25	45	140	26	0.71
28	48	118	-4	-0.28
30	50	104	-11	-0.46
35	55	76	-15	-0.54
40	60	61	-12	-0.49
45	65	52	-5	-0.31
50	70	47	-3	-0.24
55	75	42	-3	-0.24
60	80	39	-2	-0.20
65	85	36	-2	-0.20
70	90	34	-2	-0.20
75	95	33	-1	-0.14
80	100	31	-1	-0.14
85	105	30	-1	-0.14
90	110	28	-2	-0.20
100	120	27	-2	-0.20
110	130	26	-1	-0.14
120	140	25	-1	-0.14
130	150	24	-1	-0.14
150	170	23	0	0.00
170	190	22	0	0.00
190	210	21	0	0.00
200	220	21	0	0.00

Height above orifice (mm)	Y co-ordinate
	0
	Energy (mm)
2	1386
5	787
10	500
15	467
20	337
25	127
28	105
30	
35	63
40	48
45	39
50	34
55	29
60	26
65	23
70	21
75	20
80	18
85	17
90	15
100	14
110	13
120	12
130	11
150	10
170	9
190	8
200	8

S_R	Sight tube reading
H_P	Pressure head
$H_{P(V)}$	Velocity head vertical component
V_V	Velocity Vertical component
FH	Fluidised height
	Input cell

Experiment: Particle size

Flow rate (l/min)	2
Bed height (mm)	300
Ballotini sample	C
FH (measured)	19

Co-ordinates on ruler

90 Pitot tube (Facing neg X)

X	283.5	283.5	283.5	283.5	283.5	283.5	283.5	283.5
Y	301	306	311	316	321	326	331	336
Z	37							

Straight Pitot tube

X	361
Y	298
Z	20

Static Pressure reading (mm) 13

Height on Ruler (mm)	Height above orifice (mm)	Y co-ordinate															
		0		5		10		15		20		25		30		35	
		S_R	H_P	S_R	H_P	S_R	H_P	S_R	H_P	S_R	H_P	S_R	H_P	S_R	H_P	S_R	H_P
39	2	70	57	69	56	54	41	53	40	48	35	43	30	40	27	38	25
42	5	69	56														
47	10	70	57														
52	15	74	61													38	25
53	16									54	41	48	35				
56	19																
57	20	79	66											41	28	38	25
58	21							59	46								
59	22	80	67														
61	24			86	73	72	59										
62	25	79	66														
67	30	71	58														
72	35	51	38													36	23
77	40	44	31														
82	45	41	28														
87	50	37	24													35	22
92	55	35	22														
97	60	33	20														
102	65	32	19														
107	70	30	17														
112	75	28	15														
117	80	27	14														
122	85	27	14														
127	90	26	13														
137	100	25	12													25	12
147	110	24	11														
157	120	24	11														
167	130	23	10														
187	150	22	9														
207	170	21	8														
227	190	21	8														
237	200	20	7													20	7

Static Pressure reading (mm) 13

Height above orifice (mm)	Height on Ruler (mm)	Y co-ordinate		
		0		
		S_R	$H_{P(V)}$	$V_{V\,(m/s)}$
2	22	1217	1147	4.74
5	25	846	777	3.90
10	30	512	442	2.94
15	35	460	386	2.75
16				
19				
20	40	207	128	1.58
21				
22	42	161	81	1.26
24				
25	45	125	46	0.95
30	50	96	25	0.70
35	55	65	14	0.52
40	60	55	11	0.46
45	65	47	6	0.34
50	70	43	6	0.34
55	75	39	4	0.28
60	80	37	4	0.28
65	85	35	3	0.24
70	90	34	4	0.28
75	95	32	4	0.28
80	100	31	4	0.28
85	105	30	3	0.24
90	110	29	3	0.24
100	120	28	3	0.24
110	130	27	3	0.24
120	140	26	2	0.20
130	150	25	2	0.20
150	170	23	1	0.14
170	190	22	1	0.14
190	210	21	0	0.00
200	220	21	1	0.14

Height above orifice (mm)	Y co-ordinate
	0
	Energy (mm)
2	1204
5	833
10	499
15	447
16	
19	
20	194
21	
22	148
24	
25	112
30	83
35	52
40	42
45	34
50	30
55	26
60	24
65	22
70	21
75	19
80	18
85	17
90	16
100	15
110	14
120	13
130	12
150	10
170	9
190	8
200	8

S_R	Sight tube reading
H_P	Pressure head
$H_{P(V)}$	Velocity head vertical component
V_V	Velocity Vertical component
FH	Fluidised height
	Input cell

Appendix D – Raw data for the additional experiments

Experiment: Centre orifice along Y= 7 mm

Flow rate (l/min)	2
Bed height (mm)	300
Ballotini sample	A
FH (measured)	N/A

Co-ordinates on ruler

90 Pitot tube (Facing neg X)

X	283.5
Y	308
Z	37

Straight Pitot tube

X	361
Y	305
Z	20

Static Pressure reading (mm) 13

Height on Ruler (mm)	Height above orifice (mm)	Y co-ordinate 7 S_R	H_P
39	2	70	57
42	5	64	51
47	10	67	54
52	15	73	60
57	20	82	69
62	25	91	78
63	26	92	79
67	30	81	68
72	35	71	58
77	40	58	45
82	45	49	36
87	50	44	31
92	55	40	27
97	60	37	24
102	65	34	21
107	70	32	19
112	75	30	17
117	80	29	16
122	85	28	15
127	90	27	14
137	100	26	13
147	110	25	12
157	120	24	11
167	130	23	10
187	150	22	9
207	170	21	8
227	190	20	7
237	200	20	7

Static Pressure reading (mm) 13

Height above orifice (mm)	Height on Ruler (mm)	Y co-ordinate 7 S_R	$H_{P(V)}$	$V_{V\,(m/s)}$
2	22	97	27	0.73
5	25	87	23	0.67
10	30	91	24	0.69
15	35	104	31	0.78
20	40	111	29	0.75
25	45	99	8	0.40
26	46	95	3	0.24
30	50	89	8	0.40
35	55	63	-8	-0.40
40	60	54	-4	-0.28
45	65	48	-1	-0.14
50	70	43	-1	-0.14
55	75	40	0	0.00
60	80	37	0	0.00
65	85	34	0	0.00
70	90	33	1	0.14
75	95	31	1	0.14
80	100	30	1	0.14
85	105	29	1	0.14
90	110	28	1	0.14
100	120	27	1	0.14
110	130	26	1	0.14
120	140	25	1	0.14
130	150	24	1	0.14
150	170	23	1	0.14
170	190	22	1	0.14
190	210	21	1	0.14
200	220	20	0	0.00

Y co-ordinate 7 Energy (mm)
84
74
78
91
98
86
82
76
50
41
35
30
27
24
21
20
18
17
16
15
14
13
12
11
10
9
8
7

S_R	Sight tube reading
H_P	Pressure head
$H_{P(V)}$	Velocity head vertical component
V_V	Velocity Vertical component
FH	Fluidised height
	Input cell

Experiment: Side orifice along Y= 7 mm

Flow rate (l/min)	2
Bed height (mm)	300
Ballotini sample	A
FH (measured)	N/A

Co-ordinates on ruler

90 Pitot tube (Facing neg X)

X	281.5
Y	556
Z	37

Straight Pitot tube

X	361
Y	563
Z	20

Static Pressure reading (mm) 13

Height on Ruler (mm)	Height above orifice (mm)	Y co-ordinate 7 S_R	H_P
39	2	82	69
42	5	81	68
47	10	80	67
52	15	82	69
57	20	89	76
62	25	109	96
67	30	110	97
72	35	121	108
77	40	134	121
82	45	128	115
87	50	107	94
92	55	97	84
97	60	80	67
102	65	66	53
107	70	60	47
112	75	55	42
117	80	50	37
122	85	46	33
127	90	43	30
137	100	39	26
147	110	35	22
157	120	32	19
167	130	30	17
187	150	28	15
207	170	26	13
227	190	24	11
237	200	23	10

Static Pressure reading (mm) 13

Height above orifice (mm)	Height on Ruler (mm)	Y co-ordinate 7 S_R	$H_{P(V)}$	$V_{V\,(m/s)}$
2	22	113	31	0.78
5	25	103	22	0.66
10	30	102	22	0.66
15	35	103	21	0.64
20	40	109	20	0.63
25	45	119	10	0.44
30	50	130	20	0.63
35	55	138	17	0.58
40	60	140	6	0.34
45	65	126	-2	-0.20
50	70	107	0	0.00
55	75	92	-5	-0.31
60	80	77	-3	-0.24
65	85	67	1	0.14
70	90	61	1	0.14
75	95	57	2	0.20
80	100	56	6	0.34
85	105	45	-1	-0.14
90	110	42	-1	-0.14
100	120	37	-2	-0.20
110	130	34	-1	-0.14
120	140	33	1	0.14
130	150	30	0	0.00
150	170	27	-1	-0.14
170	190	25	-1	-0.14
190	210	24	0	0.00
200	220	23	0	0.00

Y co-ordinate 7 Energy (mm)
100
90
89
90
96
106
117
125
127
113
94
79
64
54
48
44
43
32
29
24
21
20
17
14
12
11
10

S_R	Sight tube reading
H_P	Pressure head
$H_{P(V)}$	Velocity head vertical component
V_V	Velocity Vertical component
FH	Fluidised height
	Input cell

APPLICATION FORM

Please Note:
Any person planning to undertake research in the Faculty of Engineering and the Built Environment (EBE) at the University of Cape Town is required to complete this form **before** collecting or analysing data. The objective of submitting this application *prior* to embarking on research is to ensure that the highest ethical standards in research, conducted under the auspices of the EBE Faculty, are met. Please ensure that you have read, and understood the **EBE Ethics in Research Handbook**(available from the UCT EBE, Research Ethics website) prior to completing this application form: http://www.ebe.uct.ac.za/usr/ebe/research/ethics.pdf

APPLICANT'S DETAILS		
Name of principal researcher, student or external applicant		Kuveshan Govebder
Department		Civil Engineering
Preferred email address of applicant:		Gvnkuv007@myuct.ac.za
If a Student	Your Degree: e.g., MSc, PhD, etc.,	MSC
	Name of Supervisor (if supervised):	Professor JE van Zyl
If this is a researchcontract, indicate the source of funding/sponsorship		WRC
Project Title		A laboratory investigation of the effect of flow rate and bedding characteristics on the interaction of a vertical water jet with an idealised soil medium.

I hereby undertake to carry out my research in such a way that:

- there is no apparent legal objection to the nature or the method of research; and
- the research will not compromise staff or students or the other responsibilities of the University;
- the stated objective will be achieved, and the findings will have a high degree of validity;
- limitations and alternative interpretations will be considered;
- the findings could be subject to peer review and publicly available; and
- I will comply with the conventions of copyright and avoid any practice that would constitute plagiarism.

SIGNED BY	Full name	Signature	Date
Principal Researcher/ Student/External applicant	Kuveshan Govender	Signed by candidate	

APPLICATION APPROVED BY	Full name	Signature	Date
Supervisor (where applicable)	Professor Kobus van Zyl	Signed by candidate	10/8/16
HOD (or delegated nominee) Final authority for all applicants who have answered NO to all questions in Section1; and for all Undergraduateresearch (Including Honours).	~~Click here to enter text.~~ M Vandersch...	Signed by candidate	Click here to enter a date.
Chair : Faculty EIR Committee For applicants other than undergraduate students who have answered YES to any of the above questions.	Click here to enter text.		Click here to enter a date.